Doctoral dissertation

Discrimination of homologous and isomeric dicarboxylic acids by gold nanoparticle-pillar[n]pyridinium ensembles

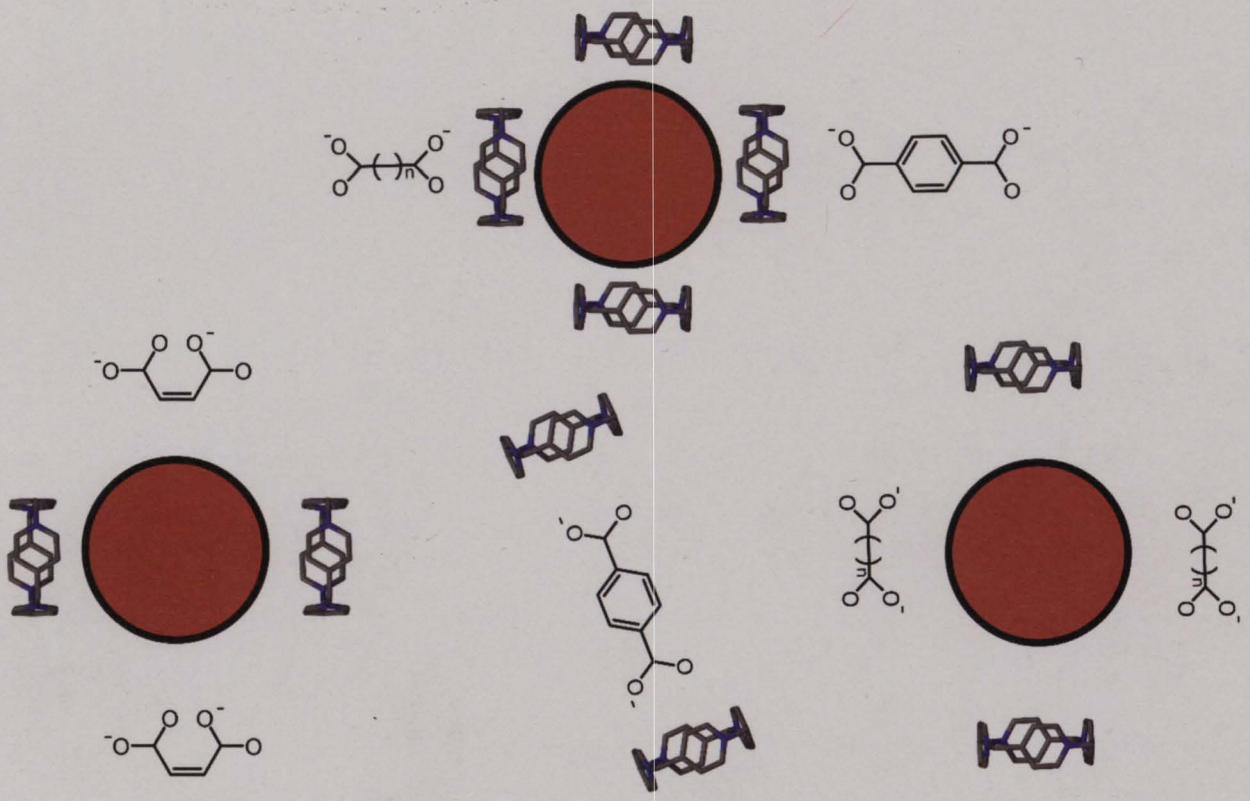

Mykola Kravets

IChF
Institute of Physical Chemistry PAS

Discrimination of homologous and isomeric dicarboxylic acids by gold nanoparticle-pillar[n]pyridinium ensembles

PhD thesis by

Mykola Kravets

Prepared under the supervision of

dr hab. **Volodymyr Sashuk** *(Assoc. Prof. IPC PAS)*

A thesis submitted in fulfilment of the requirements

for the degree of Doctor of Philosophy

under

International Doctoral Studies

Of the Institute of Physical Chemistry,

Polish Academy of Sciences

Kasprzaka 44/52

01-224 Warsaw, Poland

Warsaw, February 2023

Dedicated to
my Dearest wife Kateryna Kravets

Acknowledgment

I would like to thank the following people who contributed, supported, and encouraged me along my scientific path.

First of all, I am extremely grateful to my supervisor, **dr hab. Volodymyr Sashuk** for giving me the opportunity to work under his supervision. In particular, I would like to thank **dr hab. Volodymyr Sashuk** for his invaluable advice, constant support and feedback. His immense knowledge and plentiful experience have encouraged me through my scientific research and daily life.

Deepest thanks to **dr hab. Iwona Miszalewska-Turkowicz** from the University of Bialystok, Faculty of Chemistry, for the TEM measurements and the interpretation of obtained results and **dr hab. Oksana Danylyuk** for the determination of the structures of single X-ray crystals.

From the bottom of my heart, I would like to say a big thank you to all current and former members of the "Chemistry in Confined Spaces group" for the help and support during my PhD studies.

I also would like to say a special thank you to my former supervisor **dr hab. Yurii Ostapiuk** whose insight and knowledge of chemistry steered me to become a scientist. I deeply appreciate the help of my friend **Maksym Shehedyn** who spent a lot of time with me, discussing the different aspects of chemistry.

I am extremely thankful to my parents and brother for their love, support and confidence in me. Their belief in me has kept my spirits and motivation high during my research.

Special regards to my lovely wife **Kateryna Kravets** for her love, care, support and every little effort she is doing for me. Without her tremendous understanding and encouragement, it would be impossible for me to be the person I am now.

I acknowledge my friend **James Pogrebetsky** for proofreading my PhD thesis.

Funding

This work was financed by the National Science Centre of Poland (grant OPUS 12 no. 2016/23/B/ST5/02937) and (grant OPUS 18 no. 2019/35/B/ST4/01758).

Declaration of originality

I hereby declare that the research included within this thesis was carried out by myself or with support by others included in acknowledgments.

I state that I have exercised care to ensure that the work is original and contains no previously published material or written by another person, except where citations have been made in the text. To the best of my knowledge, the content provided here does not violate any copyrights.

I accept that the Polish Academy of Sciences has the right to use plagiarism detection software to ensure the thesis's legitimacy.

I certify that no part of my thesis has been or will be submitted for obtaining a degree or diploma by the Institute of Physical Chemistry, Polish Academy of Science, or any other educational institution.

This thesis's copyright rests with the author, and no information derived from it may be published without the author's consent.

Warsaw, February 2023

…….……
(signature)

List of scientific publications

Publications related to the thesis

1. **Kravets, M.**; Misztalewska-Turkowicz, I.; Sashuk, V., Probing E/Z Isomerism Using Pillar[4]pyridinium/Gold Nanoparticle Ensembles and Their Photoresponsive Behavior. *Langmuir* **2022**, *38*, 4942-4947. **Featured on the journal cover.**
2. **Kravets, M.**; Misztalewska-Turkowicz, I.; Sashuk, V., Plasmonic Nanoprobes Gauging the Length and Flexibility of α,ω-Alkanedicarboxylic Acids With an Optical Readout. *Sensors and Actuators B: Chemical* **2021**, *343*, 130083.
3. **Kravets, M.**; Sobczak, G.; Rad, N.; Misztalewska-Turkowicz, I.; Danylyuk, O.; Sashuk, V., Visual discrimination of aromatic acid substitution patterns by supramolecular nanocooperativity. *Chemical Communications* **2020**, *56*, 8595-8598. **Featured on the journal cover.**

Other publications

1. Ostapiuk, Y. V.; Ostapiuk, M. Y.; Barabash, O. V.; **Kravets, M.**; Herzberger, C.; Namyslo, J. C.; Obushak, M. D.; Schmidt, A., One-Pot Syntheses of Substituted 2-Aminothiazoles and 2-Aminoselenazoles via Meerwein Arylation of Alkyl Vinyl Ketones. *Synthesis* **2022,** *54*, 3658-3666.
2. Kravets, K.; **Kravets, M.**; Butkiewicz, H.; Kosiorek, S.; Sashuk, V.; Danylyuk, O., Electrostatic co-assembly of pillar[n]pyridiniums and calix[4]arene in aqueous media. *CrystEngComm* **2022,** *22*, 2213-2216. **Featured on the journal cover.**
3. Potopnyk, M. A.; **Kravets, M.**; Luboradzki, R.; Volyniuk, D.; Sashuk, V.; Grazulevicius, J. V., Carbazole-modified thiazolo[3,2-c][1,3,5,2]oxadiazaborinines exhibiting aggregation-induced emission and mechanofluorochromism. *Organic & Biomolecular Chemistry* **2021,** *19*, 406-415.

List of scientific presentations

Oral presentations

1. **Kravets, M.**; Misztalewska-Turkowicz, I.; Sashuk, V., *Recognition of E/Z Dicarboxylic Acids using Pillar[4]pyridinium Covered Gold Nanoparticles and their Photoresponsive Self-Assembly*, 2nd International Conferences on Noncovalent Interactions (ICNI 2022), 18-22.07.2022, Strasbourg, France.
2. **Kravets, M.**; Misztalewska-Turkowicz, I.; Sashuk, V., *Visual discrimination of α,ω-alkanedicarboxylic acids*, Summer School for PhD Students, 18-20.05.2022, Lublin, Poland.
3. **Kravets, M.**; Misztalewska-Turkowicz, I.; Sashuk, V., *Plasmonic nanoprobes gauging the length and flexibility of α,ω-alkanedicarboxylic acids with an optical readout*, 9th European Young Engineers Conference, 19-21.04.2021, Warsaw, Poland.
4. **Kravets, M.**; Sobczak, G.; Rad, N.; Misztalewska-Turkowicz, I.; Danylyuk, O.; Sashuk, V., *Visual discrimination of aromatic acid substitution patterns by supramolecular nanocooperativity*, Sympozjum Młodych Naukowców, Wydziału Fizyki UW, 24-27.08.2020, Warsaw, Poland.

Poster presentations

5. **Kravets, M.**; Misztalewska-Turkowicz, I.; Sashuk, V., *Probing E/Z isomerism by pillar[4]pyridinium/gold nanoparticle ensembles and their photoresponsive behavior*, Summer School for PhD Students, 18-20.05.2022, Lublin, Poland.
6. **Kravets, M.**; Sobczak, G.; Rad, N.; Misztalewska-Turkowicz, I.; Danylyuk, O.; Sashuk, V., *Visual discrimination of aromatic acid substitution patterns by supramolecular nanocooperativity*, International chemical congress of pacific basin societies, 16-21.12.2021, Honolulu, Hawaii.

List of abbreviations

ADA – Azobenzene-4,4'-dicarboxylic acid

AIE – Aggregation-induced emission

AuNPs – Gold nanoparticles

CD – Circular Dichroism

CV – Cyclic voltammetry

DCC – Dynamic covalent chemistry

DLS – Dynamic light scattering

DMC – Double mutant cycle analysis

DMF – N,N-Dimethylformamide

DMSO – Dimethyl sulfoxide

DNA – Deoxyribonucleic acid

D_2O – Deuterated water

DOSY – Diffusion-ordered NMR spectroscopy

DPAC-bisC4P – Bis-calix[4]pyrrole-appended 9,14-diphenyl-9,14-dihydrodibenzo[a,c]phenazine

DPV – Differential pulse voltammogram

EDG – Electron-donating group

ESI-FTICR – Electrospray ionization Fourier transform ion cyclotron resonance mass spectrometry

ESI-MS – Electrospray-ionization mass spectrometry

EC-SOERS – Electrochemical Surface Oxidation Enhanced Raman Scattering

EWG – Electron-withdrawing group

Fum – Fumaric acid

G – Guest

H – Host

HB – Hydrogen bonding

H_2O – Water

IDA – Indicator-displacement assays

IR – Infrared spectroscopy

K_a – Association constant

Mal – Maleic acid

MeOH – Methanol

MOF – Metal-organic frameworks

NMR – Nuclear magnetic resonance

NPs – nanoparticles

PET – Polyethylene terephthalate

PET – Photoinduced electron transfer

PnPs – Pillar[n]pyridiniums

RNA – Ribonucleic acid

SBDA – Stilbene-4,4'-dicarboxylic acid

SPR – Surface plasmon resonance

SWV – Square wave voltammetry

TEM – Transmission electron microscopy

TMA – 11-Mercapto-N,N,N-trimethylundecan-1-aminium chloride

Tris – Tris(hydroxymethyl)aminomethane

UV-Vis – Ultraviolet visible spectroscopy

VIE – Vibration-induced emission

$\Delta\delta$ – Chemical shift

Table of contents

Abstract

Dicarboxylic acids are one of the most important and well-known chemical compounds. They are used in the fabrication of dyes, perfumes, pharmaceuticals, and many other products. On the other hand, diacids play a crucial role in many biochemical processes such as energy production and storage. However, their omnipresence not only improves the quality of the life but also creates serious environmental problems and increases the risk of various diseases in humans. Therefore, their detection is of a paramount significance.

Dicarboxylic acids are colorless crystals with similar physicochemical properties. Therefore, their discrimination is extremely difficult. The methods of their detection developed so far recognize only selected diacids and often require specialized equipment. To address this issue, we have decided to develop a general and simple strategy for the recognition of dicarboxylic diacids. To this end, we have developed a supramolecular nanosensor made of gold nanoparticles coated by pillar[n]pyridinium (PnP) macrocycles.

The first part of the PhD thesis focuses on the visual discrimination of phthalic acids, which are positional isomers. Compared to previous studies, the developed by us sensor recognizes all three isomers. In the presence of the nanoparticles, these acids produce a multilevel response, including the color change observed with the naked eye. The desired optical response is attained through specific non-covalent interactions between the diacids and the NPs coated with cationic pillar[n]pyridinium hosts, resulting in the formation of NP aggregates with different interparticle gaps.

The second part of the thesis describes the recognition of aliphatic dicarboxylic acids, which are chemical homologs. The principle of the operation of the sensor, in this case, is the same and consists in cross-linking the NPs with the diacids. The obtained plasmonic coupling depends on the length, flexibility, and odd-even character of the aliphatic chain of each diacid.

The third part of the thesis concentrates on differentiating geometric isomers. Specifically, we used the dicarboxylic derivatives of ethylene, stilbene and azobenzene. As in the previous cases, the recognition of each diacid depends preliminary on the spatial position and relative distance between carboxylic groups. For short diacids, a more pronounced plasmonic response is obtained for *trans* isomer, while for long diacids for *cis* isomers. Importantly, the nanoparticles not only discriminate between *trans*- and *cis*-forms but also undergo reversible self-assembly which is controlled remotely by light.

The nanosensor we have developed stands out from other similar platforms which are more complex and are able to discriminate only selected isomers. In the future, this sensor can be also utilized for recognizing other chemically similar compounds containing anionic groups.

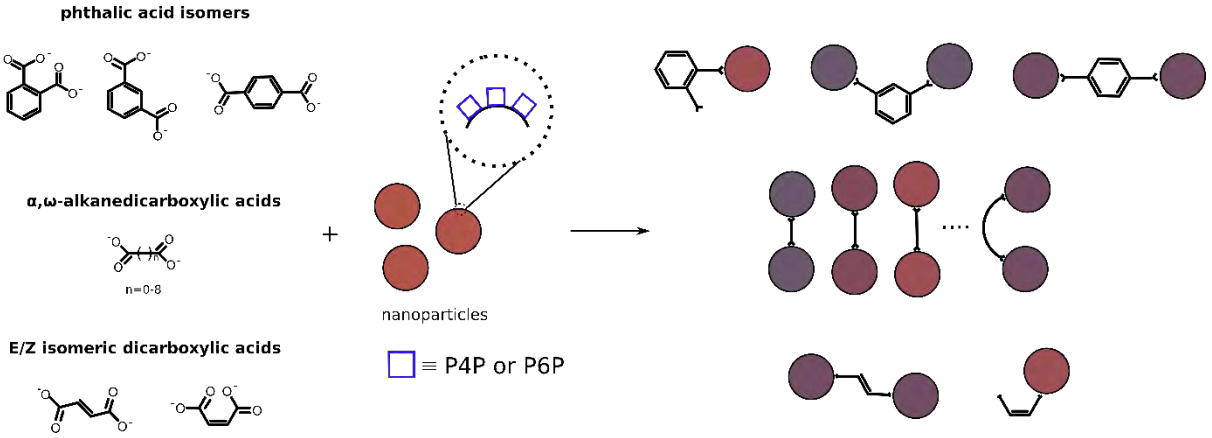

Streszczenie

Kwasy dikarboksylowe stanowią liczną grupę powszechnie znanych i niezwykle ważnych związków chemicznych. Są one wykorzystywane do produkcji barwników, perfum, leków i wielu innych produktów. Ponadto, dikwasy pełnią kluczową rolę w wielu procesach biochemicznych, takich jak produkcja oraz magazynowanie energii. Ich wszechobecność nie tylko poprawia jakość życia, ale także stanowi poważny problem dla środowiska, zwiększając ryzyko zachorowań u ludzi, dlatego ich detekcja ma ogromne znaczenie.

Kwasy dikarboksylowe to bezbarwne kryształy o zbliżonych właściwościach fizykochemicznych, dlatego ich rozróżnianie jest niezwykle trudne. Opracowane dotychczas metody umożliwiają rozpoznawanie tylko wybranych dikwasów, co wymaga zazwyczaj stosowanie specjalistycznego sprzętu. W celu rozwiązania powyższego problemu, postanowiliśmy opracować ogólną i prostą strategię rozpoznawania kwasów dikarboksylowych. Zaprojektowaliśmy supramolekularny układ złożony z nanocząstek złota pokrytych cząsteczkami dodatnio naładowanych związków makrocyklicznych - pillar[n]pirydyn (PnP).

Pierwsza część rozprawy doktorskiej skupia się na wizualnym rozpoznawaniu kwasów ftalowych, będących izomerami pozycyjnmi. W porównaniu do znanych już metod, opracowany przez nas sensor umożliwia rozróżnienie wszystkich trzech izomerów. W obecności nanocząsteczek kwasy te wywołują wielopoziomową odpowiedź, w tym zmianę barwy zauważalną gołym okiem. Obserwowany sygnał optyczny jest wynikiem specyficznych oddziaływań niekowalencyjnych między dikwasami a nanocząstkami złota pokrytymi kationowymi pillar[n]pirydynami, co prowadzi do powstawania agregatów nanocząstek z różnymi odstępami między nimi.

Druga część rozprawy dotyczy rozpoznawania homologów alifatycznych kwasów dikarboksylowych. Zasada działania sensora w tym przypadku jest identyczna i polega na łączeniu nanocząstek za pomocą dikwasów. Uzyskane sprzężenie plazmonowe zależy od długości, giętkości oraz (nie)parzystości łańcucha alifatycznego dikwasu.

Trzecia część pracy koncentruje się na rozróżnianiu poszczególnych izomerów geometrycznych pochodnych dikarboksylowych: etylenu, stilbenu oraz azobenzenu. Podobnie jak w poprzednich przypadkach, rozpoznawanie każdego dikwasu zależy od położenia przestrzennego i względnej odległości między grupami karboksylowymi. Dla krótkich dikwasów silniejszą odpowiedź plazmonową obserwuje się w przypadku izomeru *trans*, podczas gdy dla długich kwasów dikarboksylowych jest to izomer *cis*. Co ważne, nanocząstki nie tylko rozpoznają izomery, ale również ulegają odwracalnej samoorganizacji, kontrolowanej zdalnie za pomocą światła.

Opracowany przez nas nanosensor wyróżnia się na tle innych podobnych układów, ponieważ są one z reguły bardziej złożone i są w stanie odróżnić tylko wybrane izomery. W przyszłości omawiany system może być również wykorzystywany do rozpoznawania innych podobnych chemicznie związków zawierających grupy anionowe.

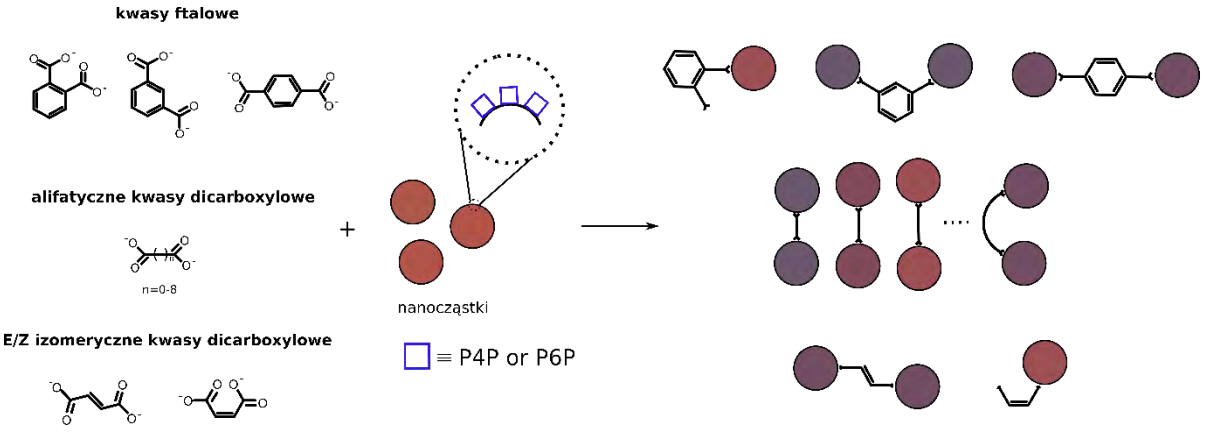

1. INTRODUCTION

1.1 Discrimination of phthalic acid isomers

Phthalic acids are aromatic dicarboxylic acids with the general formula $C_6H_4(CO_2H)_2$. They are colorless solids with similar physicochemical properties. Phthalic acids consist of three isomers: phthalic, isophthalic and terephthalic (Figure 1).

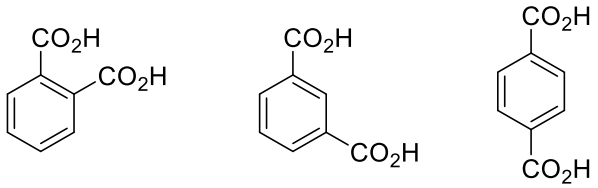

Figure 1. Structural formulae of phthalic, isophthalic and terephthalic acids.

They play a crucial role in our daily life. Although phthalic acid has no wide commercial application, its closely related derivative phthalic anhydride is utilized for the large-scale production of plasticizers for polymers. Isophthalic acid has much wider usage. For example, the fire-resistant material Nomex is made of isophthalic acid. Besides, mixed in small amounts with terephthalic acid, isophthalic acid is applied for the production of plastic bottles and food packaging. Also, this diacid is employed as an important component to produce insulation materials. Terephthalic acid is a well-known precursor for the manufacture of polyethylene terephthalate (PET). Moreover, this diacid is used in the pharmaceutical industry as a raw material. It is expected that the usage of phthalic acids will be grown in future years.

Such a large demand not only improves the quality of life but also creates serious environmental problems leading to the pollution of air[1], soil[2] and water.[3] Despite the fact that the toxicity of phthalic acids is generally low they may cause the risk of reproductive and developmental disorders in humans.[4]

Significant efforts have therefore been made in the development of a chemical sensor that would be capable of precisely recognizing phthalic acids. To date, several methods for their detection have been known from the literature: colorimetric[5-7], fluorescent[8-10], electrochemical[11-13] and others.[14-23]

1.1.1 Colorimetric discrimination of phthalic acid isomers

Since phthalic acids are dibasic acids with quite low pKa values (2.89 and 5.51 for phthalic, 3.46 and 4.46 for isophthalic, 3.51 and 4.82 for terephthalic acids, respectively), they are mostly present in the anionic form under normal conditions (aqueous solution, neutral pH).

Colorimetric methods are mostly developed for the recognition of inorganic anions[24-28], whereas only few have been reported for the discrimination of organic anions[29-32]. Such colorimetric sensors for organic anions recognition are built using the binding site-signaling unit approach in which an appropriate chromophore is attached to a specific anion sensor. Sensors for anions discrimination usually contain urea and thiourea subunits that act as H-bond donors[33,34] and these sensors are also excellent for dicarboxylate anions.[35,36]

Yen and coworkers developed[5] chromogenic receptors **1-3** for selective colorimetric discrimination of phthalic acids (Figure 2).

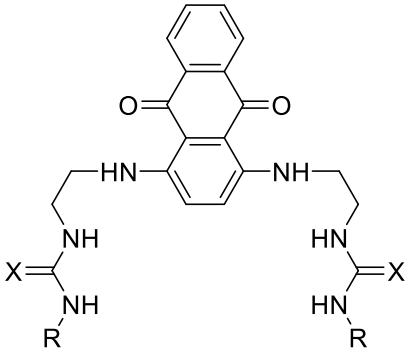

1. X=S, R=p-NO_2-phenyl
2. X=S, R=p-NO_2-naphthyl
3. X=O, R=p-NO_2-phenyl

Figure 2. Colorimetric receptors **1-3**.

Sensor **1** selectively recognizes phthalate among other isomers (Figure 3). UV-Vis spectra have shown a significant change of λ_{max} of sensor **1** in the presence of phthalate with the solution color change from blue to dark-green, while only negligible alterations have been observed upon the addition of isophthalate and terephthalate. The discrimination of phthalate by **1** has been determined by the geometry of this anion.

Figure 3. Effect of phthalate isomers on color changes of **1**: (a) **1**; (b) **1**+phthalate; (c) **1**+isophthalate; (d) **1**+terephthalate. Adapted with permission from the Elsevier. Copyright 2006.[5]

Sensor **2** had a different response to phthalates (Figure 4). The dark-red color was observed irrespective of the isomer used. In other words, receptor **2** cannot be used for the discrimination of phthalates.

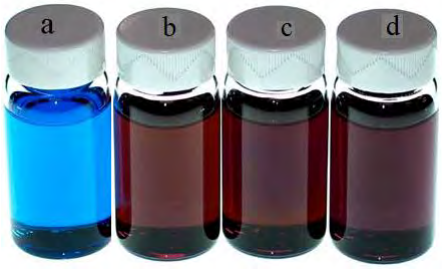

Figure 4. Effect of phthalate isomers on color changes of **2**: (a) **2**; (b) **2**+phthalate; (c) **2**+isopthalate; (d) **2**+terephthalte. Adapted with permission from the Elsevier. Copyright 2006.[5]

To get an idea how sensor **1** works the thiourea unit has been displaced by a urea unit. This gave compound **3** that has shown no significant changes in UV-Vis spectra after addition of phthalates. The strongly electronegative oxygen atom of the urea subunit, that makes little contribution to the charge-transfer process, may be the cause of the weak binding.

As an extension to this work, colorimetric sensors **1-3** have been modified by introducing electron-withdrawing substituents into one of the two binding sites to see how this might affect the binding properties of the resultant sensors **4-7** to phthalates (Figure 5).[6]

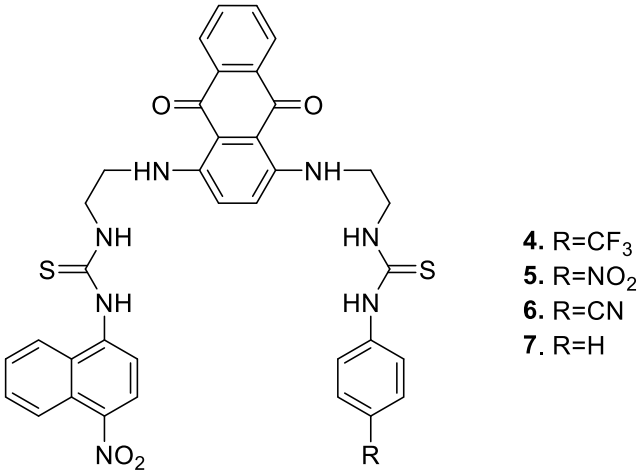

Figure 5. Colorimetric receptors **4-7**.

The authors anticipated that sensing properties would be substantially improved by the phenyl ring's substituent: the stronger electron-withdrawing group (NO_2>CN>CF_3>H), the higher binding affinity, due to the enhanced acidity of the thiourea protons was expected. Unfortunately, no well-defined color change has been observed for aromatic isomeric dicarboxylate anions (Figure 6). Hence, these sensors **4-7** are not suitable for the discrimination between phthalates.

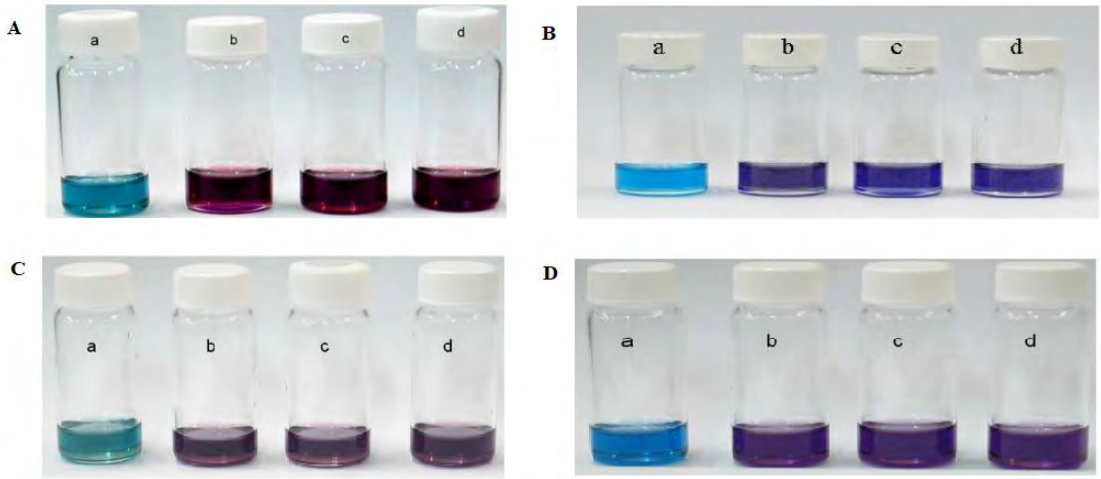

Figure 6. Effect of phthalate anions on the color changes of **4-7**: **A**: (a) **4**; (b) **4**+phthalate; (c) **4**+isopthalate; (d) **4**+terephthalate; **B**: (a) **5**; (b) **5**+phthalate; (c) **5**+isophthalate; (d) **5**+terephthalate; **C**: (a) **6**; (b) **6**+phthalate; (c) **6**+isophtalate; (d) **6**+terephthalate; **D**: (a) **7**; (b) **7**+phthalate; (c) **7**+isophthalate; (d) **7**+terephthalate. Adapted with permission from the Royal Society of Chemistry. Copyright 2007.[6]

Gold nanoparticles can also act as colorimetric sensors.[37-44] The sensing strategy in this case is based on the color change due to the aggregation of gold nanoparticles and the resulting interparticle plasmon coupling. The color change of AuNPs can be observed with the naked eye even at low concentrations.

In 2008, Ahn and coworkers[7] have reported the use of gold nanoparticles **8** decorated with a lipoic acid derivative for the detection of phthalates in water (Figure 7). In this AuNPs-based system the conformational flexibility of the carboxylate groups affects the aggregation as well as color change.

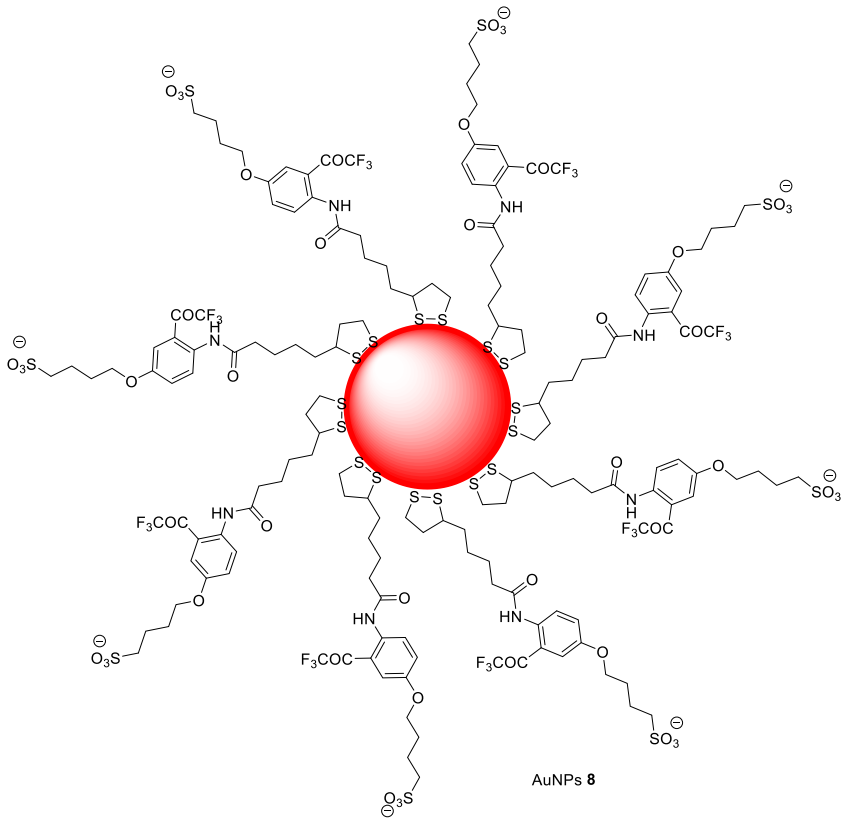

Figure 7. Schematic representation of the functionalized AuNPs **8**.

The nanoparticle probe **8** has demonstrated remarkably high sensitivity toward terephthalate over phthalate and isophthalate (Figure 8). The color of the solution has changed from red to blue through extensive nanoparticle aggregation. The interparticle cross-linking has occurred due to molecular interactions between two carboxylate groups of terephthalate and trifluoroacetyl binding site.

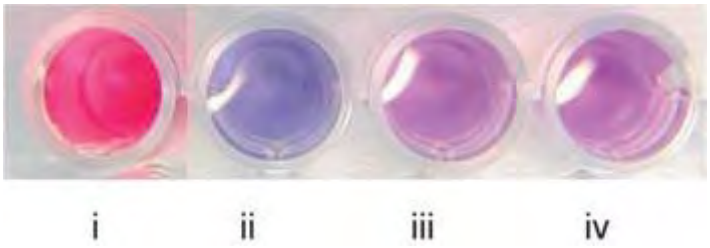

Figure 8. Effect of phthalate anions on color changes of **8**: i) before the addition of analyte and after the addition of ii) terephthalate, iii) phthalate, iv) isophthalate. Adapted with permission from the John Wiley and Sons. Copyright 2008.[7]

1.1.2 Fluorescent discrimination of phthalic acid isomers

Fluorescence is a technique that possesses a high sensitivity, real-time readout capability, design flexibility etc.[45] During the past decade various methods based on high-sensitivity fluorescence detection have been developed, for instance, DNA sequencing, DNA fragment analysis and others. Continued attempts are being made to utilize various photophysical phenomena in designing fluorescent sensors and to improve their selectivity.[46]

As in the case of colorimetry, a target host molecule has to geometrically match the size and non-covalent binding preferences of the guest.[47-49]

Phthalic acid has been reported to cause dimerization and turn-on fluorescence by aggregation-induced emission (AIE) in DMF solution upon interaction via hydrogen bonds with the pyrazole groups of the trigonal fluorinated trispyrazole sensor **9** (Figure 9).[8]

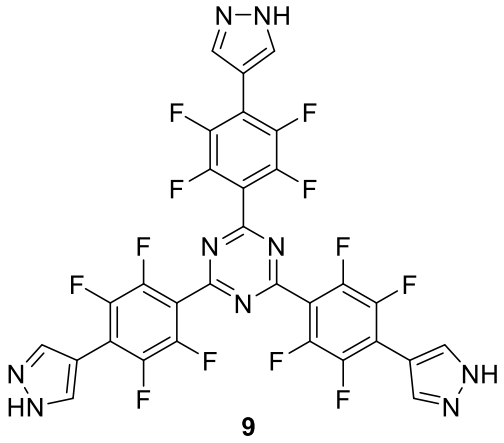

Figure 9. Fluorinated trispyrazole sensor **9**.

In this case, phthalic acid has led to the formation of a dimer when sandwiched between two sensor molecules which leads to the turn-on fluorescence response. The two carboxylic groups must be positioned correctly geometrically for this dimerization to occur. As a result, the dimer's restriction on the rotational motions of the stacked receptor molecules has caused an increase in fluorescence. This has not observed for isophthalic acid and terephthalic acid that do not bring the receptor molecules close to one another (Figure 10).

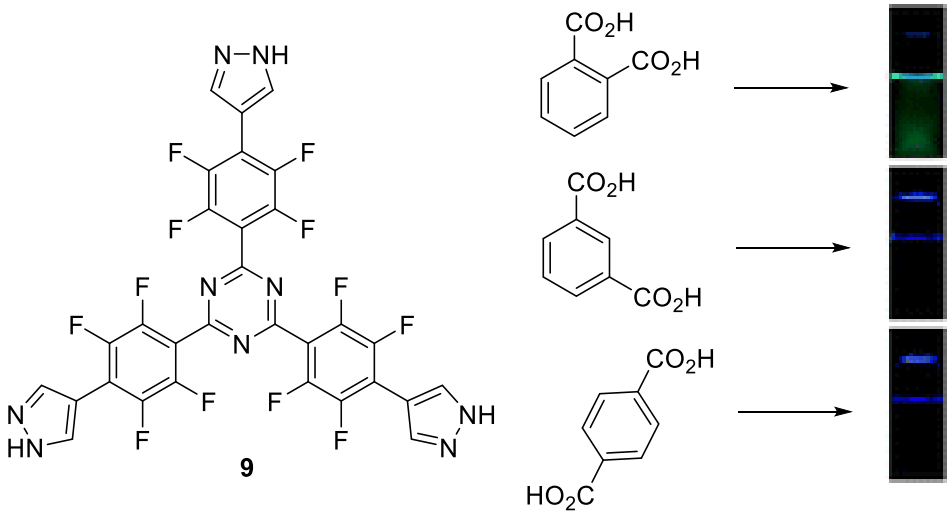

Figure 10. Fluorinated trispyrazole sensor **9** in the presence of phthalates. Adapted with permission from the Royal Society of Chemistry. Copyright 2018.[8]

In 2019, Sessler and coworkers[9] have reported the synthesis of a new fluorescent sensor system **10** based on vibration-induced emission (VIE), namely, bis-calix[4]pyrrole-appended 9,14-diphenyl-9,14-dihydrodibenzo[a,c]phenazine (**DPAC-bisC4P**) (Figure 11). This sensor recognizes aromatic dicarboxylate anions (phthalates) in the form of tetrabutylammonium salts in acetonitrile.

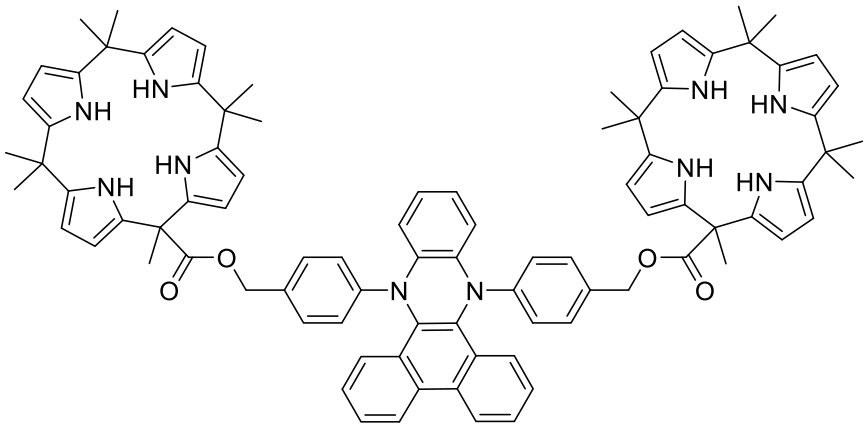

10

Figure 11. Structural formula of **DPAC-bisC4P** fluorescent sensor **10**.

Phthalate-treated receptor **10** is able to generate pseudomacrocyclic host-guest complexes through a number of hydrogen bonding interactions of phthalates with calix[4]pyrrole moieties. The emission of the phenazine core has underwent a blue-shift as a result of these interactions. Sensor **10** is able to recognize terephthalate and isophthalate but is not able to discriminate phthalate (Figure 12). The latter has been unable to support the formation of a pseudomacrocyclic structure due to the close position of two carboxylic groups. The formation of pseudomacrocyclic complexes between **DPAC-bisC4P** and both terephthalate and isophthalate has occurred at the ratio of 1:1. Since the two carboxylic groups in isophthalate are closer to each other than in terephthalate, the complexation of isophthalate by **DPAC-bisC4P** has resulted in a higher level of confinement to the **DPAC** fluorophore. Moreover, this receptor enabled to quantify these anions in acetonitrile with detection limits up to nanomolar concentrations.

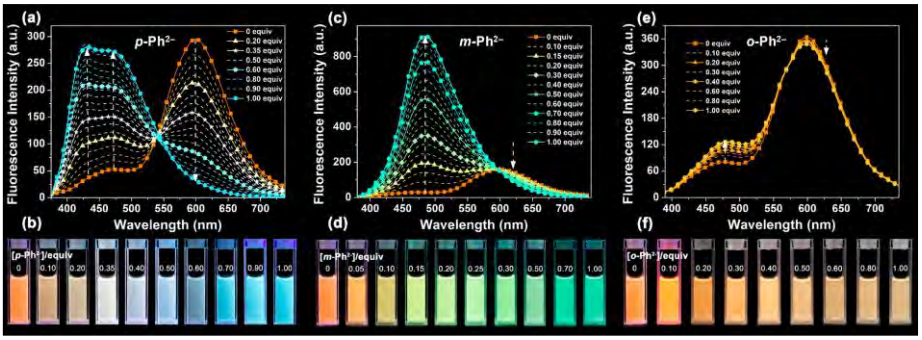

Figure 12. Fluorescence titration spectra of **DPAC-bisC4P** fluorescent sensor **10** upon the addition of (a) terephthalate (p-Ph^{2-}), (c) isophthalate (m-Ph^{2-}), and (e) phthalate (o-Ph^{2-}) and photographs showing the fluorescence features of **DPAC-bisC4P** with various amounts of (b) terephthalate, (d) isophthalate, (f) phthalate. Reprinted with permission from the American Chemical Society. Copyright 2019.[9]

A fluorescent calix[8]arene-like chemosensor **11** prepared by Zhang[10] and coworkers has selectively recognized terephthalate (Figure 13). It is the first reported fluorescent photoinduced electron transfer (PET) chemoreceptor.

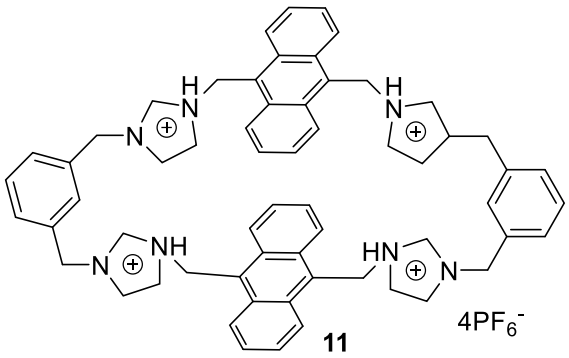

11

Figure 13. Fluorescent chemosensor **11**.

The presence of terephthalate caused a drop in the fluorescence intensity of sensor **11**, which can be attributed to the induction of PET process from the imidazolium unit's N atom to the anthracene unit due to the formation of a hydrogen bond between the sensor **11** and terephthalate.

1.1.3 Electrochemical discrimination of phthalic acid isomers

An electrochemical sensor is a device that quantitatively detects a particular chemical compound when an analyte comes in contact with an electrode surface. As a result, the analyte undergoes a redox reaction, which, in turn, produces an electrical signal that is attributed to the specific analyte.[50,51] The advantages of electrochemical sensors include simple measurement procedure, short response time and sufficient sensitivity and selectivity.[52] Basically, electrochemical analysis involves the monitoring of the changes of electron transfer occuring on an electrode. For this, cyclic voltammetry, amperometry and electrical impedance spectroscopy are used.

Considerable efforts have been devoted to the development of chemical probes capable of selectively recognizing and sensing dicarboxylic acids. Electrochemical sensors based on ferrocene, as a redox-responsive unit, exhibit a significant redox potential shift upon the formation of complexes between sensors and guest molecules. However, electrochemical discrimination of isomers still is a big challenge due to their very similar chemical and physical properties. Nevertheless, several reports on such discrimination were mentioned in the literature.

Kim and colleagues have created the electrochemical sensor **12**.[11] Sensor **12** consists of ferrocene and butylaminomethyl substituents. It has demonstrated light electrochemical oxidation of a secondary amine (Figure 14). Two anodic waves have been visible in the differential pulse voltammogram (DPV) spectra of sensor **12**, which correspond to the consecutive oxidation of ferrocene groups and the secondary amine. The presence of phthalic acid has reduced the anodic peak caused by the electrochemical oxidation of the secondary amine in receptor **12**. After the addition of 1.5 molar equivalents of phthalic acid, the peak has been fully suppressed. However, on contrary to phthalic acid, isophthalic acid and terephthalic acid have induced only a positive shift in the peak potential without a drop in peak current (Figure 15). Phthalic acid has displayed the strongest hydrogen bonding interactions between the secondary amine and carboxylic acid groups among three diacids. The electrochemical response of the sensor is the result of interactions between these groups. The phthalic acid selective electrochemical response of **12** is also fully reversible, allowing the repeated uses of **12** for the recognition of phthalic acid.

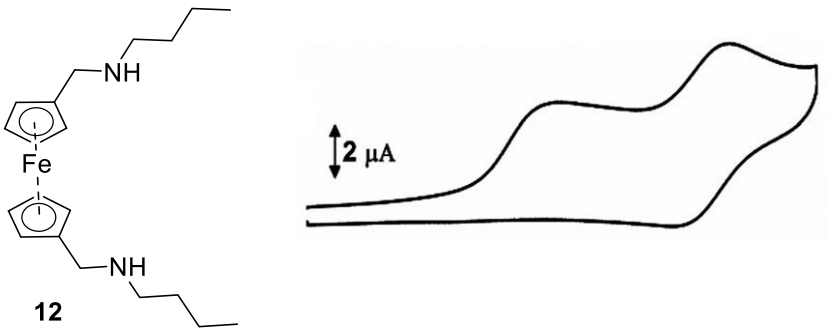

Figure 14. Electrochemical sensor **12** and its cyclic voltammogram. Reprinted with permission from the Royal Society of Chemistry. Copyright 2014.[11]

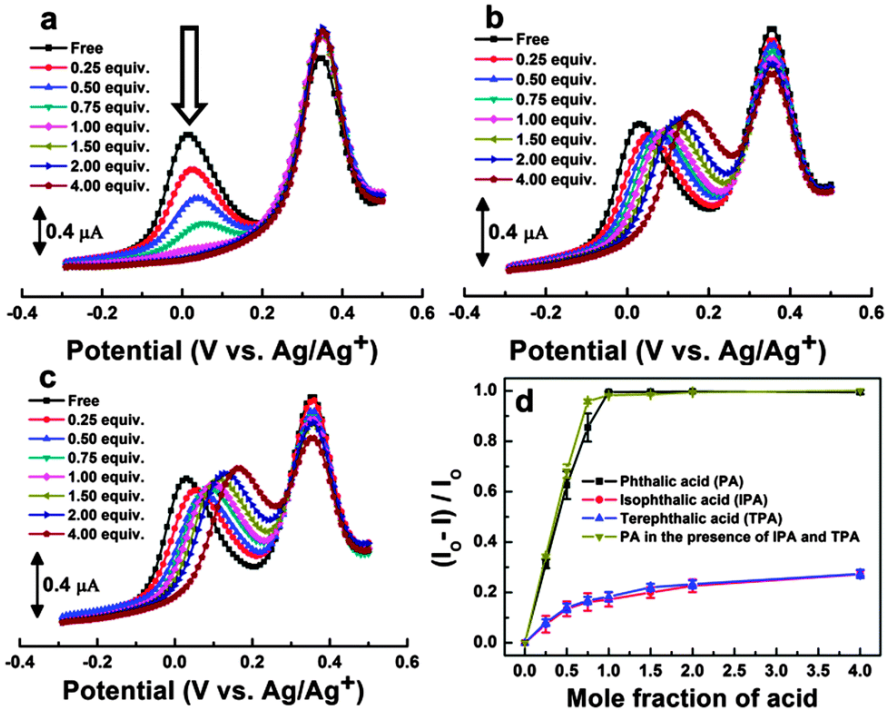

Figure 15. DPVs of **12** with 0-4 equivalents of (a) phthalic acid, (b) isophthalic acid and (c) terephthalic acid. (d) Normalized changes in the first anodic peak current (I) of **12**. Reprinted with permission from the Royal Society of Chemistry. Copyright 2014.[11]

Colina and coworkers[12] have utilized Electrochemical Surface Oxidation Enhanced Raman Scattering (EC-SOERS) phenomenon that enhances the Raman signal during the oxidation of metal surface. Authors have used this technique to differentiate phthalic acids isomers. Their research objective has been to provide additional information on how phthalic acids interact with silver substrates under specific EC-SOERS circumstances. CVs under EC-SOERS

conditions have shown very similar behaviour regardless of the studied diacids. However, some details can be found from CVs that are related to the adsorption of the target molecule (Figure 16). Depending on how well the substrate adsorbs, the maximum current seen during the oxidation of the silver electrode changes slightly. The lowest current for phthalic acid and the highest for terephthalic acid has been found. In comparison to isophthalic acid and terephthalic acid, phthalic acid had a stronger adsorption.

A similar behaviour was observed in the voltaRamangrams. When different phthalic acids have been utilized, the maximum of the Raman signal was not reached at the same potential. The maximum for phthalic acid has attained at a lower anodic potential, indicating a stronger interaction with the substrate. Whereas the maximum Raman signal for isophthalic acid and terephthalic acid has been obtained at greater anodic potentials.

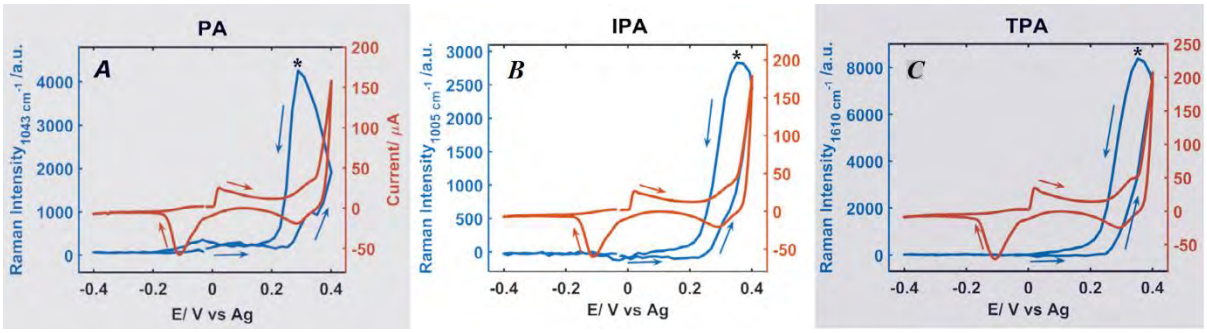

Figure 16. Comparison between CVs (orange curves) and the evolution of EC-SOERS response for the main band of each molecule with the potential applied (VoltaRamangram, blue curves) for (A) phthalic acid, (B) isophthalic acid and (C) terephthalic acid.

Tetraazamacrocycle **13** containing ferrocene moieties in a tetraprotonated form has been assessed as a sensor for phthalates recognition (Figure 17).[13] A larger binding constant has been determined by ^{1}H NMR titration for phthalic acid in comparison to isophthalic acid. By using cyclic voltammetry (CV) and square wave voltammetry (SWV), the impact of dicarboxylates on the electron-transfer mechanism of the ferrocene units of sensor **13** has been estimated. According to single crystal X-ray structures the receptor **13** has shown complexation with phthalates according to HG2 (H-host, G-guest) stoichiometry. The binding of phthalates occurred outside the macrocyclic cavity and has been assisted by N-H···O=C hydrogen bonds. The macrocycle **13** adopted different conformations depending on the phthalates used.

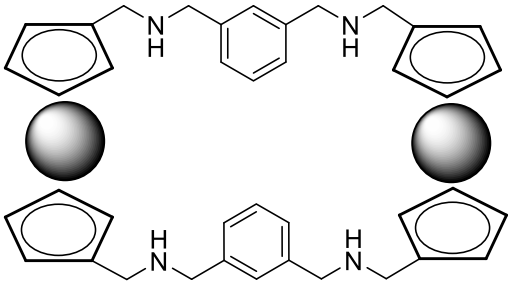

13

Figure 17. Tetraazamacrocycle **13**.

1.1.4 Other methods for discrimination of phthalic acid isomers

In addition to methods mentioned above, researchers reported a range of other techniques for the discrimination of phthalic acid isomers, for instance, gel electrophoresis[14], hydrogelation[15], complexes formation[16-18], solid state[19], anion exchange resin[20] and DOSY NMR[21].

A straightforward technique known as gel electrophoresis was developed in the 1970s and transformed molecular biology field as well as the biophysical studies of DNA and RNA. This technique is a universal method for separation of the nucleic acid in biochemistry. The separation is possible due to differences in lengths and shapes of nucleic acids. Moreover, gel electrophoresis is a crucial tool for separation of proteins. Polyacrylamide has essentially been the only material that supports proteins. However, the recovery of proteins from this gel is mediocre and the monomer of polyacrylamide is neurotoxic. To eluminate this problem, Nakajima and coauthors found a new support for gel electrophoresis such as curdlan (β-1,3-glucan) gel **14** (Figure 18).[14]

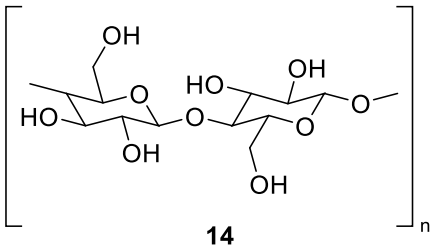

14

Figure 18. Curdlan (β-1,3-glucan) gel **14**.

Curdlan gel **14** has a similar ability to separate proteins as polyacrylamide gel, but much larger durability and therefore better suitability and reusability. Nakajima et al. used curdlan gel in the electrophoretic characterization of phthalic acid isomers. At the pH 8.7 curdlan gel gives a better resolution for the separation of phthalic acids than polyacrylamide gel. Electropherograms showed that curdlan gel had a much larger ability to separate the structural isomers. These results suggested that curdlan gel **14**, probably due to a hydrophilic interaction between the matrix and these electrolytes, is suitable for the separation of phthalic acids.

Low-molecular-weight gelators attracted considerable interest in recent years due to their application in food industry,[53] tissue engineering,[54] sensors,[55,56] template materials[57] and so on. Low-molecular-weight gelators based on carbohydrates,[58,59] amino acids[60] and other organic compounds are well-known. Two- or multi-component gels have distinct advantages over single-component gelators. Optical, mechanical and other properties can be simply tuned by changing the molar ratio between the componets.[61]

Hydrogel **15** consisting of L-histidine appended pyrenyl derivative and phthalate was fabricated by Bhattacharya and coworkers (Figure 19).[15] This hydrogelation unabled selective detection of phthalate over isophthalate and terephthalate. L-histidine derivative as a proton acceptor and phthalate as a proton donor interact to form an optically transparent hydrogel **15**. A gelation process occurred at the stoichiometric ratio of 1:1 between two components at a relatively high concentration. Since salt did not form when isomeric isophthalate and terephthalate were used in place of phthalate, hydrogelation was not seen.

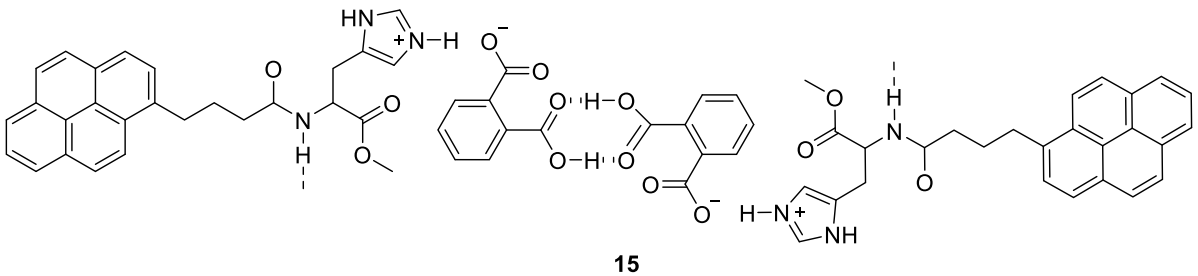

15

Figure 19. Acid-base interaction of L-histidine derivative with phthalate (hydrogel **15**).

Pritzkow and coauthors[16] demonstrated the utility of cationic complexes $[CuL^1]^{2+}$ **16**, $[Cu_2L^2]^{4+}$ **17** and $[Cu_3L^3]^{6+}$ **18** in the selective recognition of isophthalate and terephthalate (Figure 20). Complexes **16-18** are able to discriminate phthalates due to the coordination of carboxyl groups to the copper(II) ion and by stereochemical complementarity of such phthalic acid isomers to the selected receptors. UV-Vis spectra of receptor **16** did not show any changes in the presence of pthalates, while receptors **17** and **18** had different response to isophthalate and terephthalate. The best selectivity to phthalates was showed by the $[Cu_3L^3]^{6+}$ complex **18**. When reacting with isophthalate and terephthalate, receptor **18** had a differentiating impact. This could be explained by the formation of different complexes with phthalates, structure **A** in the case of isophthalate and structure **B** for terephthalate.

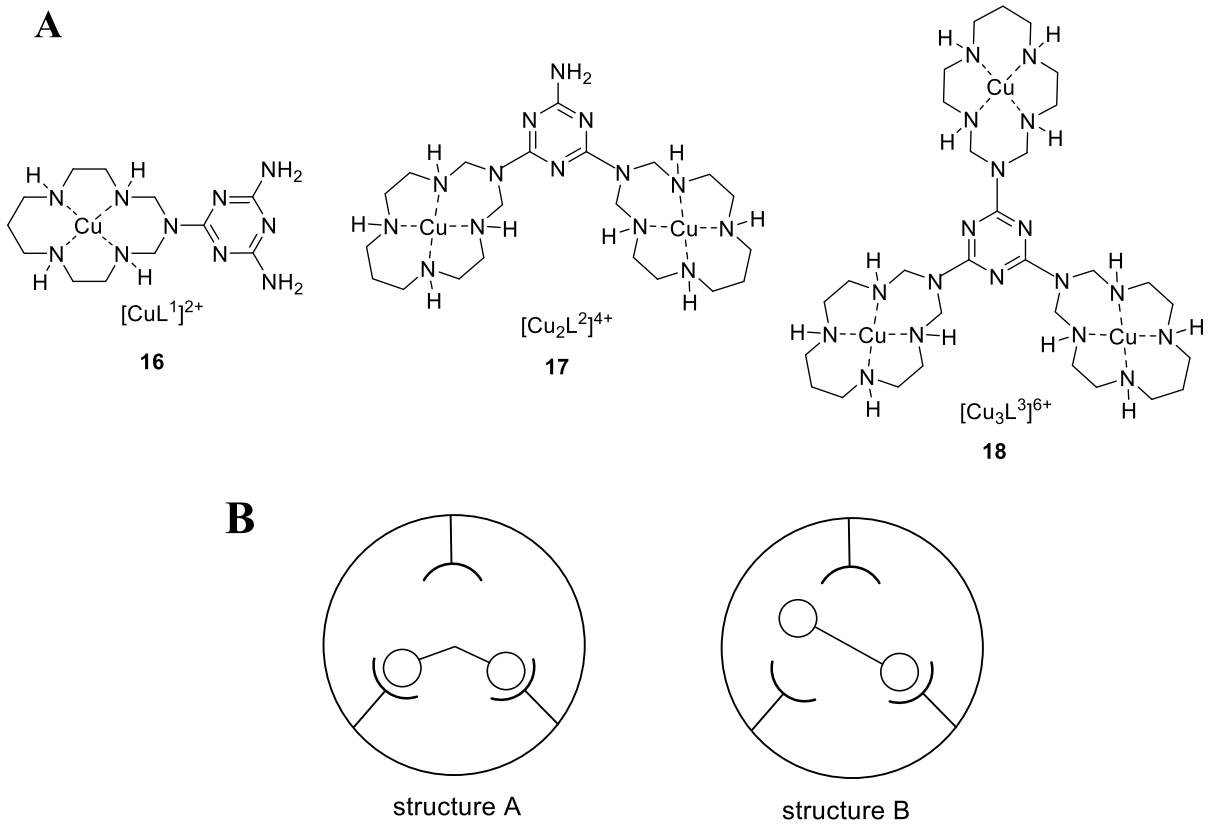

Figure 20. (A) Complexes $[CuL^1]^{2+}$ **16**, $[Cu_2L^2]^{4+}$ **17** and $[Cu_3L^3]^{6+}$ **18**; (B) schematic representation of the interaction of receptor **18** with isophthalate (structure A) and terephthalate (structure B).

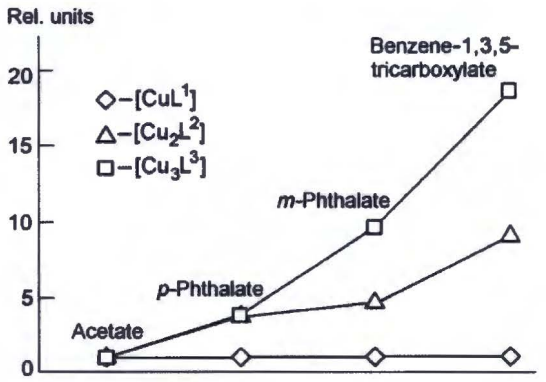

Figure 21. Diagrammatic representation of the results from UV-Vis study of the interaction of receptors **16-18** with carboxylates. Reprinted with permission from the Springer Nature. Copyright 2001.[16]

Further investigations of dicarboxylates binding were undertaken by Baruah using 1-phenyl-3-(quinolin-5-yl)urea **19** (Figure 22).[17] X-ray crystallographic investigations showed that this receptor selectively discriminates phthalic acid and terephthalic acid. Phthalic acid established a yellow colored salt with receptor **19**, whereas terephthalic acid formed a colorless co-crystal. The interaction with phthalic acid resulted in the protonation of sensor **19**, while the reaction of terephthalic acid with host **19** led to the formation of co-crystal via hydrogen bond interaction.

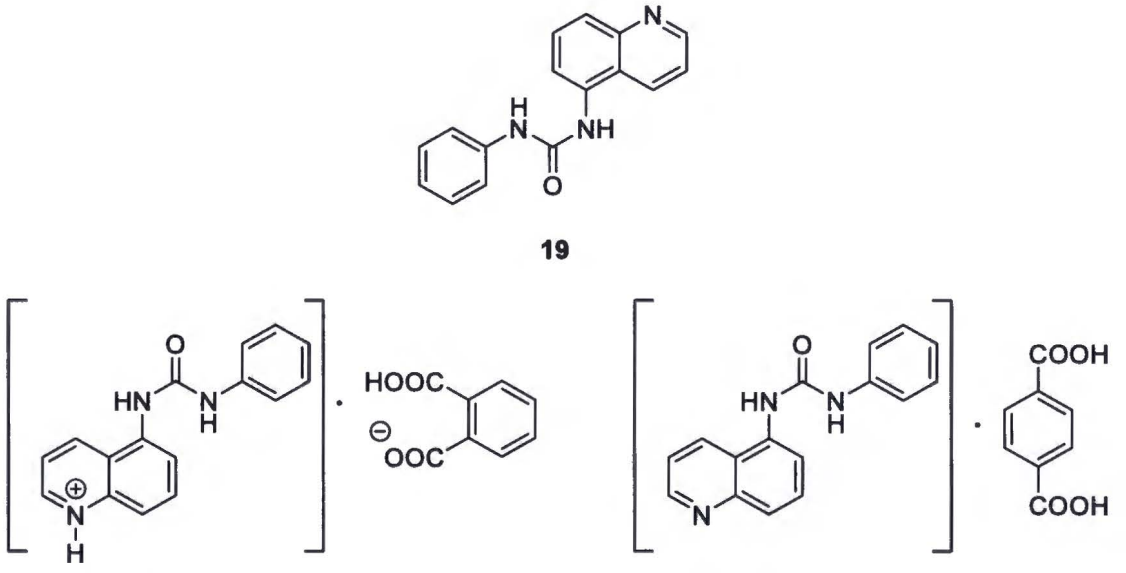

19

Figure 22. Urea derivative **19** and its complexes with phthalic and terephthalic acids.

Alvaro S. de Sousa and others investigated the binding properties of octadentate cyclen-based europium complex **20** with phthalate (Figure 23).[18] This complex exhibits fluxional ligand denticity upon phthalate recognition. The formation of a ternary phthalate complex was studied by observing the emission spectra at different pH (Figure 24). Abnormally high values of hydration states were observed for an octadentate europium(III) complex below the physiological pH. At a lower pH, the heptadenticity of the ligand was supported by the hydration states upon formation of an outer-sphere $[Eu(CyD3MA)(H_2O)_2]^{3+}$phthalate^{2-} ternary complex. At a higher pH, the deprotonation of the coordinated water took place, leading to a weaker electrostatic attraction in the ternary $[Eu(CyD3MA)(H_2O)OH]^{2+}$phthalate^{2-} complex, proved by a drop in intensity for all Eu(III) emission bands (Off-state).

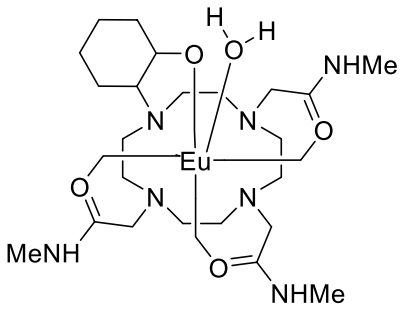

$[Eu(CyD3MA)(H_2O)]^{3+}$

20

Figure 23. Cyclen-based europium(III) complex **20**.

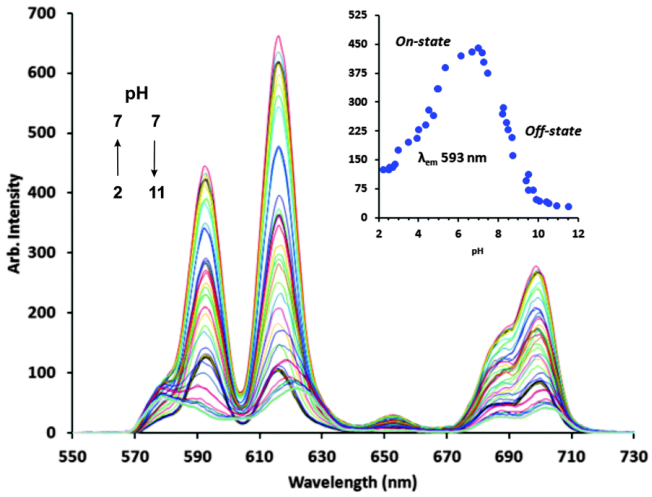

Figure 24. pH dependent emission spectra of europium(III) complex. Insert: pH dependent emission modulation of the $^5D_0$-$^7F_1$ transition.

The study of anion binding is traditionally performed in solution.[62-65] In such a situation, the host often experiences conformational freedom affording complexes with various guests. However, in most cases, a good selectivity is achieved upon crystallization.[66-68] Using mechanochemistry in this context helps to achieve selective recognition under solvent-free conditions.[69] Mechanochemistry has been utilized for solid-state differentiation of enantiomers,[70] supramolecular metathesis reactions,[71] etc.

For example, Užarević and coworkers examined the binding of polyamine host **21 (L)** with phthalic acid isomers (Figure 25).[19] They concentrated on the discrimination and separation of phthalates in either solvent-free conditions or by crystallization from solution. By forming various hydrogen-bonded frameworks, flexible polyamine sensor **21 (L)** is able to distinguish between three isomers of phthalic acid. Phthalic acid easily produced a complex HL·phthalic acid, from MeOH solution and by grinding. Isophthalic acid and terephthalic acid provided novel supramolecular complexes, HL·isophthalic acid and $(HL)_2$·terephthalic acid.

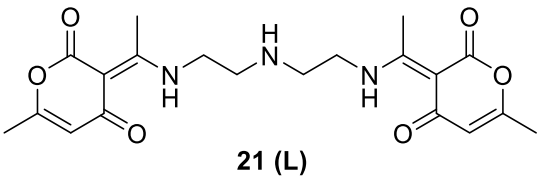

21 (L)

Figure 25. Polyamine receptor **21 (L)**. The host binds phthalic acids by the protonation of the central amino group.

Arar and others[20] demonstrated selective removal of phthalic acid and isophthalic acid from aqueous solution by using anion exchange resin (Figure 26). Absorption behaviour of phthalic and isophthalic acids was studied by changing several parameters: resin dose (g/mL), pH of the solution and temperature. For this, an extremely basic anion exchange resin (AS510GC resin) was used. The experimental results illustrated that isophthalic acid sorption on the resin is endothermic whereas phthalic acid sorption is exothermic. The most efficient sorption for phthalic acid has been shown to be in 2.0 N HCl, whereas for isophthalic acid it is in 2.0 M NaCl solution.

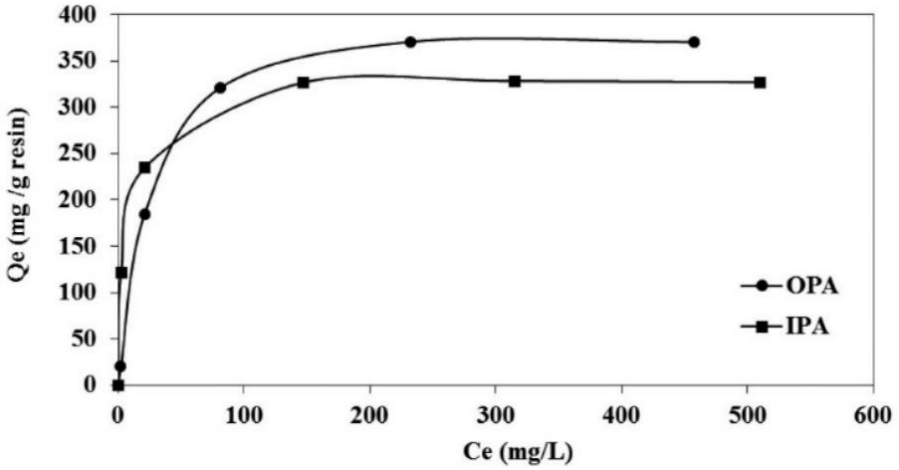

Figure 26. Sorption isotherm of phthalic acid (OPA) and isophthalic acid (IPA).

Sun and Wang reported 18-crown ether-6 (18C6) and 18C6/K^+ complexes to recognize and identify phthalic acids using ^{1}H DOSY (diffusion-ordered spectroscopy) (Figure 27).[21] Firstly, they attempted to explore 18C6 for the discrimination of positional isomers. The result clearly showed that the signals of all three phthalic acid isomers had comparable diffusion values and could not be distinguished on the diffusion dimension (Figure 27a). However, the addition of K^+ changed 18C6 from an organic cation receptor to an organic anion receptor. In alkaline environment, the presence of 18C6/K^+ complex led to a considerable drop in the diffusion coefficient for terephthalate and isophthalate. However, the highest drop was observed for phthalate (Figure 27b). This is because the carboxyl groups in terephthalate have the strongest interaction with 18C6/K^+, whereas phthalate interacts the weakest due to steric constraints.

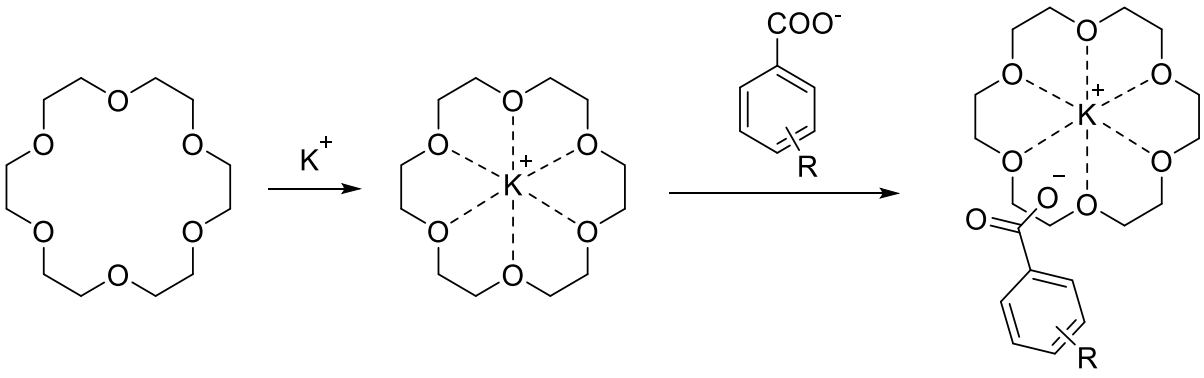

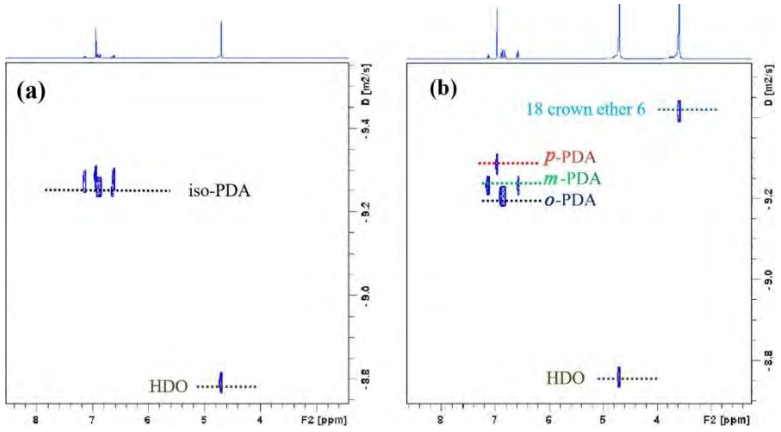

Figure 27. Schematic representation of the 18C6 and 18C6/K^+ complex in the presence of deprotonated carboxyl groups; (a) ^{1}H DOSY spectra of the mixture of phthalates with 18C6; (b) ^{1}H DOSY spectra of the mixture of phthalates with 18C6/K^+. Adapted with permission from the Elsevier. Copyright 2022.[21]

Positively charged pillar[6]pyridinium macrocycle **22** was tested in our group for its affinity to aromatic carboxylic acids (Figure 28).[22] Depending on the number of carboxylic groups as well as localization of electric charge, pillar[6]pyridinium bound guests inside or outside of the cavity. High molecular symmetry carboxylic acids, 1,3,5-tricarboxylic acid and 1,2,3,4,5,6-hexacarboxylic acid formed *endo* complexes with macrocycle **22**, while the other (phthalates) gave *exo* complexes. Guests that bound externally to the receptor showed lower binding affinities.

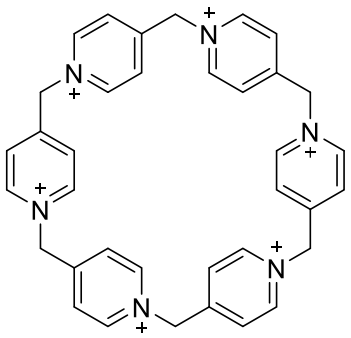

22

Figure 28. Positively charged pillar[6]pyridinium macrocycle **22**.

Glucosylcalix[4]arene derivatives **23-25** (**1-3**) developed by Castani and coauthors[23] were explored to bind phthalic acid isomers (Figure 29). They used negative ion ESI-FTICR mass

spectrometry method that enables quick analysis of noncovalent complexes formation. Glucosylcalixarenes **23-25** formed 1:1 complexes with isophthalic and terephthalic acids but did not form any complex with phthalic acid. Obviously, the position of carboxylic group has a significant impact on how selective the complexation is. Diglucosylcalixarene **23** formed the strongest complex with isophthalic acid over other isomers. On the other hand, receptors **24** and **25** had a stronger preference for isophthalic acid and terephthalic acid. The structural rigidity of **24** resulted in a higher selectivity toward terephthalic acid isomers in comparison to more flexible derivative **25**.

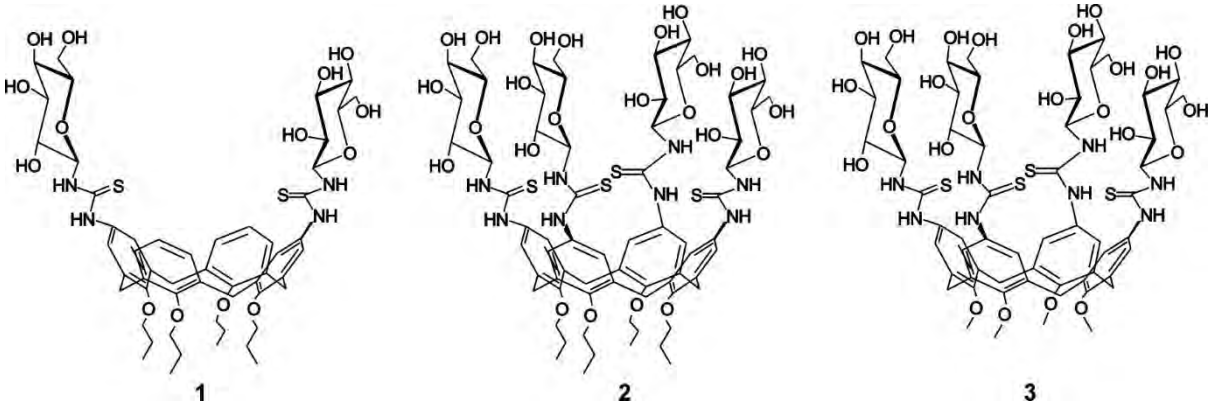

Figure 29. Tetrapropoxy diglucosylcalix[4]arene (**23** (**1**)), tetrapropoxy tetraglucosylcalix[4]arene (**24** (**2**)) and tetramethoxy tetraglucosylcalix[4]arene (**25** (**3**)). Adapted with permission from the John Wiley and Sons. Copyright 2011.[23]

1.2 Discrimination of dicarboxylic acid homologs

Dicarboxylic aliphatic acids are organic compounds with the general formula HOOC-$(CH_2)_n$-COOH. These diacids are ubiquitous on Earth. For instance, sebacic acid (C10) has a variety of uses as a component of candles, lubricants, diffusion pump oils, plasticizers, etc. It is also used in the synthesis of polyamides, like nylon. Oxalic acid (C2) acts as a reducing agent for metal oxides to remove tarnish and rust. It is also used as a bleaching agent for wood or for rinsing laundry. In addition to industrial applications, dicarboxylic aliphatic acids are involved in many biochemical processes such as energy production and storage (oxalic and malonic

(C3)), amino acid synthesis (glutaric (C5) and pimelic (C7)), regulation of cellular function (succinic (C4)).

The omnipresence of these acids may cause inflammation and metabolic disorders such as kidney and joint stones or glutaric aciduria. Therefore, their detection and recognition are of a great importance for public health and environmental protection.

The methods developed so far allowed often the recognition of only selected diacids and, in most cases, they require specialized equipment.[72-99]

1.2.1 Colorimetric discrimination of dicarboxylic acid homologs

Like phthalic acids, dicarboxylic aliphatic acids are also dibasic acids with two pKa values (pKa1, ranging from 1.25 (C2) to 4.55 (C9), and pKa2, ranging from 4.14 (C2) to 5.5 (C9)), therefore, they are present mainly in the anionic form at pH close to neutral, and anion receptors are used to recognize them.

The aforementioned report by Ahn et al. (pages 6,7) describes also the use of the functionalized AuNPs sol **8** in the discrimination of succinic (C4) and glutaric (C5) acids (Figure 30). UV-Vis analysis revealed a small decrease in the intensity of the surface plasmon resonance (SPR) band, but no apparent color changes were observed for any of the analytes even at increased concentrations. Due to the conformational flexibility of C4 and C5, intraparticle cross-linking between two carboxylate groups and the trifluoroacetyl binding sites in the same nanoparticle occurred.

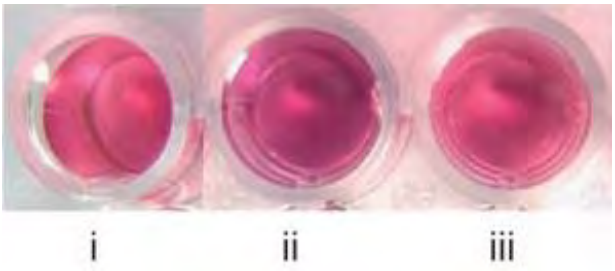

Figure 30. Colorimetric assay with aqueous solution of **8** i) without analyte; ii) in the presence of succinate (C4) and iii) in the presence of glutarate (C5) as a sodium salt. Adapted with permission from the John Wiley and Sons. Copyright 2008.[7]

Modification of gold nanoparticles **8** by Ahn et al. resulted in a new AuNPs sensor **26** (Figure 32).[72] Gold sol **26** recognized oxalate (C2) over malonate (C3), succinate (C4) and glutarate (C5) (Figure 31). The aggregation of gold nanoparticles was caused by interparticle cross-linking.

Figure 31. Color change of AuNPs **26** upon addition of analyte. From left to right: fumarate, maleate, oxalate (C2), malonate (C3), succinate (C4), glutarate (C5), propionate and 4-pentenoate. Adapted with permission from the Elsevier. Copyright 2008.[72]

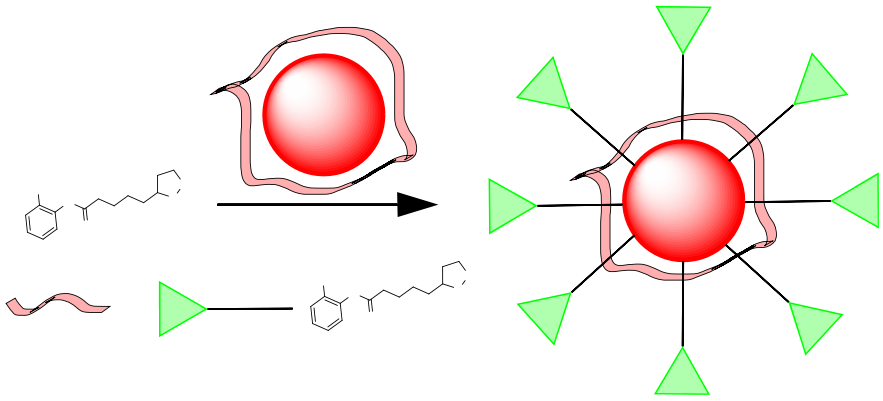

Figure 32. Synthesis of functionalized AuNPs **26**.

Gold nanoparticles, with thiourea arms, **27** have been tested for the recognition of dicarboxylic acid homologs (Figure 33).[73] UV-Vis experiments were carried out to detect dicarboxylates. However, a color change (from red to blue) of gold nanoparticles (GNP1) was observed only with succinate (C4) (Figure 34).

The appearance of a new surface plasmon peak at 615 nm was responsible for the color change. For other diacids, only minor bathochromic shifts in the SPR band were observed. The reason may be the propensity of the thiourea ligand to create bridging interparticle interactions via hydrogen bonds with C4.

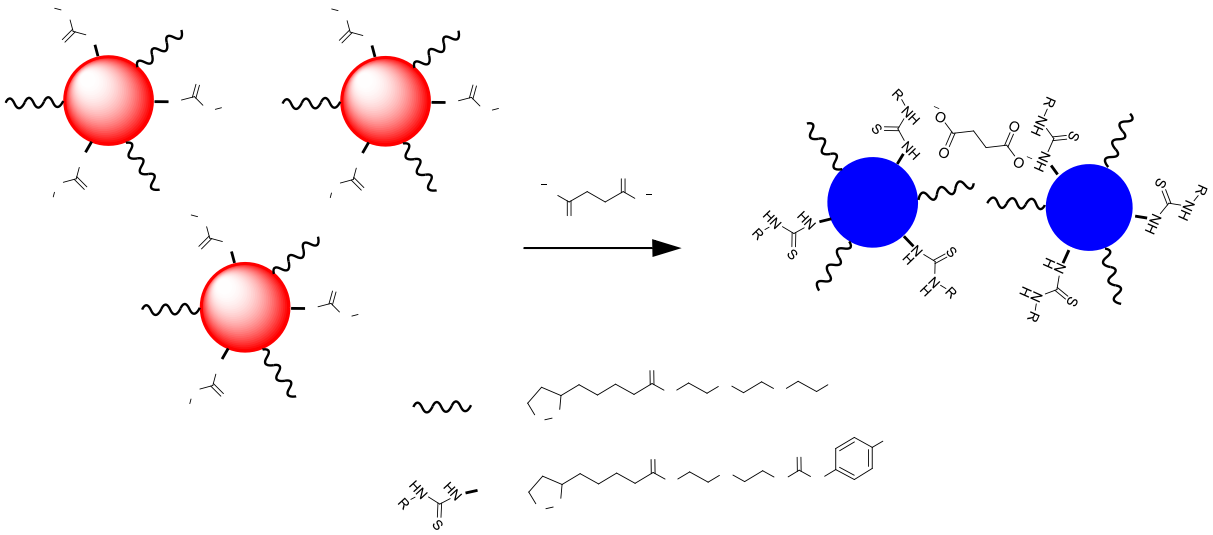

Figure 33. Complexation of succinate (C4) with thiourea group of functionalized GNP1s **27** induces aggregation, and, hence, the color change.

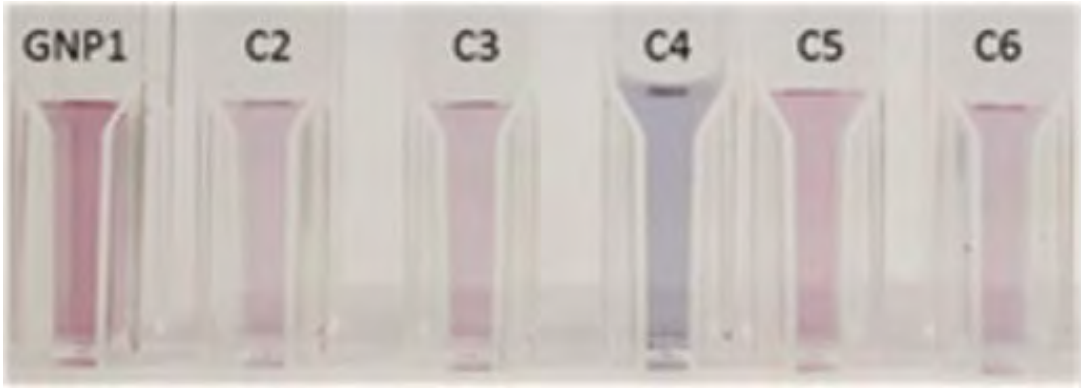

Figure 34. Colors of gold nanoparticles **27** solutions before and after the additions of excess of dicarboxylates C2-C6. Reprinted with permission from the John Wiley and Sons. Copyright 2016.[73]

Jiahui and colleagues synthesized functionalized gold nanoparticles **28** and **29** (Figure 35).[74] The behaviour of these AuNPs in the presence of aliphatic dicarboxylates was investigated in DMSO solution.

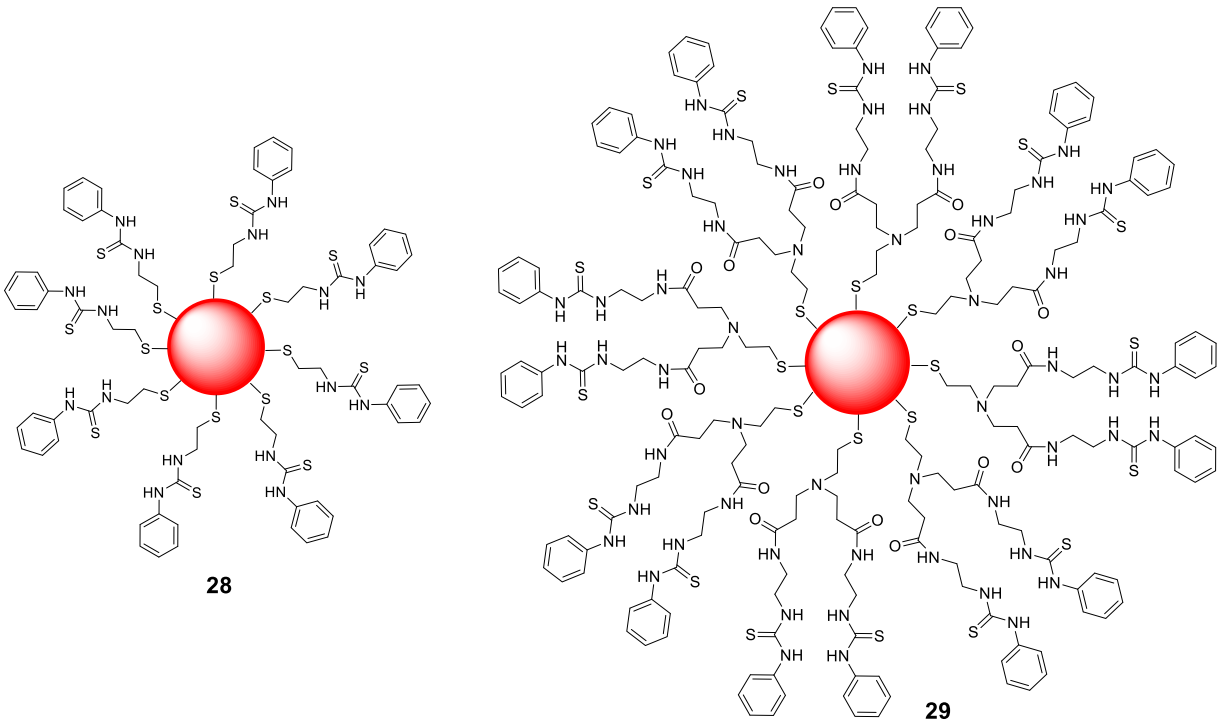

Figure 35. Gold nanoparticles-based receptors **28** and **29**.

Significant changes in UV-Vis spectra of **29** were observed in the presence of malonate (C3), succinate (C4), glutarate (C5) and pimelate (C7). This was attributed to the interaction of gold nanoparticles with dicarboxylates rather than to a change in the ionic strength or permittivity around the nanoparticle surface. An increase in the plasmon band intensity was possible due to the conformational changes of the immobilized ligands.

On the other hand, the nanoparticles **28** covered with less flexible ligands did not exhibit any significant changes in the presence of the same dicarboxylates.

1.2.2 Fluorescent discrimination of dicarboxylic acid homologs

Gunnlaugsson group synthesized a fluorescent sensor **30** for the recognition of malonic (C3) and glutaric (C5) acids (Figure 36).[75] Titration with the salts of these acids led to the quenching of its emission.

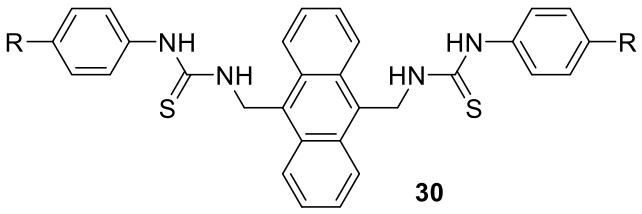

Figure 36. PET anion chemosensor **30**.

The emission spectra of **30** were "switched off" by 70% for C5, and 86% for C3 because of the alteration of the electron transfer rate, making the standard free energy change (ΔG_{ET}) more negative.

Chemical modification of receptor **30** gave new chemosensors **31-33** (Figure 37).[76] Similarly to chemosensor **30**, the fluorescence quenching of **31-33** was observed in the presence of malonate (C3) and glutarate (C5). However, in this case different stoichiometries were observed depending on the length of the diacid and the nature of the receptor. C3 interacted with **31** and **32** equimolarly, while C5 exhibited a 1:2 binding mode. However, for the urea-based sensor **33** for both diacids the binding ratio was 1:1.

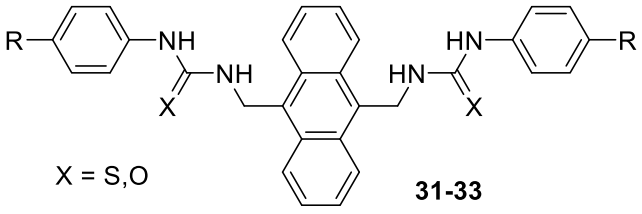

Figure 37. PET anion chemosensor **31-33**.

Furthermore, triphenylamine-based **34** has been studied as a fluorogenic receptor for aliphatic dicarboxylates of different chain lengths (Figure 38).[77] In acetonitrile solution, receptor **34** selectively recognized only suberate guest (C8), while in DMSO, a color change was also noticeable in the presence of malonate (C3). The observed behaviour is due to the adaptation of the binding sites of the receptor to the above two diacids. Interestingly, the interactions can be observed not only fluorescently but also colorimetrically.

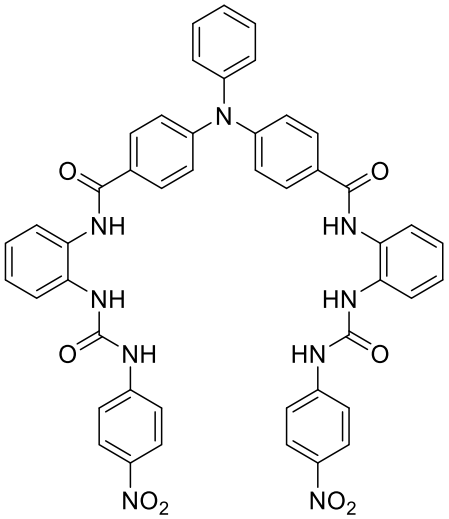

34

Figure 38. Triphenylamine-based chemosensor **34**.

With an excess of C3, the color of solution changed from bright yellow to deep yellow and finally to red (Figure 39).

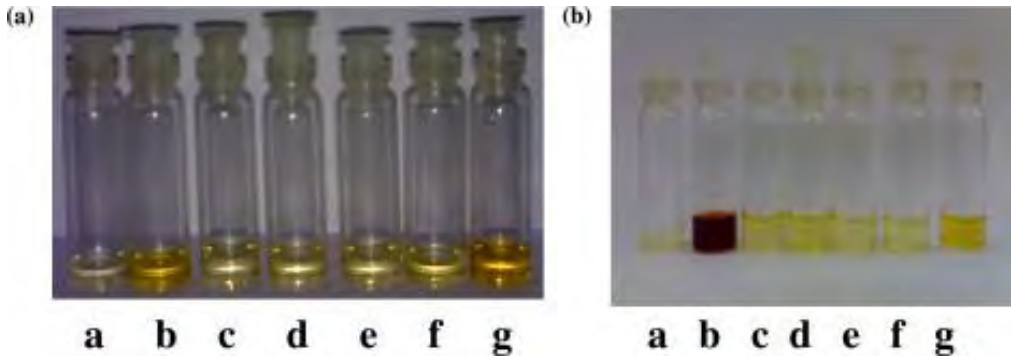

Figure 39. Color of **34** solutions in the presence of 1 equiv. (**a**) and 4 equiv. (**b**) of: a: receptor **34**, b: with malonate (C3), c: with succinate (C4), d: with glutarate (C5), e: with adipate (C6), f: with pimelate (C7) and g: with suberate (C8). Reprinted with permission from the Elsevier. Copyright 2010.[77]

Costero et al. reported a fluorescent bis(calix[4]pyrrole)-substituted BODIPY ditopic receptor **35** for linear aliphatic dicarboxylates (Figure 40).[78] The coordination of diacids to the receptor **35** was manifested by changes in UV-Vis spectra and strong quenching of the fluorescence emission. Receptor **35** formed a 1:1 complex with all dicarboxylic aliphatic acids (C2, C5, C7-C12). Interestingly, the strongest binding constant was observed for sebacic

dianion (C10, n=8). This was likely due to the formation of a cyclic 1:1 complex with terminal carboxylate groups of the guest dianion interacting with calixpyrrole units of **35**. For other acids, the formation of such complexes was less likely.

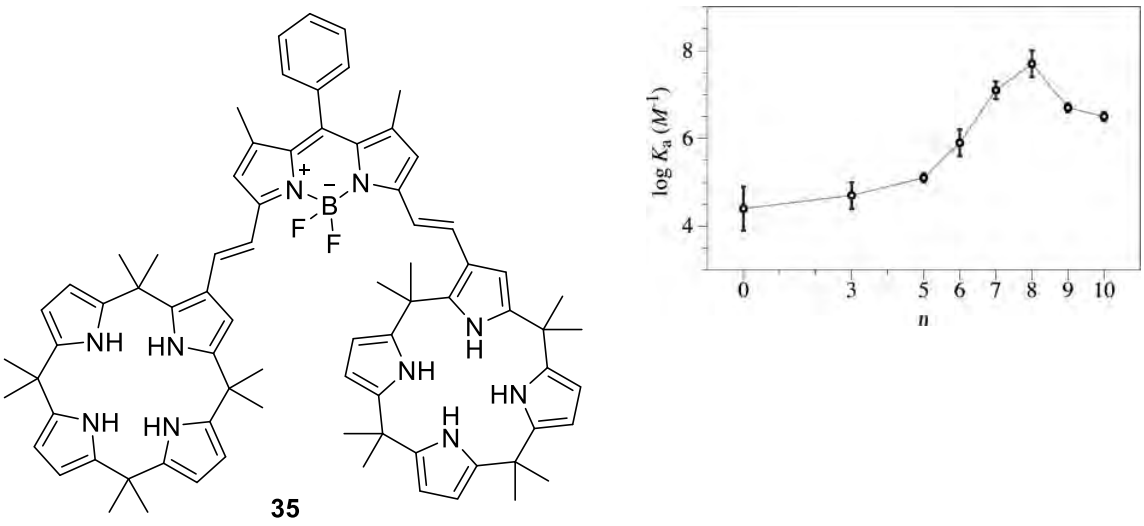

Figure 40. Bis(calix[4]pyrrole)-substituted BODIPY ditopic receptor **35** and associated constants for the 1:1 complexes between **35** and several aliphatic dicarboxylates. Adapted with permission from the John Wiley and Sons. Copyright 2013.[78]

The rigid carbazole-based dicarboxylate receptor **36** was reported by Curiel and coworkers in 2016 (Figure 41).[79] This sensor selectively recognized glutarate (C5) over succinate (C4) and adipate (C6) in DMSO by forming a 1:1 complex. C5 had a good geometric match with receptor **36**, and, therefore, a larger binding constant than C4 and C6.

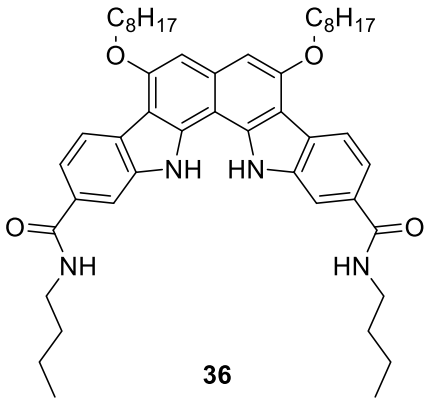

Figure 41. Fluorescence chemosensor **36**.

Miljanic et al. demonstrated that trigonal fluorinated trispyrazole **9** (pages 7,8) in addition to phthalic acids can also discriminate aliphatic dicarboxylic acids.[8] The intensity of the emission of **9** combined with oxalic (C2), malonic (C3), and succinic (C4) acids decreased as the distance between carboxylic groups increased.

Anzenbacher investigated dicarboxylates binding to a series of calixpyrrole sensors **37-41** (Figure 42).[80]

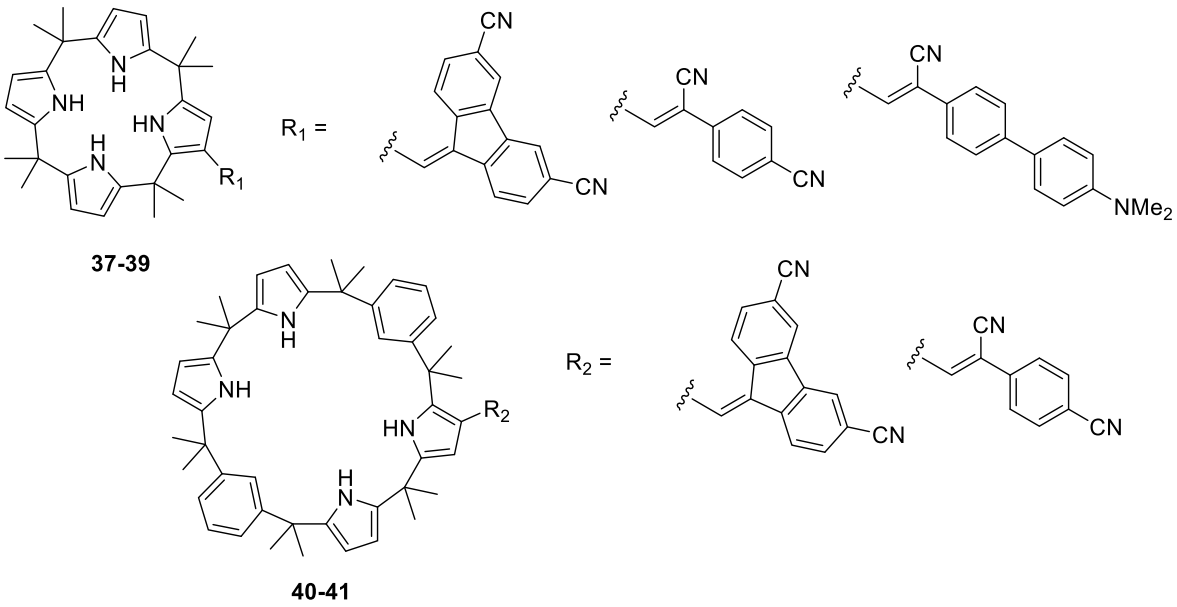

Figure 42. Structures of corresponding fluorescent sensors **37-41**.

These sensors differing by the size of the macrocyclic ring and fluorophore were utilized in a microchip fluorescence-based array. The studies revealed perfect classification of 18 analytes based on only five sensors. With an inaccuracy of less than 2%, quantitative assessments of aqueous solutions of oxalate (C2), malonate (C3), glutamate (C5), and aspartate were shown.

Receptor **10** reported by Sessler[9] and coworkers in 2019 (pages 9,10) was also able to discriminate aliphatic dicarboxylic acids (Figure 43). The longest aliphatic diacid (C12) in acetonitrile caused no changes in fluorescence intensity. However, when the distance between two carboxylic groups decreased, the emission wavelengths underwent hypsochromic shifts resulting in color change. Notably, the sensor was responsive to dicarboxylates and unresponsive to monocarboxylates. Moreover, the quantification of dicarboxylate anions was made possible due to the ratiometric response.

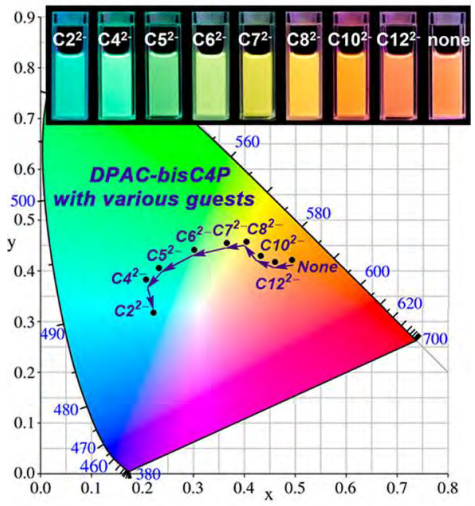

Figure 43. Chromaticity coordinates of **DPAC-bisC4P 10** in the presence of aliphatic dicarboxylic acids. Inset: fluorescence images of the same ensembles upon irradiation (UV). Reprinted with permission from the American Chemical Society. Copyright 2019.[9]

Fluorescence sensing of dicarboxylates has been reported for macrocyclic copper(II) complex **42** (Figure 44).[81] The formation of a strong complex with oxalate (C2) was evidenced in aqueous solution at neutral pH. Sensor **42** also showed high selectivity towards C2 in the presence of other dicarboxylic aliphatic acids by using fluorescent indicator-displacement assays (IDA), with fluorescein and Eosin Y.

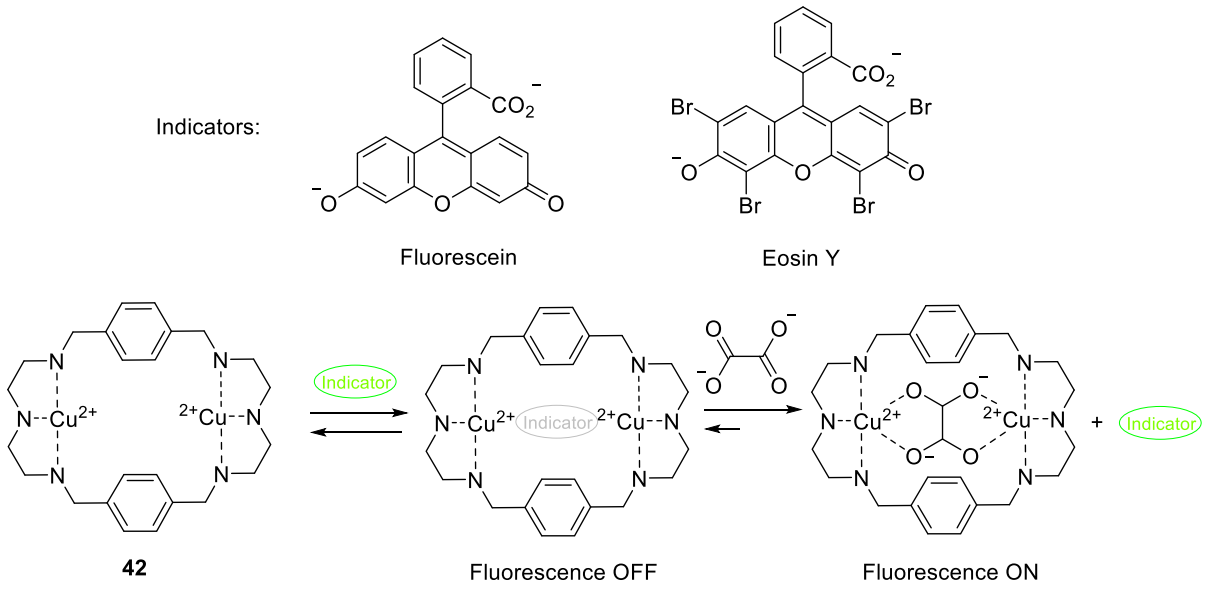

Figure 44. Macrocyclic copper(II) complex **42**, indicators and sensing of oxalate (C2).

The addition of one equivalent of complex **42** reduced emissions of both indicators practically completely, demonstrating the effective competitive binding of C2.

Nabeshima and coauthors reported metallomacrocycle **43** (Zn-hexapap) which was studied in dicarboxylate recognition (Figure 46).[82] ^{1}H NMR spectra revealed that only adipate (C6) and pimelate (C7) formed 2:2 complexes with Zn-hexapap resulting in wavy-stacked dimeric structures. This was also confirmed by a stronger red emission in fluorescence spectra (Figure 45). For other C3-C12 diacids, more sophisticated complexes were observed.

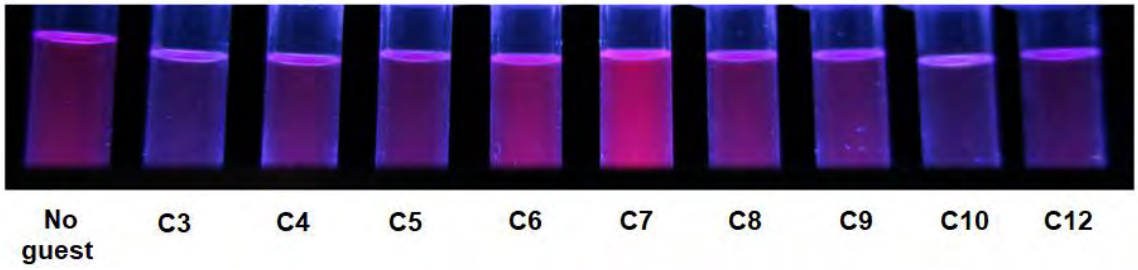

Figure 45. Photographs of Zn-hexapap **43** solutions upon binding of aliphatic dicarboxylic acids under UV irradiation.

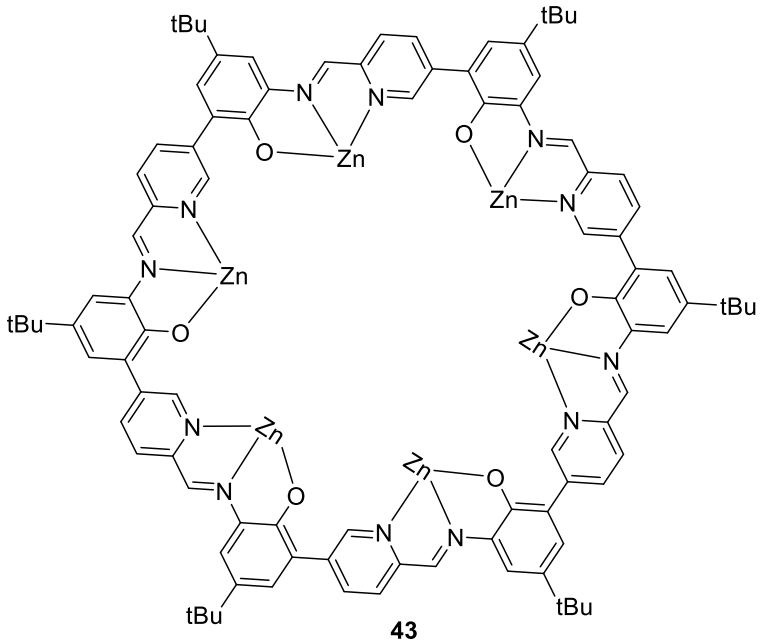

Figure 46. Chemical structure of metallomacrocycle, Zn-hexapap **43**.

1.2.3 Other methods for discrimination of dicarboxylic acid homologs

Delgado et al. developed ditopic polyamine macrobicyclic receptor **44** for the recognition of dicarboxylates when complexed with copper(II) (Figure 47).[83] The association constants with succinate (C4), glutarate (C5), adipate (C6) and pimelate (C7) were also determined by potentiometry.

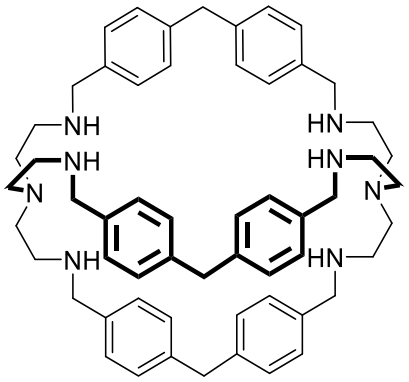

44

Figure 47. Structure of polyamine cryptand receptor **44**.

The binding affinities increased with the increase in chain length and reached its maximum for C6. The extraordinarily large binding constants suggested that all dicarboxylates were bound in a bridging mode.

The triazine derivative **45** has found application in the recognition of aliphatic dicarboxylic acids (Figure 48).[84] Its co-crystallization with various diacids (C2-C6) gave two types of host-guest assemblies. In three-dimensional arrangement, complexes have voids or channels. This dissimilarity came from differences in the acidity of the diacids. At $pK_a<3.0$, various host networks consisting of **45** and the corresponding aliphatic dicarboxylic acids with water and other solvents were observed, however, at $pK_a>3.0$ only a neat **45** was detected.

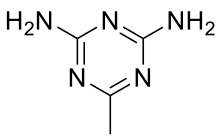

45

Figure 48. Structure of 2,4-diamino-6-methyl-1,3,5-triazine **45**.

Biswas and coworkers prepared compound **46**, a derivative of **45**, that was probed in the recognition of aliphatic dicarboxylic acids (Figure 49).[85] Various supramolecular assemblies with C2 (**a**), C3 (**b**), C4 (**c**), C5 (**d**) and C6 (**e**) acids have been identified.

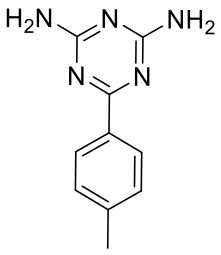

46

Figure 49. Structure of 2,4-diamino-6-(4-methyl-phenyl)-1,3,5-triazine **46**.

Depending on the solvents and type of guests used in the crystallization process (CH_3OH or DMSO) anhydrous or methanol containing molecular adducts were obtained. Structure analysis revealed a 2:1 host:guest interaction mode in most cases, with the exception of **b** and **c**, likely due to the involvement of one of the carboxylic groups in the intermolecular hydrogen bonding. Moreover, carboxylic group of **a** exhibited interaction with receptor **46** via amino groups, while other diacids (**b-e**) interacted with hetero -N atoms.

The discrimination between aliphatic dicarboxylates has been described by Rybak-Akimova et al.[86] The group has investigated how dicarboxylates (C2-C7) bind to receptor **47** (Figure 50) depending on the length of their chain. Although the pK_a of all examined diacids was nearly the same (with the exception of C2), a strong correlation of the binding with the chain length was found.

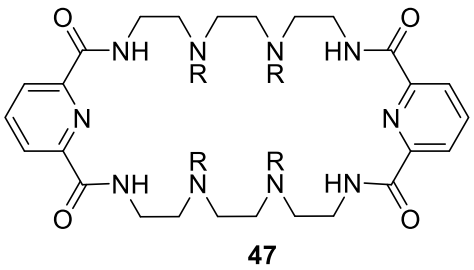

47

R = H, Me

Figure 50. Amino-based 30-membered receptor **47**.

The highest binding constant was observed for succinate (C4) with a four-carbon chain perfectly matching to the receptor cavity. Decreasing the number of hydrogen bonds in receptor **47** (R=Me instead of H) resulted in generally lower binding constants for all dicarboxylates.

Zonta and others[87] have utilized dynamic covalent chemistry (DCC) of molecular cages **48** (seven zinc(II) and eight copper(II) complexes) in the presence of aliphatic dicarboxylic acids (Figure 51). Selectivity profiles of sensors **48** towards diacids (C5-C14) were investigated by ESI-MS. The binding affinities of **48** were in strong correlation with the dicarboxylic acid alkyl chain length. Adipic (C6) and suberic (C8) acids were best fitted to the cages. For shorter and longer diacids, reduced binding affinities were observed.

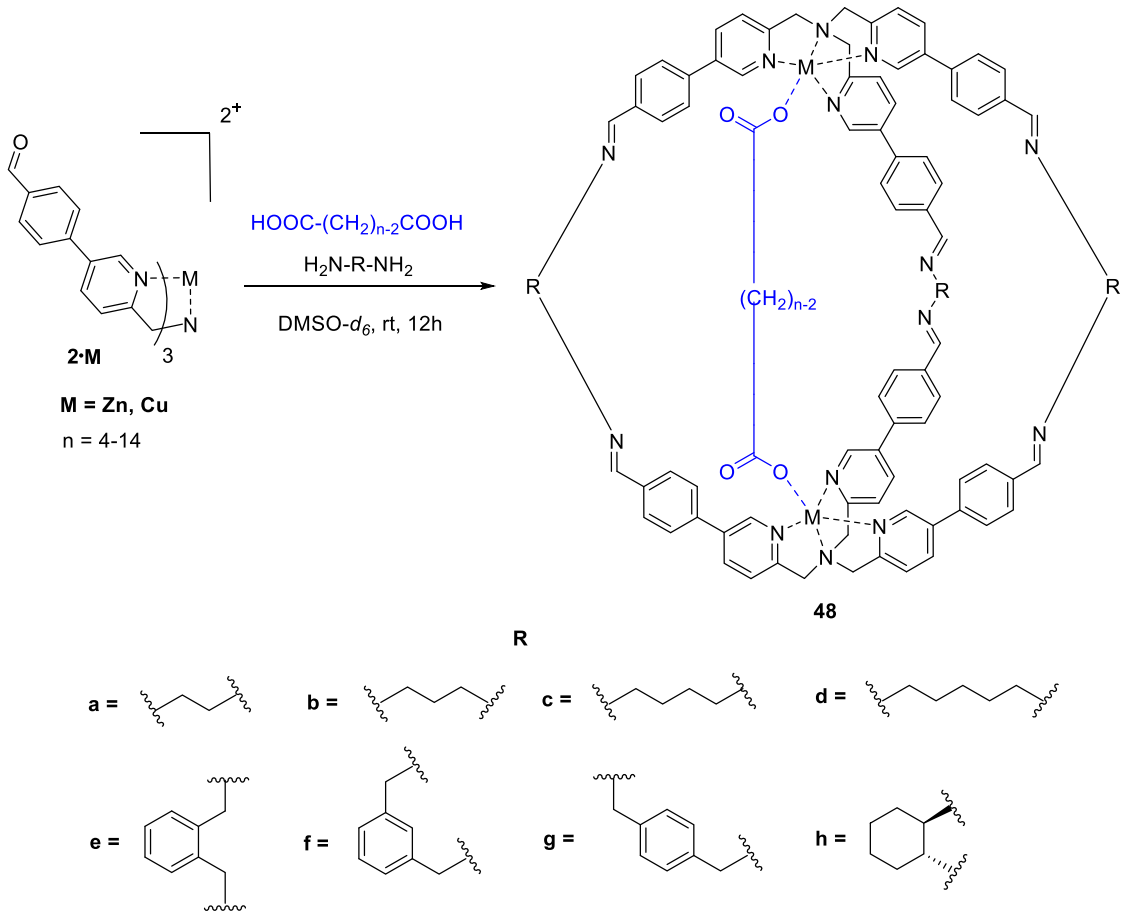

Figure 51. Binding of **48** with various aliphatic dicarboxylic acids (C5-C14).

Making chiral sensor **49** gave an opportunity to observe structural changes in the presence of dicarboxylic acids (C4-C10) by using Circular Dichroism (CD) spectroscopy (Figure 52).[88] For long dicarboxylic acids, the formation of cages with the chiral diamine unit substituents

twisted into an antiperiplanar arrangement was observed, while short acids were arranged in a gauche manner.

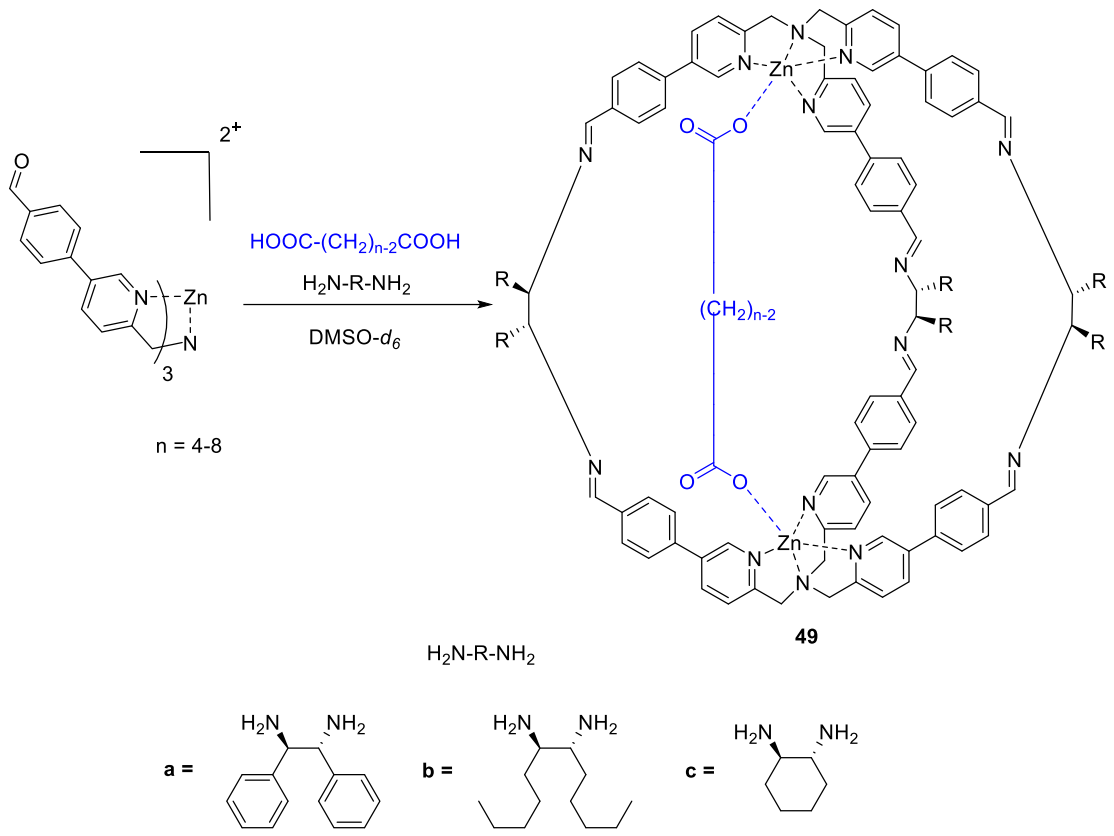

Figure 52. Binding of **49** with various aliphatic dicarboxylic acids (C4-C8).

He and coauthors developed two-armed neutral receptors **50** and **51** (Figure 53).[89] Calix[4]arenes **50** and **51** selectively recognize aliphatic dicarboxylates (C3-C6) over other anions (AcO^-, Cl^-, Br^-, I^-, $H_2PO_4^-$). The results showed a 1:1 stoichiometry between the hosts and anion guests due to multiple hydrogen interactions in DMSO solution. The addition of MeOH led to the disruption of hydrogen bond network and the destruction of the formed complexes. In all cases, receptors **50**, **51** displayed good selectivity, however, the binding affinity depended on the chain length of dicarboxylates, decreasing with the chain length increase: C6 > C5 > C4 >C3.

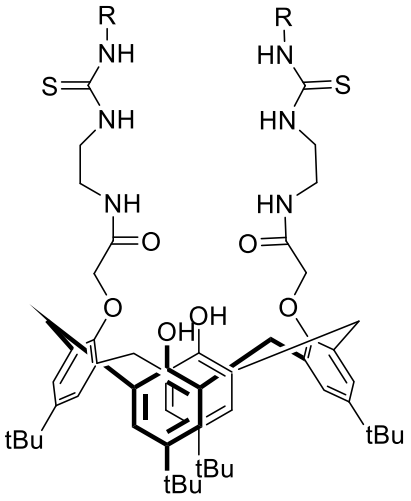

50 R = p-nitrophenyl
51 R = 1-naphthyl

Figure 53. Calix[4]arene-based receptors **50**, **51**.

A library of new p-tert-butylthiacalix[4]arenes **52-54** (**4-6**) was prepared to study the binding properties with dicarboxylates (Figure 54).[90] The effectiveness of the interaction with **52** dropped from oxalic (C2) to malonic (C3) to succinic (C4) acids. The association constant changed due to the increasing length and decreasing acidity of dicarboxylic acids. Macrocycles **53** and **54** showed a similar tendency. In all cases, UV-Vis spectroscopy disclosed the role of substituents in the binding.

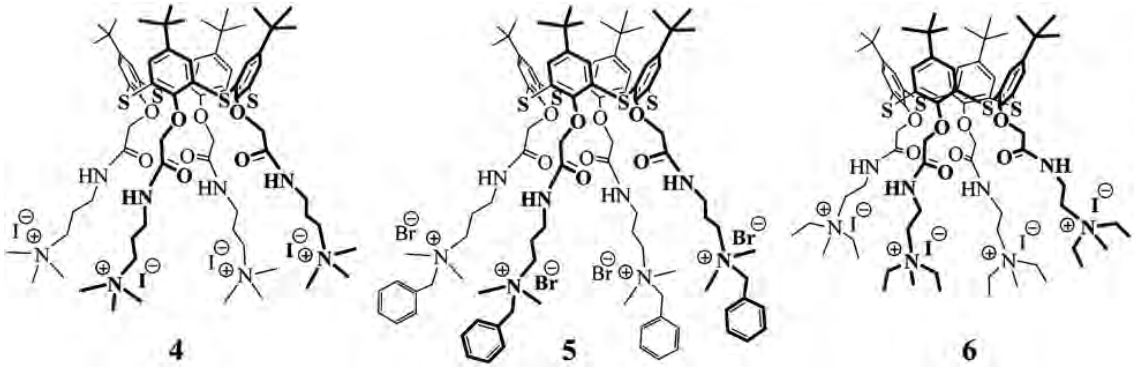

Figure 54. Structures of p-tert-butylthiacalix[4]arenes **52-54 (4-6)**. Adapted with permission from the Royal Society of Chemistry. Copyright 2014.[90]

"Texas-sized box" **55** (Figure 55) synthesised by Sessler and coworkers had been intensively studied as a dicarboxylate receptor.[91-96] It was found that small aromatic dicarboxylates

(monoprotonated 1,4-acid) formed a pseudorotaxane structure, while aliphatic dicarboxylates (C2-C10) bound outside the cavity of **55**. In most cases, the stoichiometry between host and guests was 1:1. Host-guest complex formation was pH-dependent and reversible: at a lower pH, the decomposition of the complexes was observed, while at a higher pH pseudorotaxane regeneration occurred.

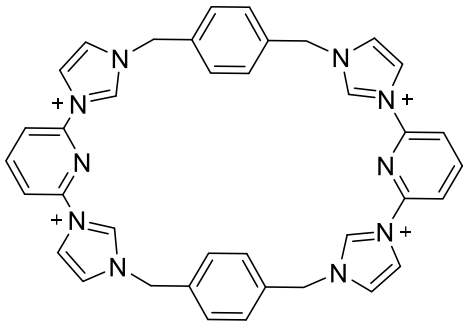

55

Figure 55. "Texas-sized box" macrocycle **55**.

Lu et al. investigated the recognition of aliphatic dicarboxylic acids (C3-C8) by a water-soluble pillar[6]arene dodecaamine **56** (Figure 56).[97] Their interactions produced deep inclusion complexes with a stoichiometry 1:1. Association constants K_{as} increased with an increasing chain length of the dicarboxylic acids. This is due to an increase in the number of methylene groups of the aliphatic chain, which leads to a stronger hydrophobic effect.

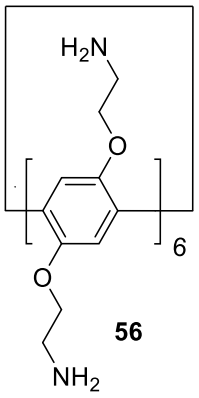

56

Figure 56. Water-soluble pillar[6]arene dodecaamine **56**.

Tetrathiourea macrocycles **57** and **58** (Figure 57) have also showed good efficiency in dicarboxylates sensing.[98] For **57** and **58** the largest affinity was observed for adipate (C6), and similar selectivity for other aliphatic dicarboxylates. In all cases, a 1:1 binding stoichiometry was found. Similar binding properties of receptors **57** and **58** were attributed to the flexibility and adaptability of their structures. With a dicarboxylate larger than C6, the binding strength decreased dramatically, because these anions were too large to fit into the macrocycle cavities. Double mutant cycle analysis (DMC) revealed negative cooperativity effects for malonate (C3), suberate (C8) and azelate (C9) and a strong positive cooperativity for adipate (C6).

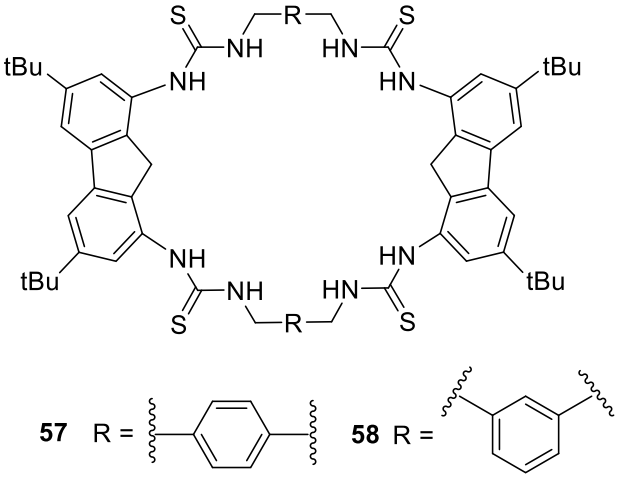

Figure 57. Carbazole tetrathiourea receptors **57**, **58**.

Receptor $[H_6Me_2[28]py_2N_6]^{6+}$ **59** reported by Delgado in 2004 was examined for the discrimination of aliphatic dicarboxylates (Figure 58).[99]

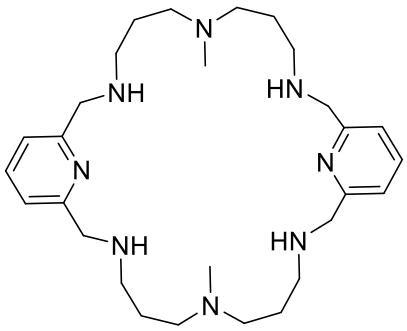

59

Figure 58. Structure of 28-membered octaazamacrocycle $Me_2[28]py_2N_6$ **59**.

A number of dicarboxylate anions (C2-C6) was assessed by ^{1}H NMR spectroscopy and single crystal X-ray crystallography. The ^{1}H NMR studies revealed that receptor **59** binds two carboxylic groups of dicarboxylic acids in each case. No particular selectivity was discovered; however, the largest association constant was determined for C6.

1.3 Discrimination of dicarboxylic acid geometric isomers

Geometric isomers, containing either double bonds or else ring structures that prevent functional groups from freely rotating around a chemical bond are important chemical substances for many fields. Among them butendioic acid is arguably one of the most well-known compounds, the *trans* form of which (fumaric acid) is an intermediate in Krebs cycle, while the *cis* isomer (maleic acid) is an important chemical commodity. Other noted geometrical isomers are azobenzene-4,4'-dicarboxylic acid (ADA) and stilbene-4,4'-dicarboxylic acid (SBDA) which can regulate mechanical properties of thin films,[100] macroscale motion of MOFs,[101] molecular self-assembly,[102,103] enzyme-like catalysis,[104] drug delivery and release.[105]

Despite the fundamental importance and broad application of these acids, their recognition remains challenging and greatly unexplored. Although, several reports on detecting butendioic acid are known,[106-112] the general strategy for the detection of E/Z dicarboxylic acids (Figure 59) has not yet been developed.

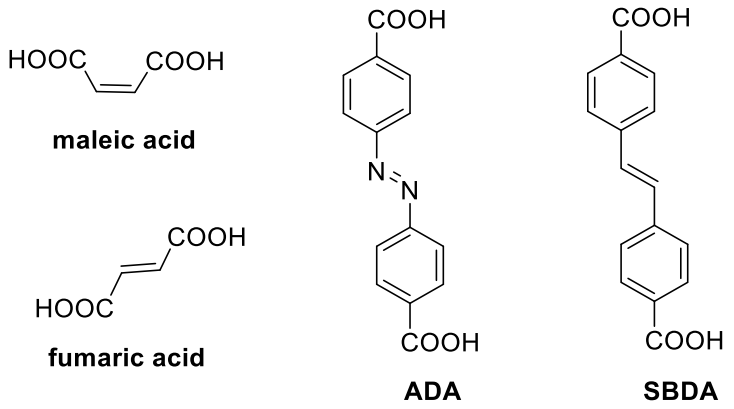

Figure 59. Structures of E/Z-diacids.

1.3.1 Colorimetric discrimination of geometric isomers of diacids

In this approach, the sensors are built in such a way that they can colorimetrically identify only one particular isomer.[113-118] An appropriate chromophore is attached to a specific anion receptor to selectively discriminate the chosen diacid (in most cases).[119]

The receptors **1-3** (pages 3,4) and **4-6** (pages 4,5) synthesised by Yen et al.[5,6] were also examined in the discrimination of E/Z-diacids. When maleate and fumarate were added to receptor **1** in DMSO/H_2O (80:20), the color change from blue to green was observed for maleate, and no color change was visible for fumarate (Figure 60). This indicated the formation of a complex with maleate through hydrogen bonding. Similar studies were conducted using sensor **2**. The solution only changed color in the presence of maleate, changing from blue to pink (Figure 61). The addition of these isomers to the solution of receptor **3** did not give rise to any color change.

Figure 60. Photographs of the solutions: (a) **1**; (b) **1**+maleate; (c) **1**+fumarate. Adapted with permission from the Elsevier. Copyright 2006.[5]

Figure 61. Photographs of the solutions: (a) **2**; (b) **2**+maleate; (c) **2**+fumarate. Adapted with permission from the Elsevier. Copyright 2006.[5]

The interaction of receptor **4** with maleate in DMSO led to change in the color of the solution from dark-blue to dark-red. Other receptors also changed color in the presence of maleate, from blue to violet in case of the receptor **5**, and from blue-green to purple in the presence of **6** (Figure 62). The addition of fumarate led to a color change only in the case of sensor **4**. Besides, it was shown that the efficiency of the receptors is strongly dependent on the substituent. The highest binding affinity for the maleate anion was observed in the case of using the strongest electron-withdrawing group.

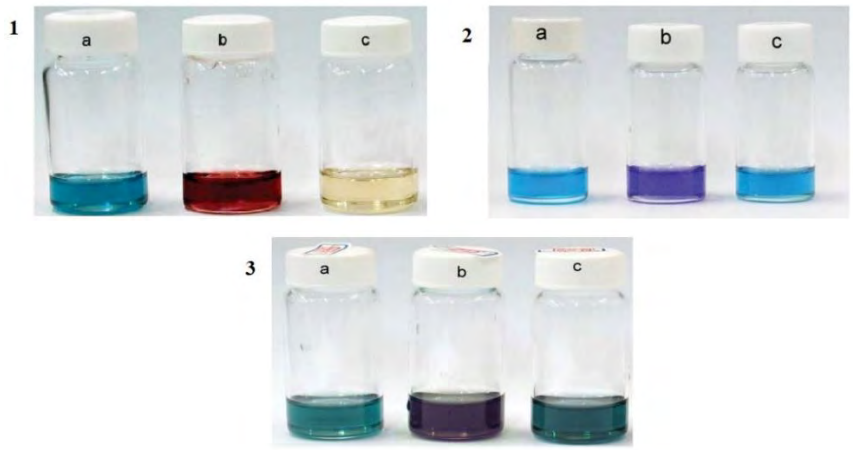

Figure 62. Photographs of the solutions: **1**: (a) **4**; (b) **4**+maleate; (c) **4**+fumarate; **2**: (a) **5**; (b) **5**+maleate; (c) **5**+fumarate; **3**: (a) **6**; (b) **6**+maleate; (c) **6**+fumarate. Adapted with permission from the Royal Society of Chemistry. Copyright 2007.[6]

Sensor **8** (pages 6,7) was also used for the discrimination of maleate and fumarate. The modified gold nanoparticles selectively sensed fumarate over maleate due to the geometric match of the former (Figure 63). A color change from red to purple was due to the shift toward longer wavelength and broadening of the plasmon band.

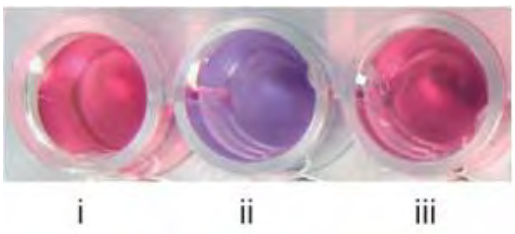

Figure 63. Effect of phthalate anions on color changes of **8**: i) without analyte and with ii) fumarate, iii) maleate. Adapted with permission from the John Wiley and Sons. Copyright 2008.[7]

In 2009, Yen et al. continued work on the discrimination of geometric isomers. They synthesised a new receptor **60** that selectively discriminates maleate anion (Figure 64).[106]

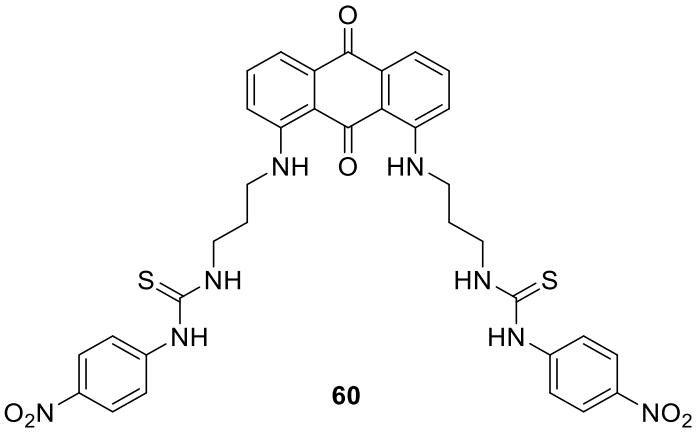

60

Figure 64. Colorimetric receptors **60**.

A 1:1 complex was formed with maleate anion which implied that two thiourea groups of **60** acted as cooperative binding sites. At low concentrations of maleate, the initial purple color changed to violet-red, probably due to the formation of a charge-transfer complex via hydrogen bond interactions. At a higher concentration of maleate, the violet-red color changed to red, likely due to the deprotonation of the N-H proton of the thiourea moiety (Figure 65). However, receptor **60** was silent toward the fumarate guest. Evidently, the observed selectivity refers to anion stereochemistry. While fumarate did not affect the receptor's conformation, the maleate guest perfectly fitted the receptor's cleft.

Figure 65. Effect of maleate and fumarate anions on color changes of **60**: (a) **60**; (b) **60** with 0.1 equiv. of maleate; (c) **60** with 2.0 equiv. of maleate; (d) **60** with 2.0 equiv. of fumarate. Reprinted with permission from the Royal Society of Chemistry. Copyright 2009.[106]

Trivedi and coauthors designed and synthesised two new receptors **61** and **62** for the recognition of E/Z-diacids (Figure 66).[107] In the presence of maleate, a significant change in

the UV-Vis spectrum of receptor **61** was observed. However, the addition of fumarate did not cause any changes. The same behaviour was also displayed by receptor **62**. Upon addition of maleate to sensor **61** and **62**, the color changes from colorless to red and yellow, respectively (Figure 67). The Job plot revealed a 1:1 stoichiometry between maleate and the receptors. Obviously, the selective discrimination of maleate is related to the receptor structure. Maleate anion can readily fit with the benzohydrazide functionality of the receptors **61** and **62**, and, therefore form complementary hydrogen bond sustained complexes. On the other hand, fumarate guest cannot accommodate within these receptors due to its larger size.

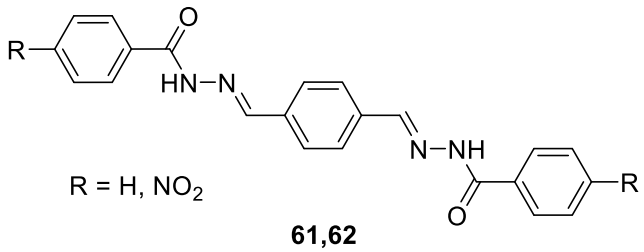

61,62

Figure 66. The molecular structures of receptors **61**, **62**.

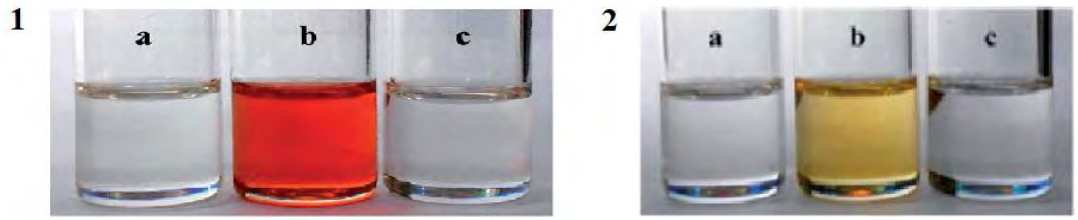

Figure 67. Effect of maleate and fumarate anions on color changes of **61** and **62**: **1**: (a) **61**; (b) **61**+maleate; (c) **61**+fumarate; **2**: (a) **62**; (b) **62**+maleate; (c) **62**+fumarate. Adapted with permission from the Royal Society of Chemistry. Copyright 2014.[107]

In 2020, Trivedi synthesised two new colorimetric receptors **63(R1)** and **64(R2)**, which were used in visual discrimination of maleate.[108] Receptors **63(R1)** and **64(R2)** selectively recognize maleate guest over fumarate. In the presence of maleate, color changes from pale yellow to wine red, and from pale yellow to orange-red was observed for **63(R1)** and **64(R2)**, respectively (Figure 68). Addition of fumarate to the solution had no considerable effect on color change. Since maleate is more basic than fumarate, it strongly binds with the acidic proton of receptors **63(R1)**, **64(R2)**, and, hence, a huge bathochromic shift in the absorption band of

the final solution was observed. Additionally, the presence of -NO_2 groups makes the NH proton extremely acidic, and, therefore, the binding of maleate to **63**(**R1**) is stronger than to **64**(**R2**), resulting in a different color change.

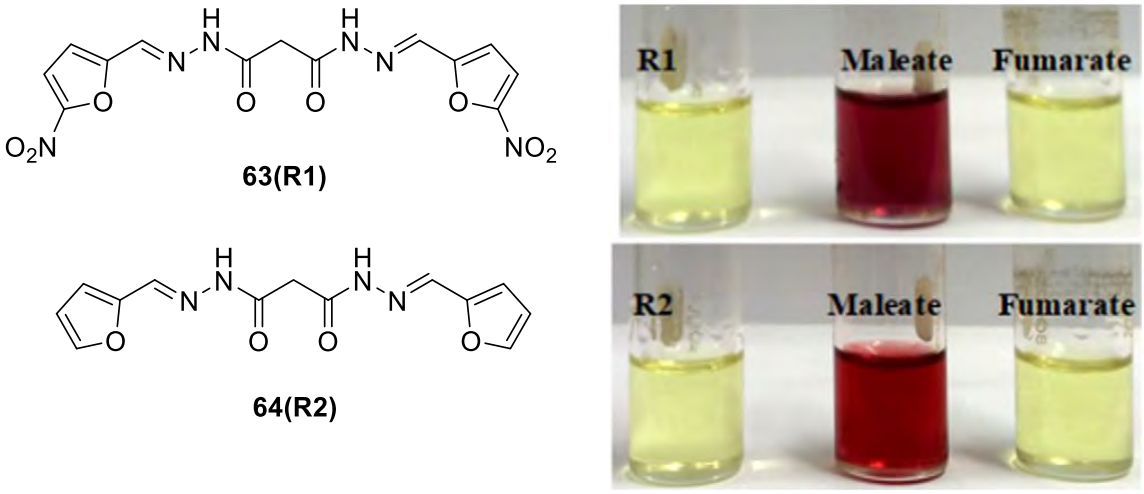

Figure 68. The molecular structures of receptors **63**(**R1**), **64**(**R2**) and their solutions in the presence of maleate and fumarate. Adapted with permission from the Elsevier. Copyright 2020.[108]

Lee et al. prepared a series of water-soluble polymers that were utilized for visual discrimination of geometric isomers.[109] Depending on the type of -R groups, these polymers gave different responses to maleic and fumaric acids. Polymer **65**(**P1**) with an aldehyde group discriminated between maleic and fumaric acids with a color change seen by the unaided eye.

Because the pK_a of polymer **65**(**P1**) is lower than the pK_{a1} of fumaric acid, but higher than the pK_{a1} of maleic acid, only maleic acid can protonate the *β*-nitrogen atoms of the azo chromophore of **65**(**P1**), resulting in discrimination between two geometric isomers. Polymer **66**(**P2**) that comprises thiazolidine units did not show any discrimination because its pK_a is higher than the pK_a values of these two diacids. No response was also observed for polymer **67**(**P3**) due to the presence of a strong electron-withdrawing nitrile group (EWG) that significantly reduces the chance to protonate *β*-nitrogen atoms (Figure 69).

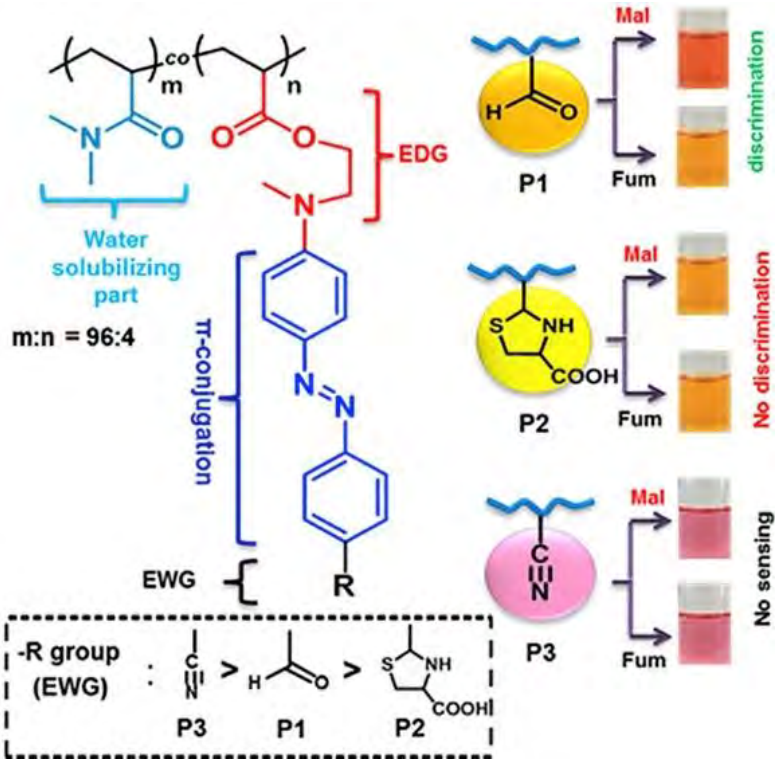

Figure 69. Structures of a series of water-soluble polymers **65**(**P1**), **66**(**P2**) and **67**(**P3**) and their efficiency in the colorimetric discrimination of maleic (Mal) and fumaric (Fum) acids. EDG: electron-donating group: EWG: electron-withdrawing group. Reprinted with permission from the Elsevier. Copyright 2020.[109]

1.3.2 Fluorescent discrimination of the geometric isomers of dicarboxylic acids

Compound **68**(**L**) with two heteroimine bonds has been explored in geometric diacids recognition.[110] This sensor discriminates maleic acid over fumaric acid through fluorescence response. Addition of maleic acid yielded a considerable shift in the emission spectrum of ligand **68**(**L**). On the other hand, its geometric isomer, fumaric acid, practically did not have any effect (Figure 70). Since only maleic acid has a lower pK_{a1} than the receptor, it protonated the -NMe_2 group leading to the generation of a new complex that gave a deep red color.

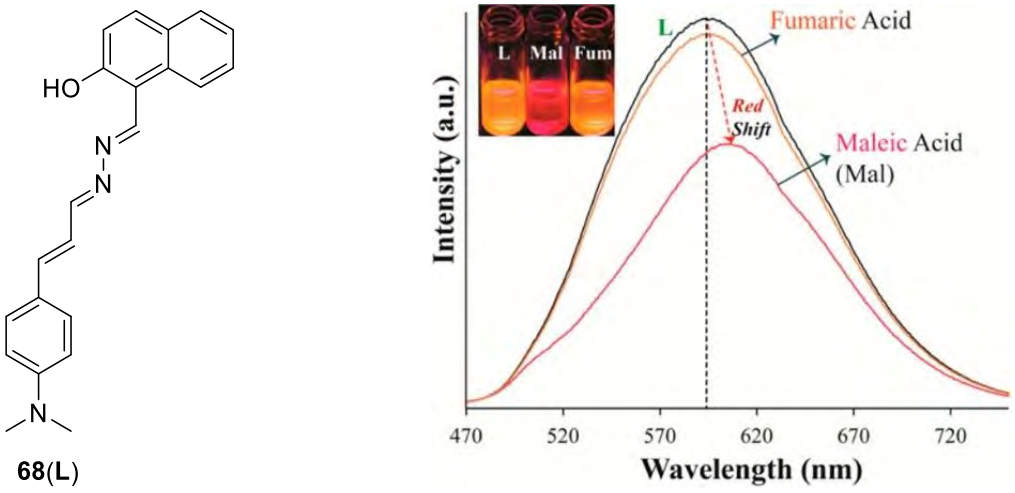

Figure 70. Structure of receptor **68**(**L**) and its fluorescence spectra in the presence of maleic and fumaric acids. Adapted with permission from the American Chemical Society. Copyright 2015.[110]

Mukherjee and coauthors used **69** (Figure 71) in the discrimination of maleic acid over fumaric acid.[111] Maleic acid formed a 2:1 complex, which led to an increase in the emission intensity. The obvious reason for this was the *cis*-configuration of the acid, which perfectly fitted to the amide functionalized cavity. In the presence of fumaric acid, no changes in emission spectra were observed.

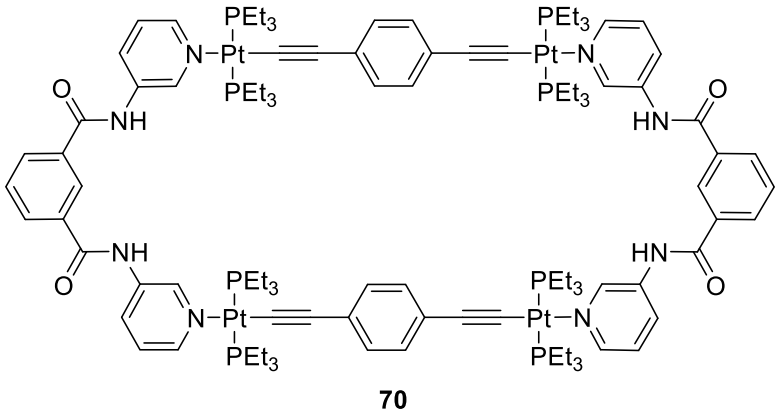

Figure 71. [2+2] Self-assembled macrocycle **70**.

1.3.3 Other methods for the discrimination of the geometric isomers of the dicarboxylic acids

Delgado et al. described two receptors **70** and **71** (Figure 72) which were studied in the discrimination of geometric isomers.[112] Utilizing ^{1}H NMR titration, a 1:1 binding stoichiometry was only observed for fumarate ion. The highest association constants were found for hexaprotonated receptors with fully deprotonated fumarate. Since maleate has a higher second pK_a it was not fully ionized in the pH region where both receptors were hexaprotonated. Therefore, maleate did not form any complex with receptors **70** and **71**. Notably, receptor **71** binds fumarate with a larger association constant than receptor **70** due to its less rigid structure.

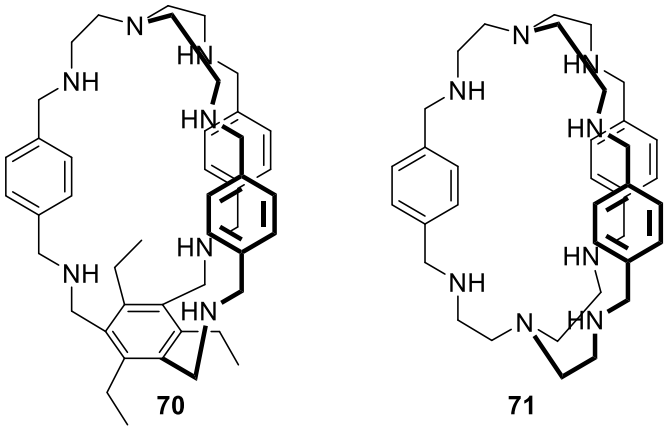

Figure 72. Macrobicyclic receptors **70**, **71**.

Receptor **21**(**L**) reported by Užarević and coworkers (page 19) showed specific selectivity to maleate anion.[19] The binding affinity of this receptor toward maleate and fumarate was examined both in solution and in the solid state. Competitive crystallization analysis showed the formation of only **21**(**L**)-maleate complex in the presence of both ions. The same manner of complexation was observed under solvent-free conditions. When **21**(**L**) was milled with maleate and fumarate, again only the complex with maleate was obtained.

2. RESULTS AND DISCUSSION

2.1 Concept of supramolecular nanosensor

As can be seen from the literature, many receptors have been developed for the recognition of dicarboxylic acids. However, most receptors recognize single acid and only few of them more than one acid. For example, phthalic acid was discriminated by receptors developed in Yen,[5] Miljanić,[8] and Kim[11] groups. Ahn[7] and Zhang[10] were also able to recognize terephthalic acid, but only Sessler[9] managed to distinguish isophthalic and terephthalic acids over phthalic acid. On the other hand, in most reports on the discrimination of aliphatic dicarboxylic acids, either oxalic (C2) or succinic (C4), or adipic (C6) acids[8,72,73,81,83,86,98,99] were recognized. Only in few cases, the discrimination of several aliphatic acids was possible (malonic (C3) and suberic (C8),[77] adipic (C6) and pimelic (C7),[82] adipic and suberic (C8)[87]). Versatile sensors are also absent for geometric isomers. Despite several reports on detecting butenedioic acid,[5-7,106-110] a general approach to the recognition of E/Z isomers was not developed. Therefore, we were looking for a universal sensor that would be easy to prepare and that could recognize the largest number of diacids.

Recently, in our group, we developed a new family of prismatically shaped positively charged macrocycles (Figure 73) called pillar[n]pyridiniums (PnPs, n=4,6). These macrocycles have a high affinity for negatively charged species.[22,120] For example, P4P, the smallest macrocycle, can interact with negatively charged guests such as PF_6^- and F^-. But only F^- anion can bind inside the cavity due to its smaller size. P6P, which has a larger cavity, has been shown to bind aromatic oligocarboxylic acids. Depending on the magnitude and distribution of electric charge in the guest molecules, the complexation occurred either internally or externally. We have also noticed that P6P in the presence of terephthalic acid and 1,2,4-benzenetricarboxylic acids gave white precipitates. This suggested the formation of polymeric species due to the cross-linking of P6P macrocycles with the carboxylic groups on the opposite ends of the aromatic rings. For other acids, this was impossible due to the unfavourable geometry of the carboxylic groups. Nevertheless, despite the formation of white precipitates, terephthalic acid and 1,2,4-benzenetricarboxylic acids remained undifferentiated. Thus, we wondered if we could discern even more subtle differences in the interaction patterns, paving the way to distinguish more acids.

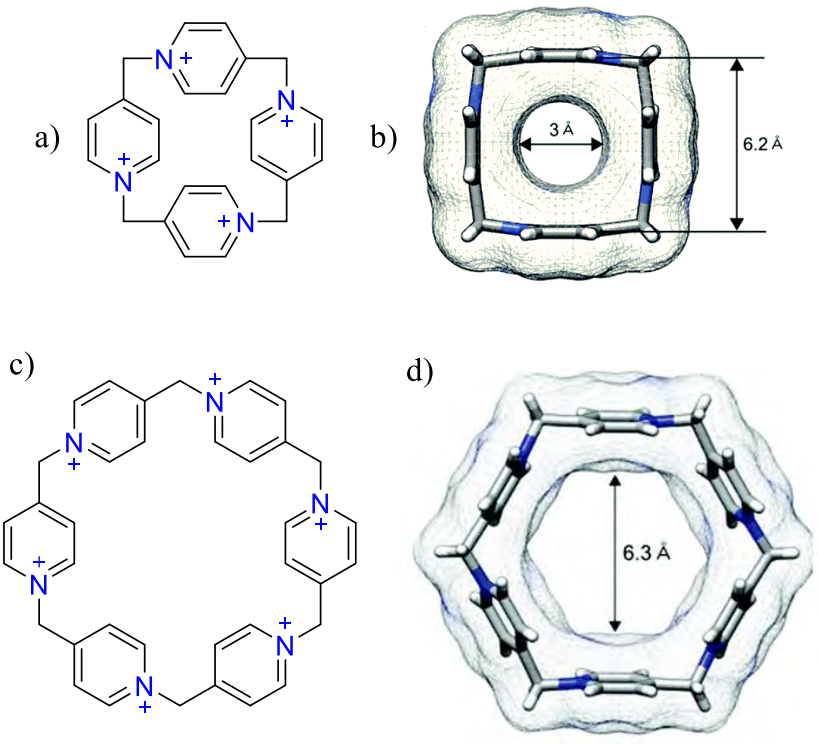

Figure 73. a) Structural formula of pillar[4]pyridinium (P4P); b) top view of P4P; c) structural formula of pillar[6]pyridinium (P6P); d) top view of P6P.

We draw our attention to gold nanoparticles (AuNPs) which are characterized by a plethora of different colors depending on their size and shape as well as the distance between them.[121-124]

We thus hypothesized that a negative charge typically present on the surface of gold nanoparticles would prompt the deposition of positively charged pillar[n]pyridinium macrocycles (Figure 74). Moreover, once formed these modified nanoparticles should be cross-linked by diacids (in dianionic form) to produce interparticle gaps that correspond to the distance between carboxylic groups, and consequently, give different plasmonic responses (colors).

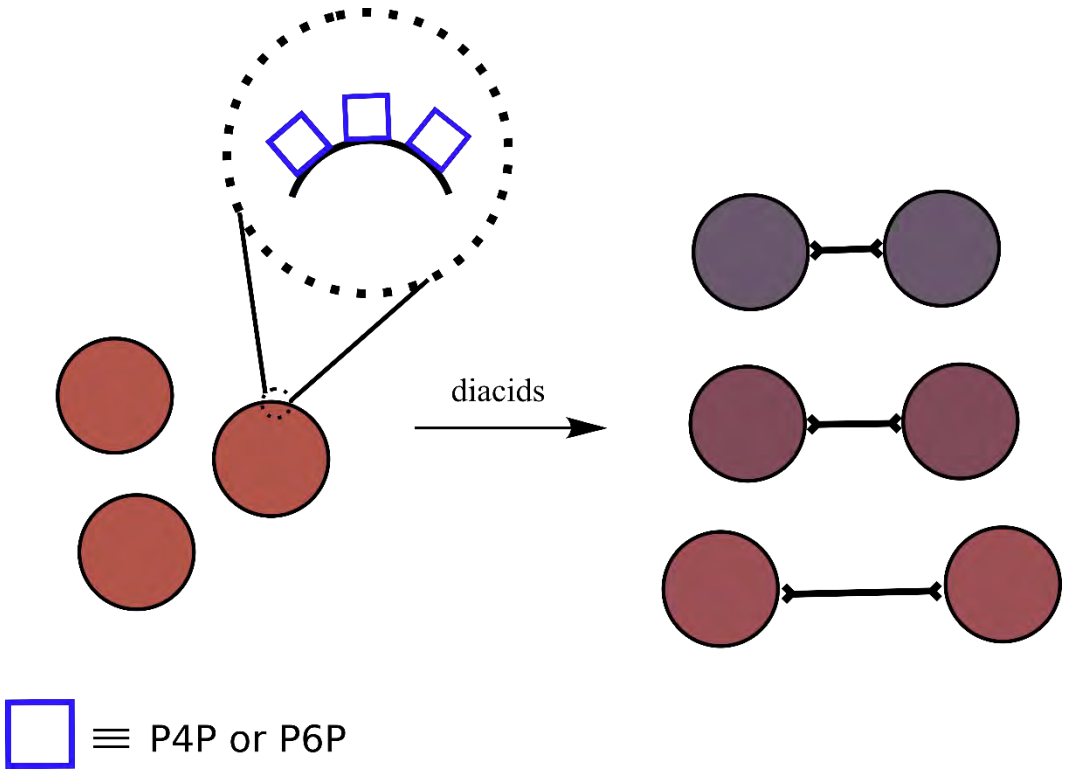

Figure 74. Cartoon representation of supramolecular nanosensor (red circles denote gold nanoparticles, whereas blue squares stand for P4P and P6P macrocycles adsorbed on the nanoparticles) and its interaction with different diacids in anionic form.

Based on these considerations, we started to design a suitable nanosensor to be employed further for the discrimination of three groups of carboxylic acids: a) phthalic acids, which are positional isomers; b) α,ω-alkanedicarboxylic acids belonging to chemical homologs; and c) dicarboxylic acids with double C-C and N-N bonds that display geometric isomerism.

phthalic acid isomers

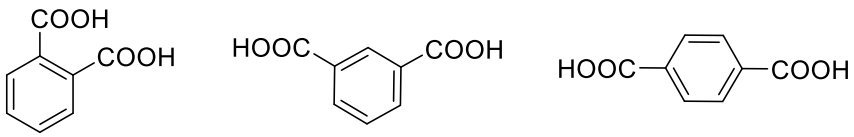

α,ω-alkanedicarboxylic acids

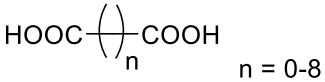

E/Z isomeric dicarboxylic acids

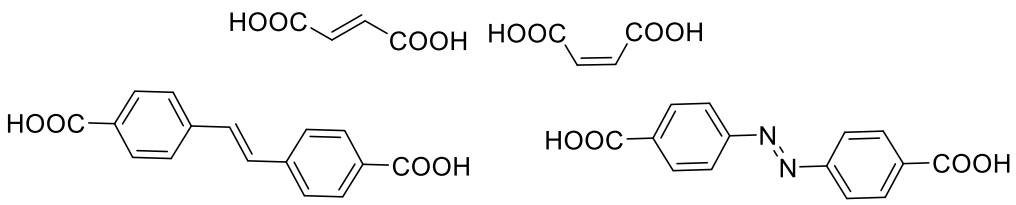

2.2 Nanosensor design

We began our study with P4P, the smallest representative of PnPs, which later turned out to be a good choice. First, we thought to deposit P4P macrocycles on the NP surface in situ as Weiss and Yang reported[125] for carboxylatopillar[5]arenes (CP[5]A). We mixed $HAuCl_4 \cdot 3H_2O$, P4P, and $NaBH_4$ solutions at different ratios. Unfortunately, in all cases, we obtained unstable gold nanoparticles which almost immediately underwent aggregation.

Therefore, we decided to introduce PnPs into solutions after the NPs were formed. The concentration of gold nanoparticles we obtained by this method was 1.08 mM in term of gold atoms. Dynamic light scattering (DLS) analysis showed that the average hydrodynamic size of the NPs was equal to 6.9 nm as well as ξ-potential of = -31.5 mV (Figure 75). The observed high negative charge is due to the presence of adsorbed anions left after the reduction of gold(III) chloride rendering the formed colloid very stable (for more than one month).

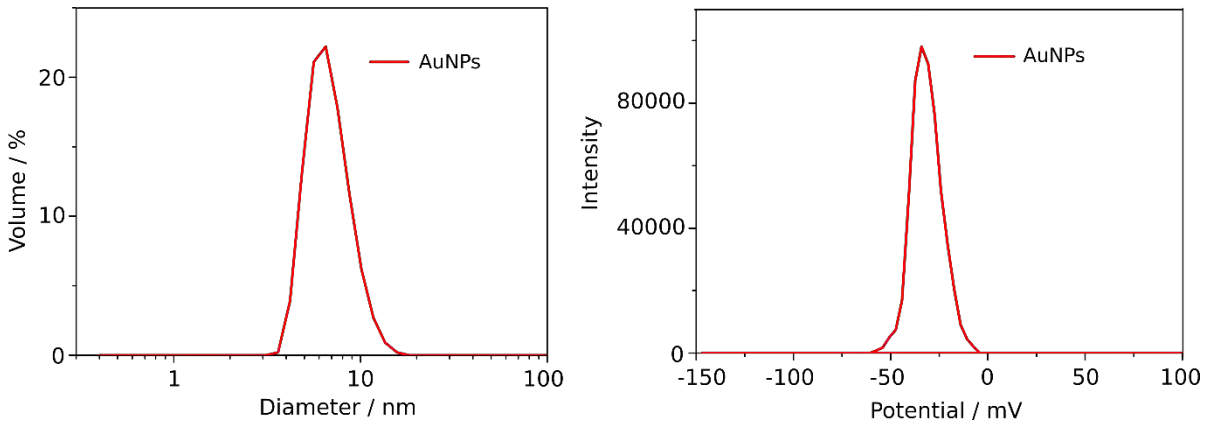

Figure 75. Particle size distribution and ξ-potential of freshly obtained gold NPs.

Next, we proceeded to the decoration of these NPs with P4P. UV-Vis spectra revealed that the nanoparticles aggregated when the concentration of P4P used was lower than the concentration of gold nanoparticles (Figure 76), most probably due to the cross-linking of negatively charged particles by positively charged macrocycles. However, the more P4P was used, the more stable the NPs became. The optimal ratio between P4P and AuNPs was found to be 4:1 (P4P@AuNPs). At this ratio, the obtained NPs remained stable for at least 24 hours. UV-Vis spectrum of P4P@AuNPs showed the plasmon peak with a maximum at 517 nm (Figure 77A). The average hydrodynamic size of AuNPs increased from 6.9 nm to 7.7 nm indicating the presence of P4P on the surface (Figure 77C). Another evidence of the successful adsorption of the macrocycle was the inversion of the ξ-potential from -31.5 mV to +1.3 mV (Figure 77D). The lack of aggregation in the obtained P4P@AuNPs sol was also confirmed by TEM analysis (Figure 78).

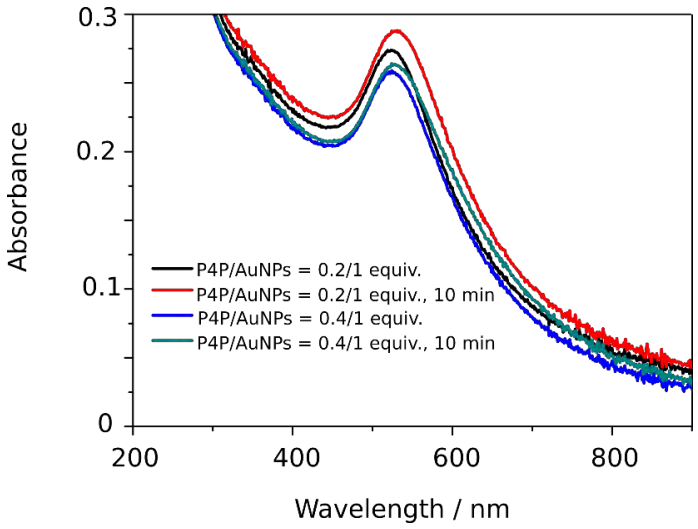

Figure 76. Absorption spectra of P4P/AuNPs at different ratios.

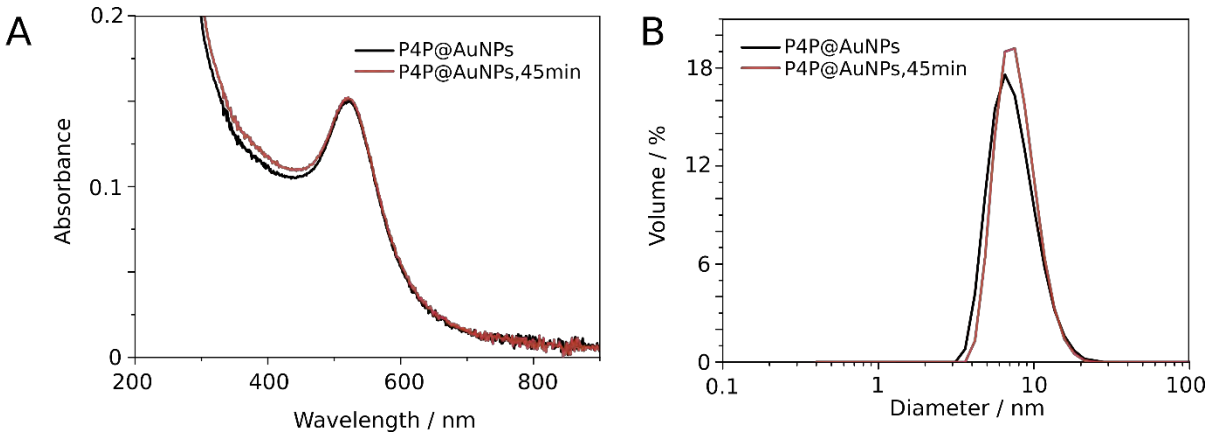

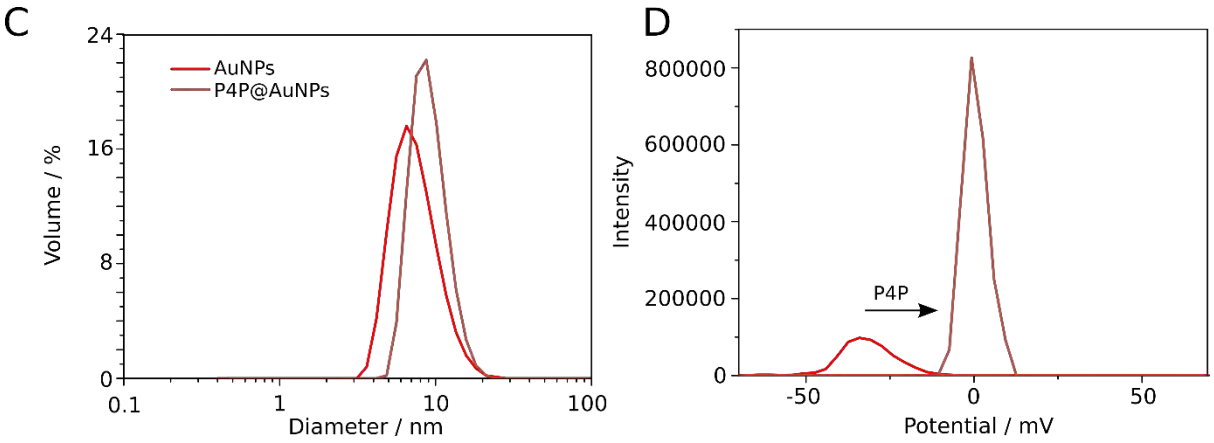

Figure 77. (A) Progress in time of the absorption spectra of P4P@AuNPs; (B) progress in time of the particle size distribution of P4P@AuNPs; (C) particle size distribution of AuNPs vs. P4P@AuNPs; (D) ξ-potential of AuNPs vs. P4P@AuNPs.

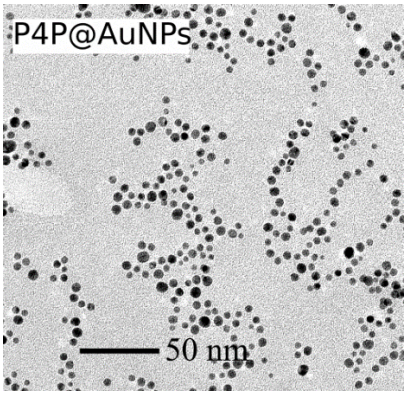

Figure 78. TEM image of P4P@AuNPs.

2.3 Recognition of phthalic acid isomers

First, we verified whether P4P itself (without nanoparticles) could interact with diacids. As a model, we used phthalic acid isomers. 12.6 mM aqueous solution of P4P was divided into four portions. To each portion, we added a single isomer (in the form of sodium salt, 6.3 mM). One portion was left as a blank. While the phthalic acid (1,2-acid) containing solution remained transparent, isophthalic acid (1,3-acid) and terephthalic acid (1,4-acid) produced white precipitates. Notably, the heaviest sediment appeared for 1,4-acid. First, we considered a scenario that since P4P is acidic, the precipitation may be due to a decrease in the pH of the

solution, which reduces the solubility of 1,3-acid and 1,4-acid. We found the resulting pH of the solution to be 5.61. On the other hand, bringing the pH to the same value with HCl in solutions containing only diacids did not cause any precipitation. This indicated that the formation of white precipitates is due to cross-linking of P4P with the carboxylic groups of 1,4-acid and 1,3-acid.

For 1,3-acid, in which the carboxylic groups are more away from each other: two guest molecules can interact with one host molecule, one guest with one host, and one guest with two hosts. The same is true for 1,4-acid, in which two carboxylic groups are opposite to each other. As a result, the feasible multiple interactions of 1,3-acid and 1,4-acid with P4P, especially at high concentrations, lead to a growing supramolecular chain, giving insoluble aggregates. In the case of 1,2-acid, one guest molecule can only interact with one host molecule (P4P). The interaction of one guest with two hosts, or the opposite, and as a result the formation of supramolecular polymers, is practically impossible in the latter due to steric reasons (Figure 79).

To get a deeper insight into the structure of phthalic acids-P4P complexes, we attempted to grow single crystals suitable for X-ray diffraction analysis. First, we attempted crystallization by slowly adding P4P solutions to the aqueous solutions of phthalic acids. Unfortunately, using this approach we were not able to grow suitable crystals for X-ray analysis. Then, we proceeded to the slow evaporation approach. We mixed aqueous solutions of P4P with aqueous solutions of phthalic acids using high dilution (5 mM) at pH=6 and left the solvent to evaporate. In this case, we managed to obtain a suitable crystal only for 1,4-acid-P4P complex. The obtained X-ray structure showed the tendency of 1,4-acid and P4P to linear arrangement (Figure 80). In the addition to electrostatic attraction, the supramolecular chain composed of alternate tetracations and dianions was sustained by charge-assisted hydrogen bonding of $(C\text{-}H)^{+}\cdots O^{-}$ type. Extra dianions fulfilling electroneutrality of the supramolecular assembly were intercalated between external skeletons of the two adjacent macrocycles in the crystal lattice. The supramolecular chain was composed of P4P (in cornflower blue) and 1,4-acid (in red). The P4P inner cavity is filled by water molecules (in cyan), and two extra water molecules are located close to the portals. There are multiple charge-assisted hydrogen bonds of $(C–H)^{+}\cdots O^{–}$ type between P4P serving as a donor and 1,4-acid serving as an acceptor (hydrogen bonds demonstrated as dashed red lines) (A). Figure 80 (B and C) further shows two modes of intercalation of 1,4-acid between the outer skeletons of adjacent P4P macrocycles. Such

insertion is assisted *via* $\pi^{+}\cdots\pi^{-}$ interactions between macrocyclic tetracations and guest dianions. The closest contacts are depicted as red dashed lines.

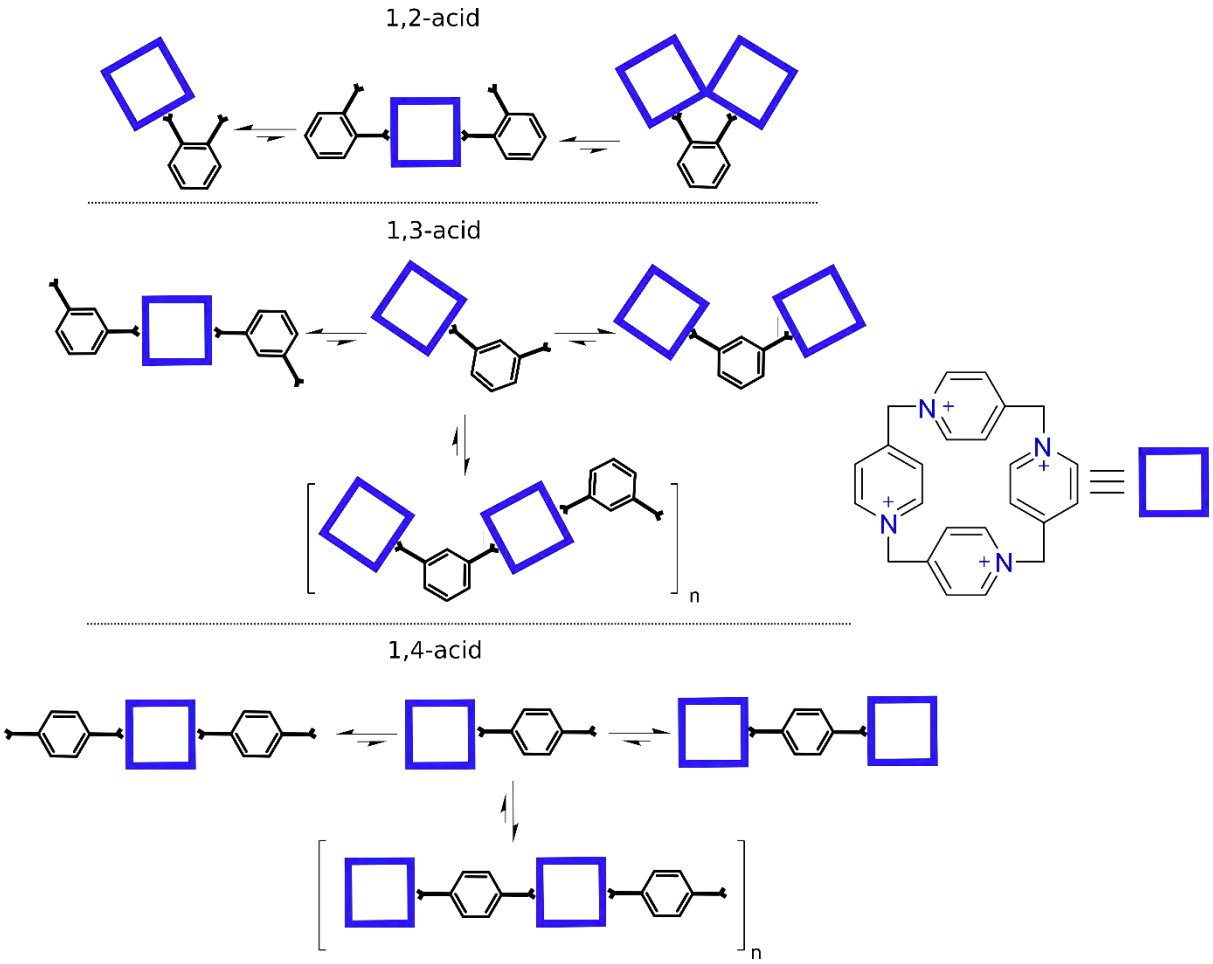

Figure 79. Plausible thermodynamic equilibria in aqueous phthalic acids-P4P solutions.

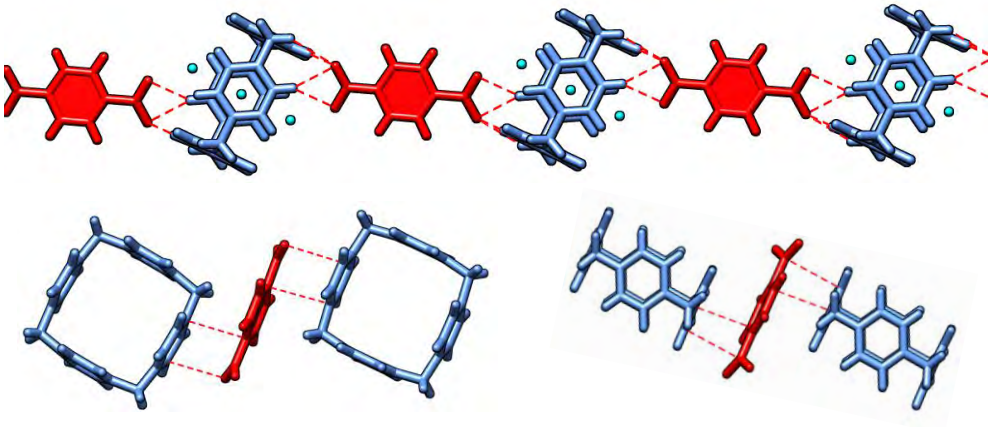

Figure 80. 1,4-Acid-P4P complex structure.

Having confirmed the interaction of phthalic acid isomers with P4P, we began experiments with P4P-nanoparticle ensembles. First, we started with diluted solutions of the sensor (0.75 mM) and analytes (0.25 mM). However, no color change was seen. Then, we increased the concentration of the acids by two times, but still no color change was observed. Eventually, a 5-fold increase in the acid concentration lead to apparent color differences of the prepared solutions.

The color change occurred almost immediately, and with the extension of time these differences became more noticeable. After 1h, all solutions had different colors – pink for 1,2-acid, blue for 1,3-acid and violet for 1,4-acid (Figure 81).

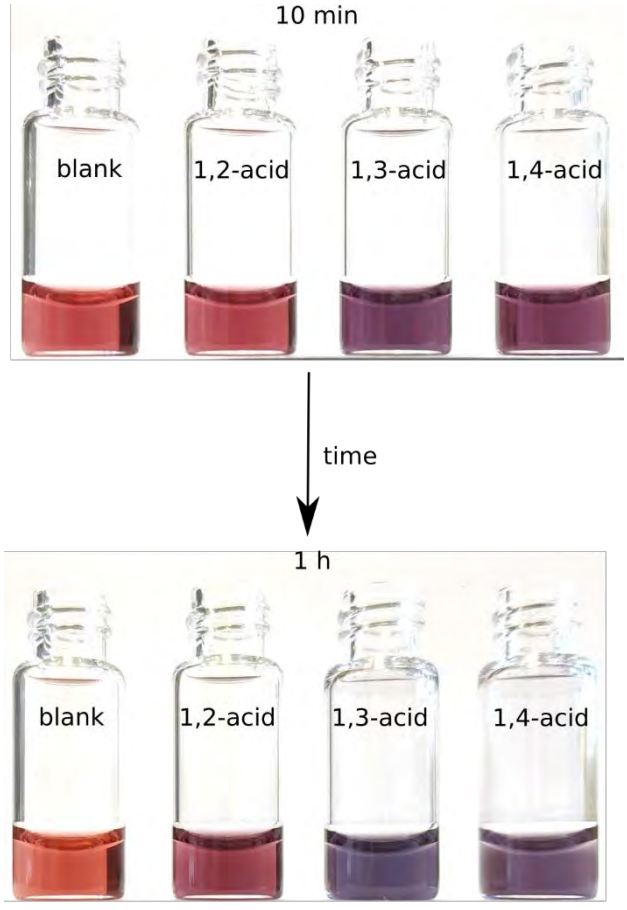

Figure 81. Photograph of P4P@AuNPs solutions taken 10 min and 1 h after mixing with phthalic acids.

The next day, in all vials containing phthalic acids, the solutions turned grey as the nanoparticles aggregated. UV-Vis spectra showed changes in plasmon peak for all acid-containing samples.

UV-Vis spectra were in line with the observed color changes. While the plasmon band in the presence of 1,2-acid changed a little, considerable changes were noticed for the remaining two acids. The bathochromic shift and intensity increase of the plasmon peaks indicated that NPs were approaching each other and plasmon coupling.[126-128] With the decrease in the distance between NPs, their absorption intensity increased, while the absorption band shifted toward the red region. As time elapsed (1h), the differences became even more pronounced. The largest change was observed for 1,3-acid, indicating the shortest interparticle distance in this case (Figure 82).

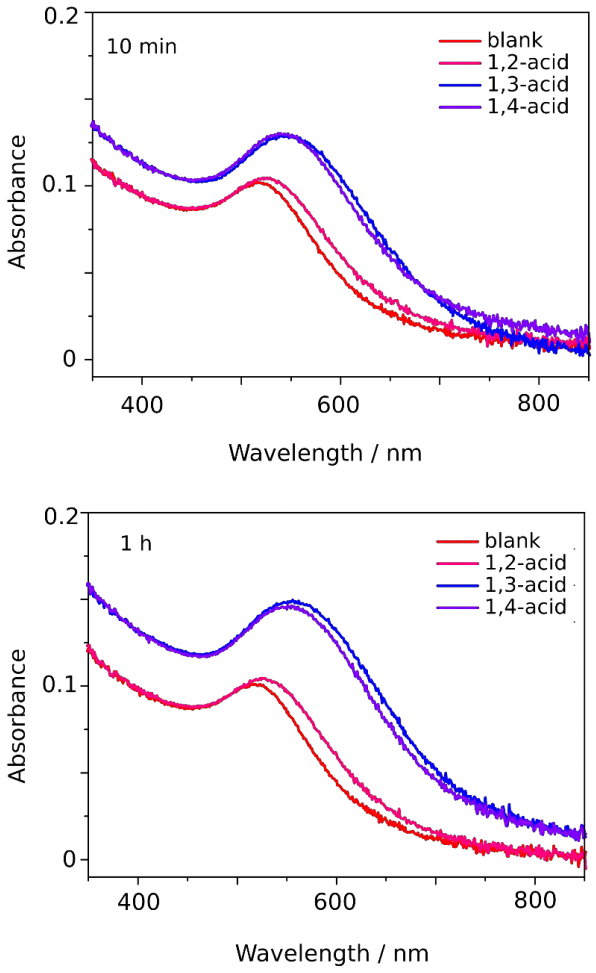

Figure 82. Absorption spectra of P4P@AuNPs recorded 10 min and 1 h after mixing with phthalic acids.

DLS analysis revealed the presence of small aggregates for 1,2-acid and large aggregates for 1,3-acid and 1,4-acid. The average hydrodynamic size of the particles was 30 nm, 460 nm and 1270 nm in the case of 1,2-acid, 1,3-acid and 1,4-acid, respectively (Figure 83). This corresponds well with the directionality of carboxylic groups. 1,4-Acid with opposite carboxylic groups should exhibit the best cross-linking ability and therefore give rise to the largest aggregates.

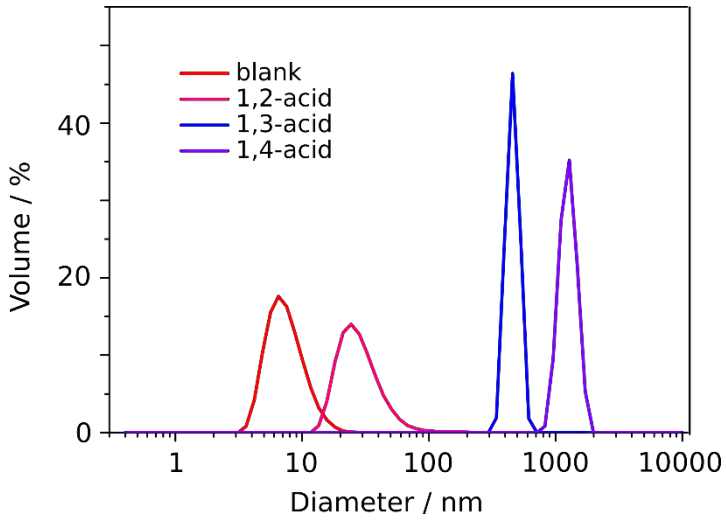

Figure 83. Particle size distributions.

The extent of aggregation of the samples in correlation with the type of used acid was also confirmed by TEM analysis (Figure 84).

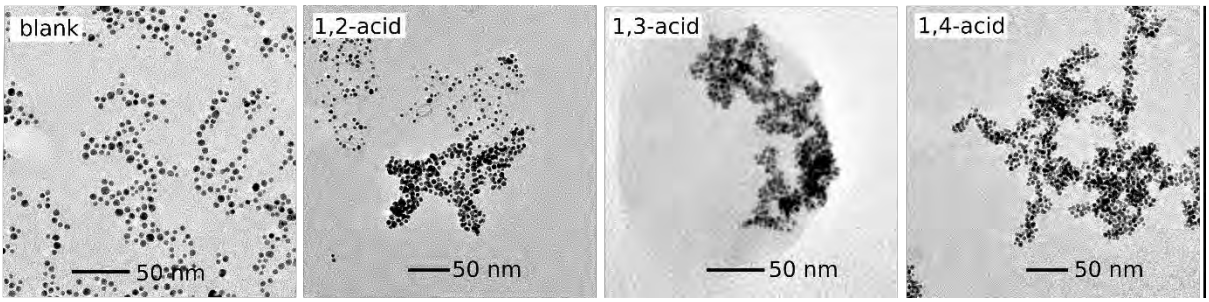

Figure 84. TEM images of P4P@AuNPs and P4P@AuNPs after the addition of phthalic acids.

Moreover, 1,3-acid and 1,4-acid based aggregates displayed a worm-like topology. This may suggest that the NPs undergo aggregation in the same fashion as P4P interacts with phthalic acids in the solution. To get more insight into the interaction patterns, we analyzed

TEM images with ImageJ software. We found that the average particle size was practically the same for all samples: 4.54±0.62 nm (without acids), 5.48±1.35 nm (1,2-acid), 5.40±0.68 nm (1,3-acid), and 5.35±1.42 nm (1,4-acid) (Figure 85).

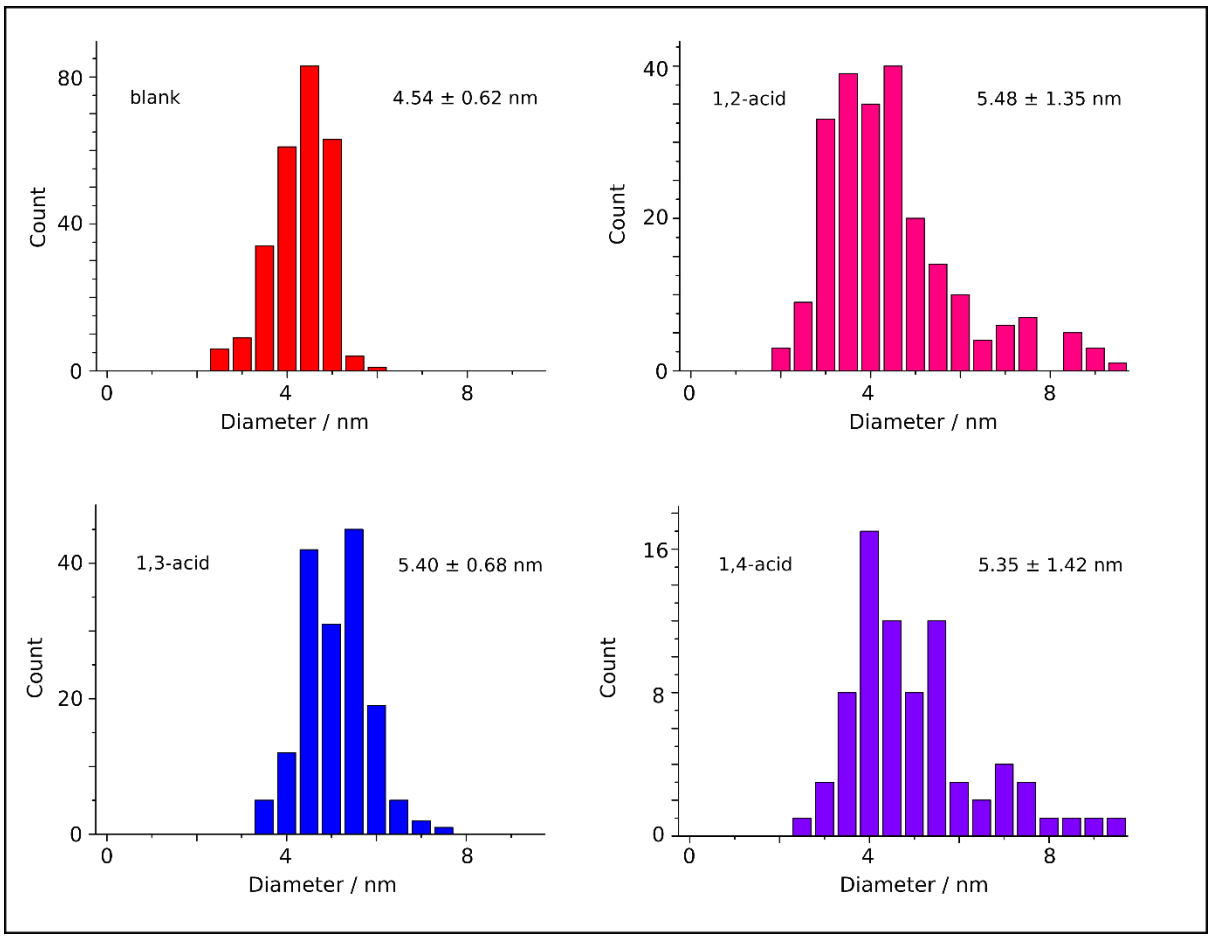

Figure 85. Particle size distribution for P4P@AuNPs and P4P@AuNPs mixed with phthalic acids determined from TEM images.

However, the centre-to-centre interparticle distances were quite different: 7.44±1.37 nm for 1,2-acid, 6.69±2.04 nm for 1,3-acid and 7.05±1.61 nm for 1,4-acid (Figure 86).

By subtracting the diameter of a single NP we were able to obtain the distances between their surfaces: 1.96 nm for 1,2-acid, 1.29 nm for 1,3-acid, and 1.70 nm for 1,4-acid. These data are in good agreement with theoretically calculated values (2.09, 1.34, and 1.56 nm, respectively) obtained by summing up the heights of two P4P macrocycle molecules and the lengths of single acid molecules (measured between oxygen atoms of carboxylic groups).

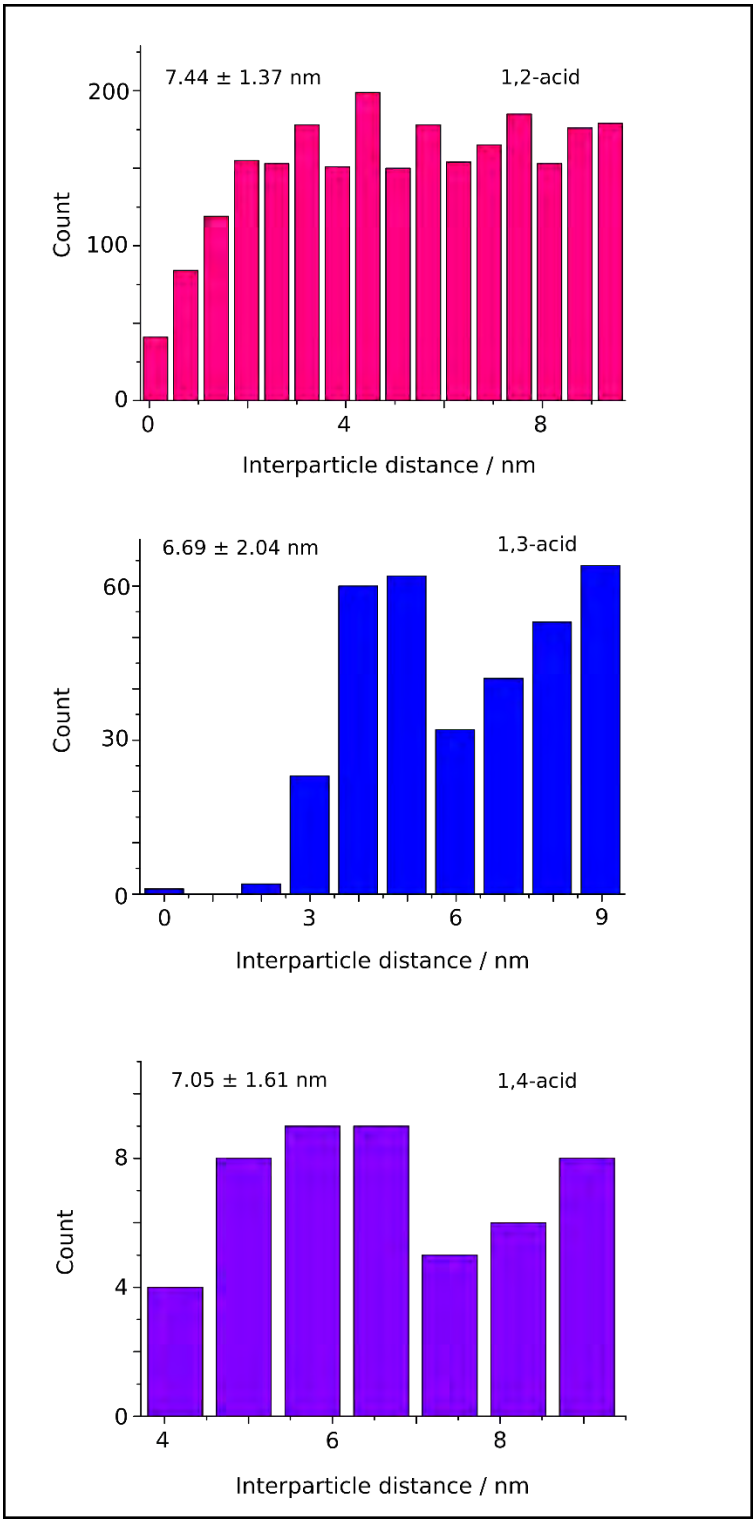

Figure 86. Center-to-center particle size distribution for P4P@AuNPs and P4P@AuNPs mixed with phthalic acids determined from TEM images.

Based on the obtained data, we proposed the plausible mechanism of the aggregation (Figure 87). In the case of 1,2-acid, the aggregation is probably due to the partial hydrophobization of

gold nanoparticles' surface by phenyl rings. Therefore, it is not as heavy as in the remaining samples. The distance between the NPs remains quite large as they are separated by two phenyl rings. So, the final color does not differ much from red. For 1,3-acid and 1,4-acid containing samples, P4P@AuNPs approach one another at the distance of a single acid molecule due to the cross-linking of these acids with NPs. Thus, a sharp change in the position of the absorption band was observed. The difference in optical response stems from the directionality of the carboxylic groups. For 1,3-isomer, the interparticle gap was a bit shorter than for 1,4-acid, and consequently, the color of the aggregates was more bluish.

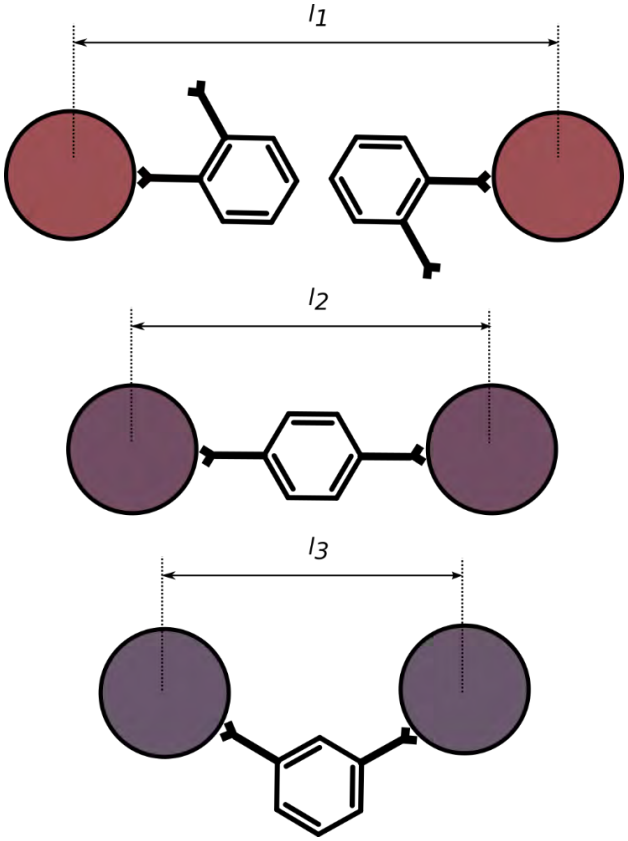

Figure 87. Plausible mechanism of the interaction of P4P-modified gold nanoparticles with phthalic acids.

Note that the method we developed is very sensitive. To find the detection limit for each acid, we prepared solutions of different concentrations (Figure 88). To a solution of P4P@AuNPs a single isomer was added at different concentrations and UV-Vis spectra were recorded. Based on these data, the detection limit, arbitrarily defined as the analyte concentration at which a noticeable shift in the absorption band is seen, was found to be 5×10^{-5} M for 1,2-acid, 1×10^{-6} M for 1,3-acid, and 5×10^{-6} M for 1,4-acid.

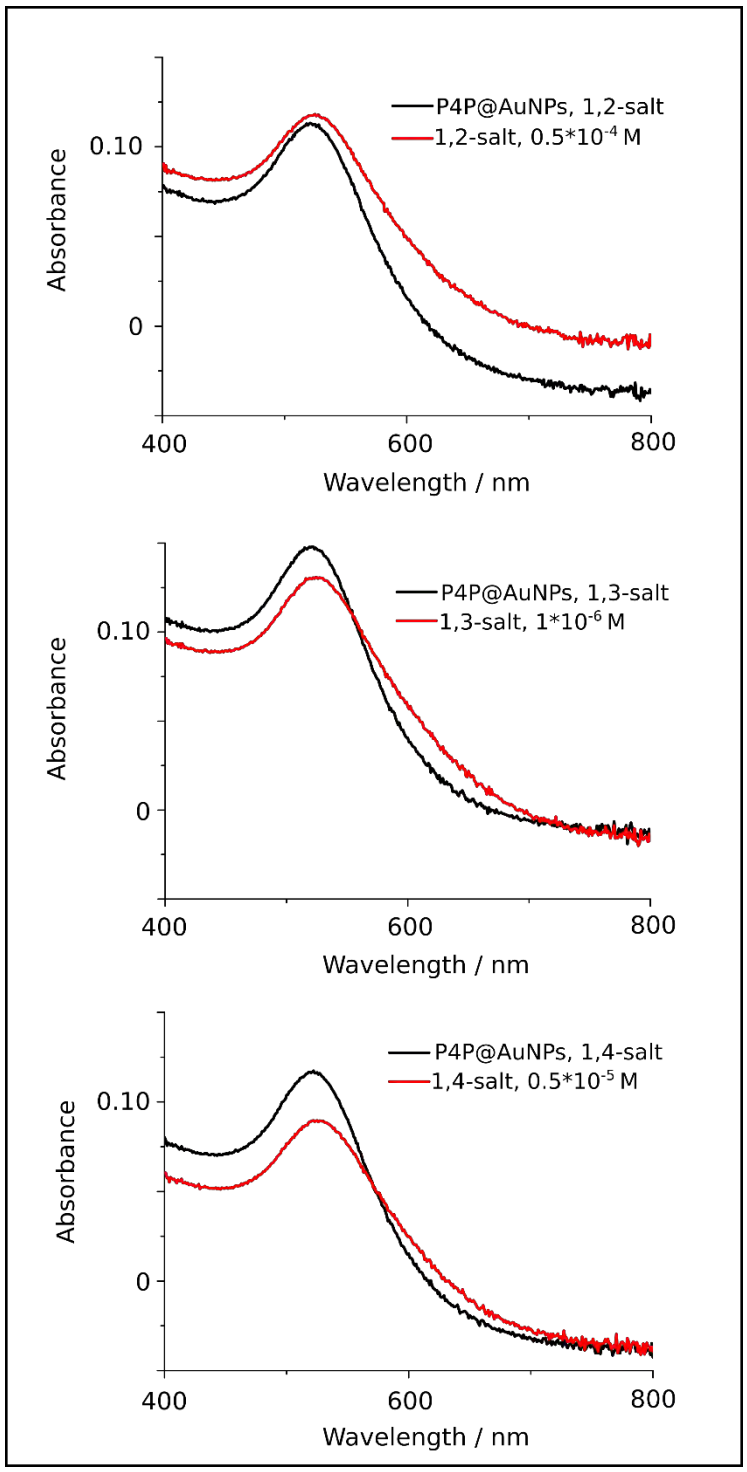

Figure 88. UV-Vis spectra of P4P@AuNPs with phthalic acids at different concentration (detection limit).

To show the crucial role of P4P in the visual differentiation of phthalic acid isomers we conducted a control experiment. We covered AuNPs with positively charged aliphatic thiol ligand (11-mercapto-*N,N,N*-trimethylundecan-1-aminium chloride (TMA)), which does not contain an internal cavity.

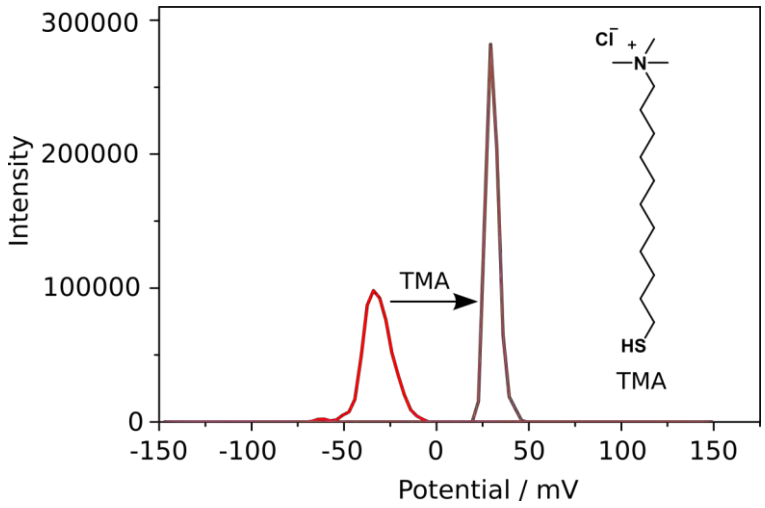

Figure 89. Change of ξ-potential of AuNPs after the addition of TMA.

ξ-potential changed from -31.5 mV to +28.5 mV, confirming the presence of TMA ligands (Figure 89). The TMA coated NPs were then mixed with phthalic acid solutions. The observation was carried out visually and by recording UV-Vis spectra.

Although the addition of phthalic acids to the final solution led to some changes in the color appearance, this was not sufficient to discriminate each acid (Figure 90). After 10 min, the plasmon band of gold nanoparticles changed only a little (+5 nm) with a small increase in intensity (by ≈+3%) for each isomer. As time elapsed (1h), the situation did not change much with the exception of 1,4-acid where further shift of the plasmon peak (+5nm) and increase of its intensity (by ≈+9%) was observed (Figure 91).

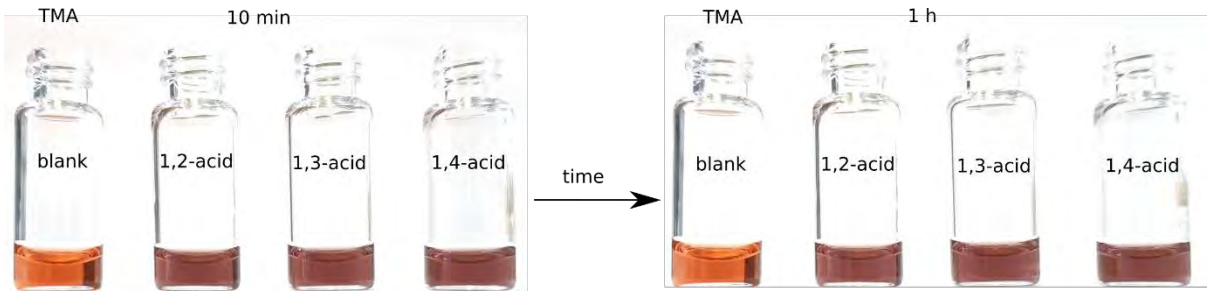

Figure 90. Photograph of glass vials filled with TMA coated NPs taken 10 min and 1 h after mixing with phthalic acids.

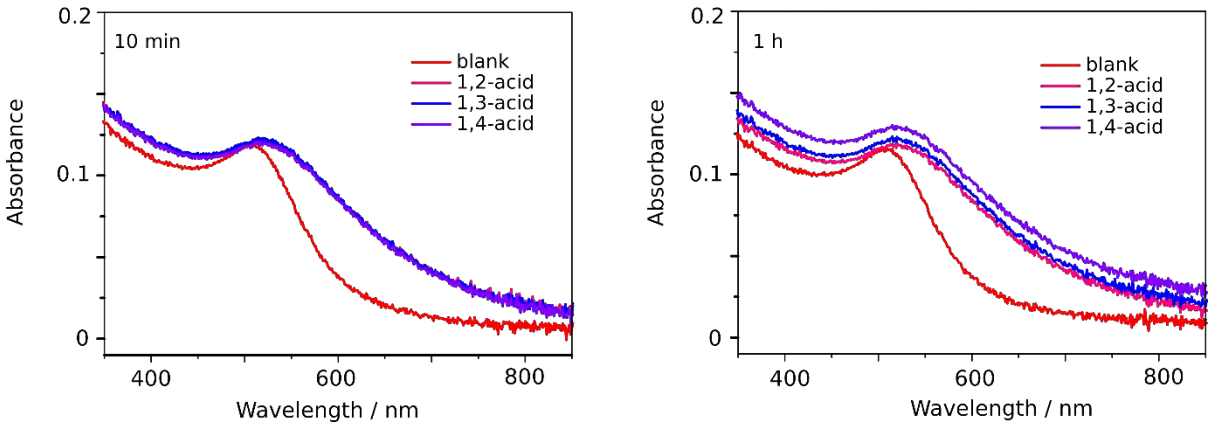

Figure 91. UV-Vis spectra of TMA coated gold NPs recorded after 10 min and 1 h after mixing with phthalic acids.

Also, we performed DLS measurements of TMA coated gold nanoparticles before and after the addition of phthalic acids (Figure 92).

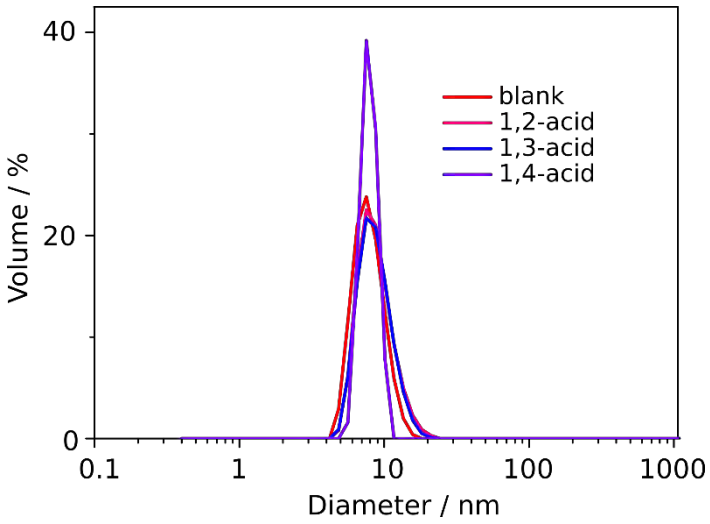

Figure 92. Particle size distributions for TMA coated gold nanoparticles measured by DLS 1h after the addition of phthalic acids.

We found that the addition of phthalic acids practically did not affect the hydrodynamic sizes of the NPs: 8.70 nm for 1,2-acid, 8.75 nm for 1,3-acid, and 7.89 nm for 1,4-acid, as compared to 7.99 nm at the beginning. This indicates that the acids do not cross-link the NPs.

These experiments confirmed the important role of host-guest interactions in the nanoparticles self-assembly.

2.4. Recognition of dicarboxylic acid homologs

Having established that our sensor is very sensitive to the spatial positions of carboxylic groups in phthalic acids, we hypothesized that the same should be true for other types of diacids. Therefore, as for the next target, we chose alkanedicarboxylic acids differing by the length of the aliphatic chain.

In these studies, for comparison, we also used a plasmonic sensor based on the larger macrocycle (P6P). It was prepared in a similar way as the one containing P4P. P6P was added to the "naked" AuNPs obtained by the reduction of gold(III) chloride with sodium borohydride. The charge of the particles changed from -31.5 mV to +45 mV, while the size and absorbance spectra remained almost the same, indicating the efficient surface coating (Figure 93). We also found that if the "naked" NPs were left agitating for 2 days, the stability of the resultant macrocycle coated NPs could be extended for several days. This is due to the decomposition of unreacted BH_4^- ions, the excess of which probably reduced the positively charged P4P or P6P molecules and caused aggregation.

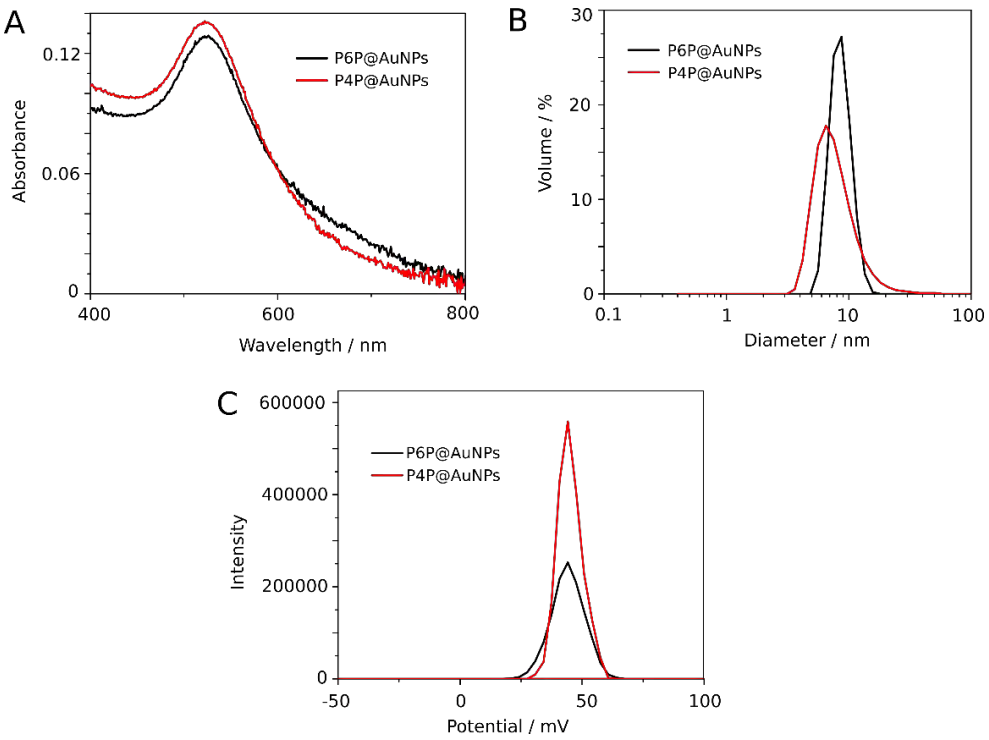

Figure 93. (A) Absorption spectra of P6P@AuNPs vs. P4P@AuNPs; (B) particle size distribution of P6P@AuNPs vs. P4P@AuNPs; (C) ξ-potential of P6P@AuNPs vs. P4P@AuNPs.

Similarly to the procedure used for phthalic acids we also prepared 5 mM (140 µL) solutions of aliphatic diacids in the form of sodium salt and added them to obtained P4P@AuNPs or P6P@AuNPs solutions (final C_{AuNPs} = 1 mM), divided into ten 300 µL portions. However, the color of the resultant solutions did not change. Therefore, we increased the concentration of acids to 9 mM. To each portion we added a single acid homolog (9 mM, 240 µL). Correspondingly, the blank solution was diluted with the same volume of pure water. Upon adding oxalic (C2) and sebacic (C10) acids to P4P@AuNPs, the red-to-blue color change was observed. Color change was also clearly visible for malonic (C3), suberic (C8) and azelaic (C9) acids. The color in the remaining analytes left practically undisturbed. As time elapsed (30 min), the differences became more pronounced due to progressive NPs aggregation (Figure 94). A similar color change was also observed for P6P@AuNPs, but it was not as pronounced (Figure 95).

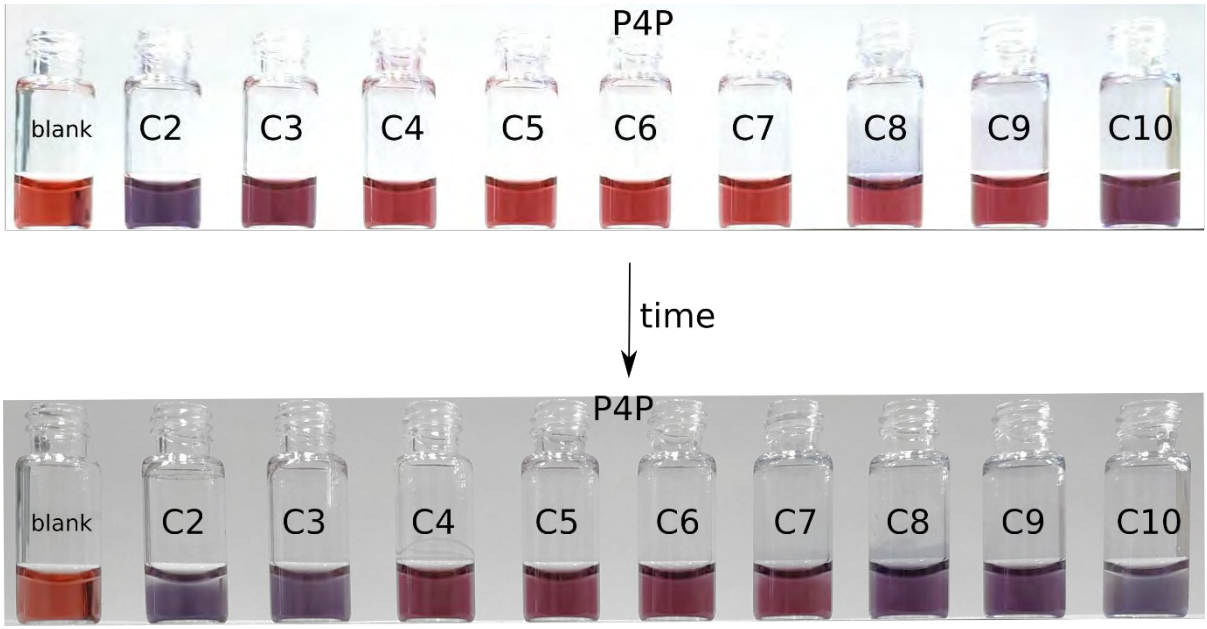

Figure 94. Photograph of glass vials filled with P4P@AuNPs taken 10 min and 30 min after mixing with the α,ω-alkanedicarboxylic acids.

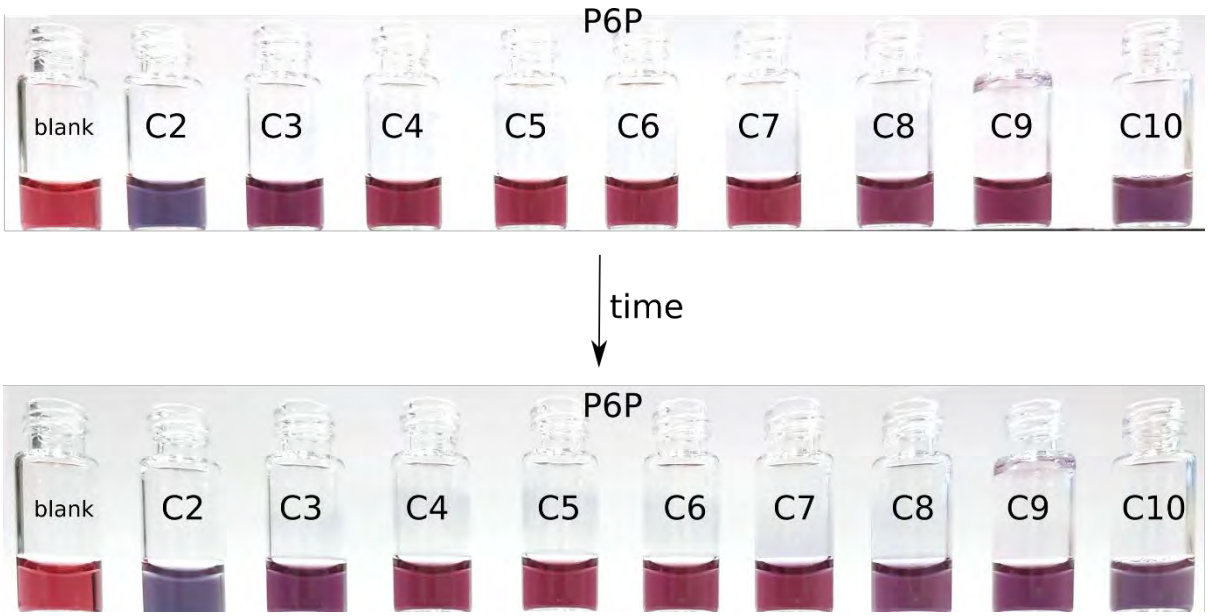

Figure 95. Photograph of glass vials filled with P6P@AuNPs taken 10 min and 30 min after mixing with the α,ω-alkanedicarboxylic acids.

Color changes are better seen in chromaticity diagrams. For both macrocycles, the color of gold nanoparticles evolved from red to purple. For pillar[6]pyridinium (Figure 97), however, color range was narrower with lower contrast between the analytes, indicating its lower versatility compared to pillar[4]pyridinium (Figure 96). Thus, P4P@AuNPs and P6P@AuNPs sensors clearly differentiated short and long aliphatic dicarboxylates over medium-length ones.

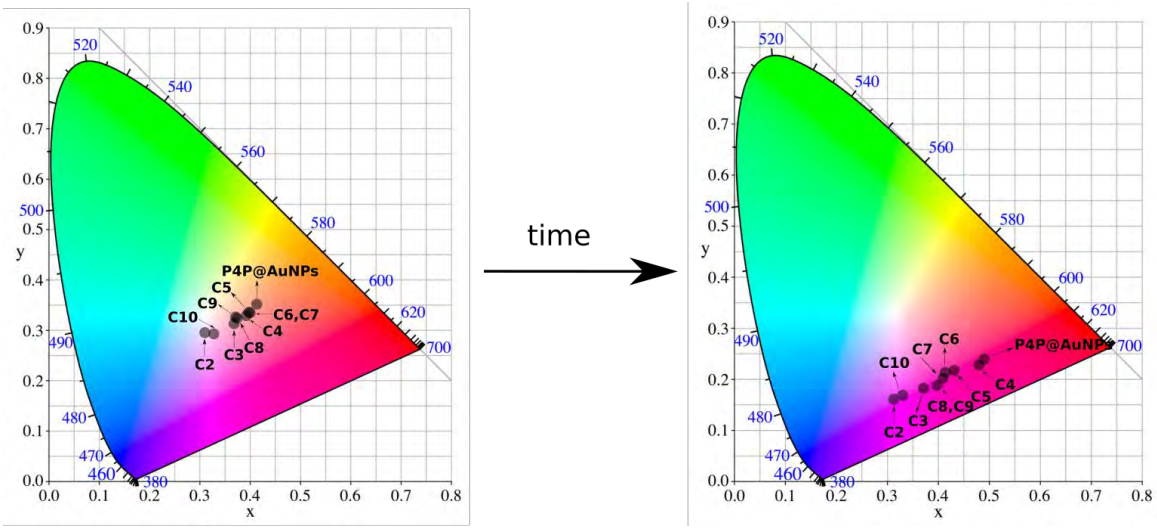

Figure 96. Chromaticity diagrams showing the evolution of color 10 min and 30 min after the addition of diacids (P4P@AuNPs).

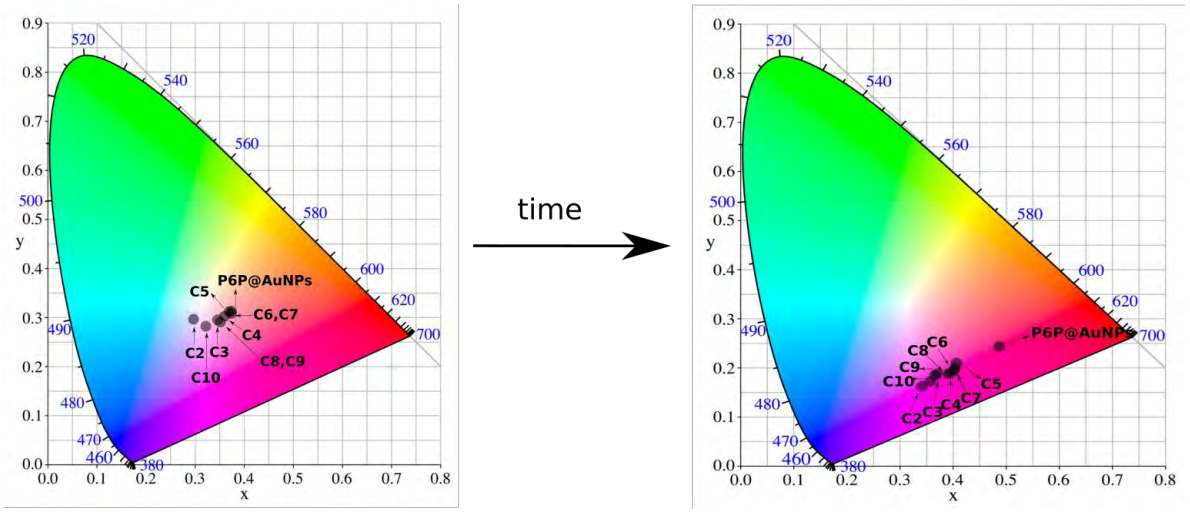

Figure 97. Chromaticity diagrams showing the evolution of color 10 min and 30 min after the addition of diacids (P6P@AuNPs).

UV-Vis spectra of P4P@AuNPs and P6P@AuNPs with aliphatic dicarboxylic acids showed a similar tendency (Figure 98 and Figure 99). The largest shift in the position of the plasmon, which is the measure of nanoparticle interactions, was caused by the shortest diacid (C2). Malonic (C3) and succinic (C4) diacids caused a smaller shift, indicating an increase in the distance between the nanoparticles. However, at a certain point (C4 for P4P@AuNPs and C5 for P6P@AuNPs), the plasmon shift increased, indicating nanoparticle re-approach. The increase in the shift of the plasmon band firstly was slow and boosted at the end (for C10). It is worth mentioning that this trend was general and did not change in time (Figure 100A). The tendency of the change in plasmon intensity was similar (Figure 100B). Additionally, UV-Vis spectra provided the information about the concentration of AuNPs, revealing better stability of C3-C9 analytes compared with C2 and C10 samples. Summary of UV-Vis spectra of P4P@AuNPs and P6P@AuNPs with aliphatic dicarboxylic acids is presented in **Table 1** and **Table 2**.

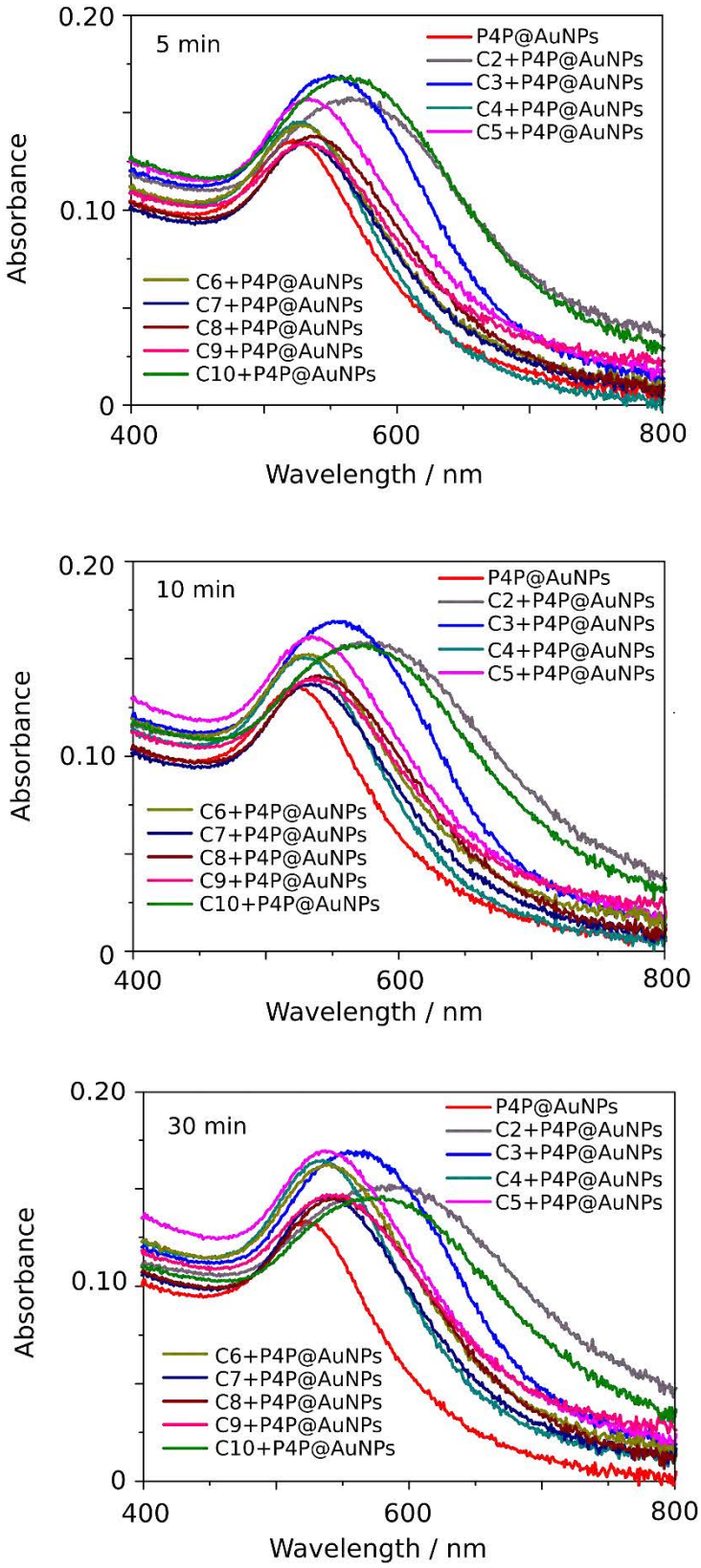

Figure 98. UV-Vis spectra of P4P@AuNPs with diacids at different time intervals.

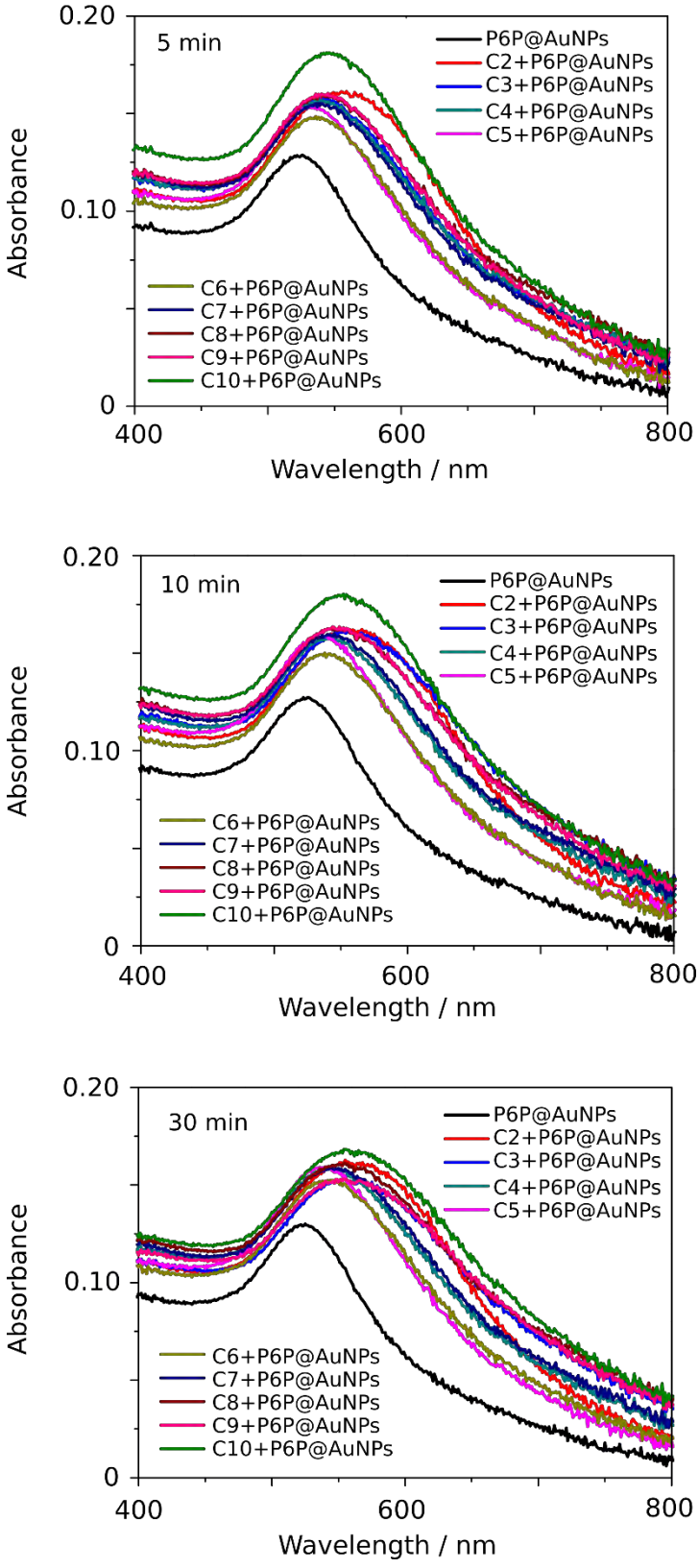

Figure 99. UV-Vis spectra of P6P@AuNPs with diacids at different time intervals.

Table 1. Summary of absorption peaks for P4P@AuNPs-containing samples at different time intervals.

5 min	$\lambda_{max, nm}$	10 min	$\lambda_{max, nm}$	30 min	$\lambda_{max, nm}$
P4P@AuNPs	522	**P4P@AuNPs**	522	**P4P@AuNPs**	522
C2+P4P@AuNPs	575	**C2+P4P@AuNPs**	581	**C2+P4P@AuNPs**	585
C3+P4P@AuNPs	549	**C3+P4P@AuNPs**	551	**C3+P4P@AuNPs**	554
C4+P4P@AuNPs	522	**C4+P4P@AuNPs**	525	**C4+P4P@AuNPs**	535
C5+P4P@AuNPs	534	**C5+P4P@AuNPs**	534	**C5+P4P@AuNPs**	537
C6+P4P@AuNPs	527	**C6+P4P@AuNPs**	535	**C6+P4P@AuNPs**	541
C7+P4P@AuNPs	535	**C7+P4P@AuNPs**	537	**C7+P4P@AuNPs**	540
C8+P4P@AuNPs	540	**C8+P4P@AuNPs**	540	**C8+P4P@AuNPs**	544
C9+P4P@AuNPs	535	**C9+P4P@AuNPs**	540	**C9+P4P@AuNPs**	550
C10+P4P@AuNPs	565	**C10+P4P@AuNPs**	572	**C10+P4P@AuNPs**	579

Table 2. Summary of absorption peaks for P6P@AuNPs-containing samples at different time intervals.

5 min	$\lambda_{max.}$, nm	10 min	$\lambda_{max.}$, nm	30 min	$\lambda_{max.}$, nm
P6P@AuNPs	522	**P6P@AuNPs**	522	**P6P@AuNPs**	522
C2+P6P@AuNPs	559	**C2+P6P@AuNPs**	566	**C2+P6P@AuNPs**	568
C3+P6P@AuNPs	544	**C3+P6P@AuNPs**	552	**C3+P6P@AuNPs**	555
C4+P6P@AuNPs	538	**C4+P6P@AuNPs**	542	**C4+P6P@AuNPs**	545
C5+P6P@AuNPs	532	**C5+P6P@AuNPs**	536	**C5+P6P@AuNPs**	540
C6+P6P@AuNPs	538	**C6+P6P@AuNPs**	538	**C6+P6P@AuNPs**	545
C7+P6P@AuNPs	540	**C7+P6P@AuNPs**	540	**C7+P6P@AuNPs**	545
C8+P6P@AuNPs	540	**C8+P6P@AuNPs**	543	**C8+P6P@AuNPs**	554
C9+P6P@AuNPs	545	**C9+P6P@AuNPs**	549	**C9+P6P@AuNPs**	554

C10+P6P@AuNPs	546	**C10+P6P@AuNPs**	554	**C10+P6P@AuNPs**	556

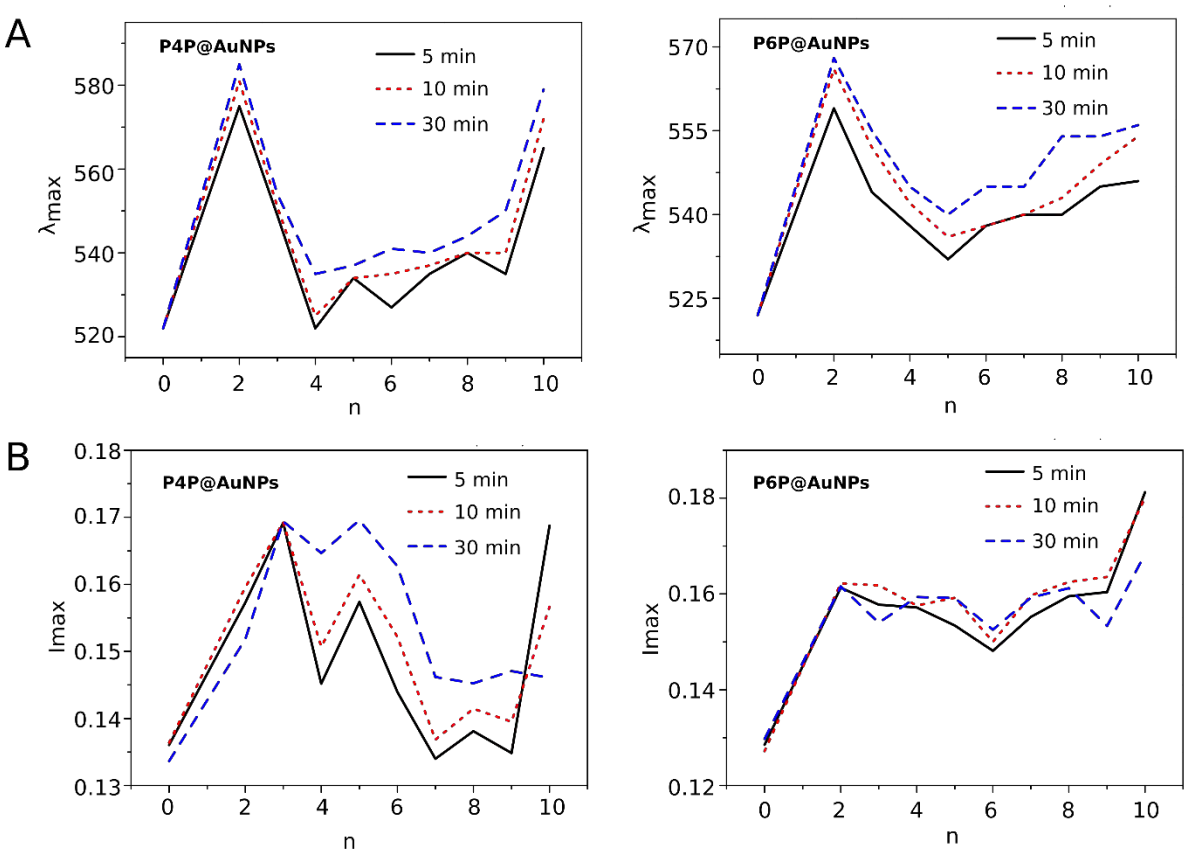

Figure 100. A) Dependencies of plasmon shift with respect to the diacid length (n denotes the number of carbon atoms in the diacid); B) dependencies of plasmon intensity with respect to the diacid length.

The observed trends required further clarification. While the decrease of λ and *I* with the increase of diacid length was understandable, the reverse tendency (after the diacids reached 4-5 carbons length) was quite surprising. This indicated that gold nanoparticles approached to each other, probably through the bending of the aliphatic chain, which is known to happen under hydration.[129-132] To prove the bending of the aliphatic chain, we carried out infrared spectroscopy (IR) measurements for medium length (C5, Figure 101A) and long (C10, Figure 101B) samples. Since the spectra of C5 overlapped with the spectra of the macrocycles, we were able to analyze only the spectra of C10. The experiments showed that the symmetric stretching bands of CH_2 groups in the aliphatic chain were shifted toward the higher frequencies (from 2847 cm^{-1} to 2853 cm^{-1} for P6P@AuNPs and 2855 cm^{-1} for P4P@AuNPs) after the addition of the NPs. This is an indication of the increasing amount of gauche

conformations, present due to the bending of the aliphatic chain.[133,134] The shift induced by the P4P@AuNPs was larger (by 2 cm^{-1}) than that brought by the P6P@AuNPs, indicating stronger bending in the presence of the P4P@AuNPs sensor. This might be due to a deeper inclusion of C10 in the cavity of P6P.

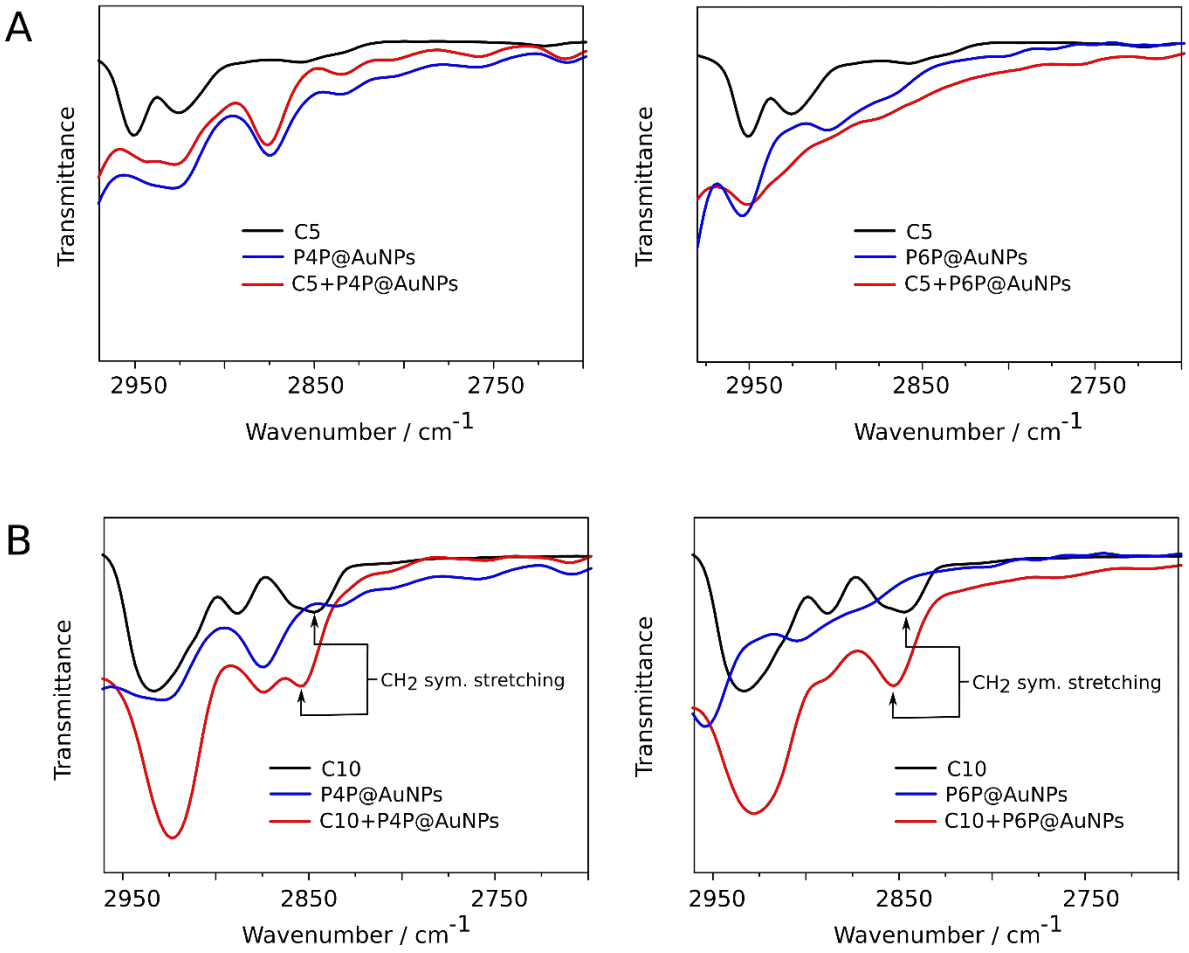

Figure 101. A) Partial Fourier-transform infrared spectroscopy (FTIR) spectra of C5 before and after mixing with the modified gold nanoparticles; B) partial FTIR spectra of C10 before and after mixing with the modified gold nanoparticles.

To get more evidence of the chain bending of aliphatic dicarboxylic acids we imaged the samples on TEM (Figure 102). The detailed analysis of NP aggregates demonstrated that the NPs are closest in the presence of C2. The average interparticle distance for the P4P@AuNPs and the P6P@AuNPs was found to be 0.80 nm and 0.76 nm, respectively. These values were relatively close to theoretical value (1.07 nm, calculated as the sum of the weight of the macrocycle (2×0.417 nm) and the length of the diacid (0.259 nm)). In the case of C5, the NPs were the farthest away from one another (1.17 nm and 1.05 nm found vs. 1.37 nm (obtained

from theoretical calculations), for P4P@AuNPs and P6P@AuNPs, respectively). However, for C10 the distance shortened again 0.89 nm (P4P@AuNPs) and 0.84 nm (P6P@AuNPs), confirming the chain bending. The disparities between the found and calculated values might be due to the inclusion of the carboxylic groups inside the macrocyclic cavity. The shorter distances for P6P@AuNPs (in comparison to P4P@AuNPs) may indicate deeper penetration of the diacids. These results provided an additional proof that the length and flexibility of the aliphatic chain affect the interparticle distance, and, hence, the color of the sample.

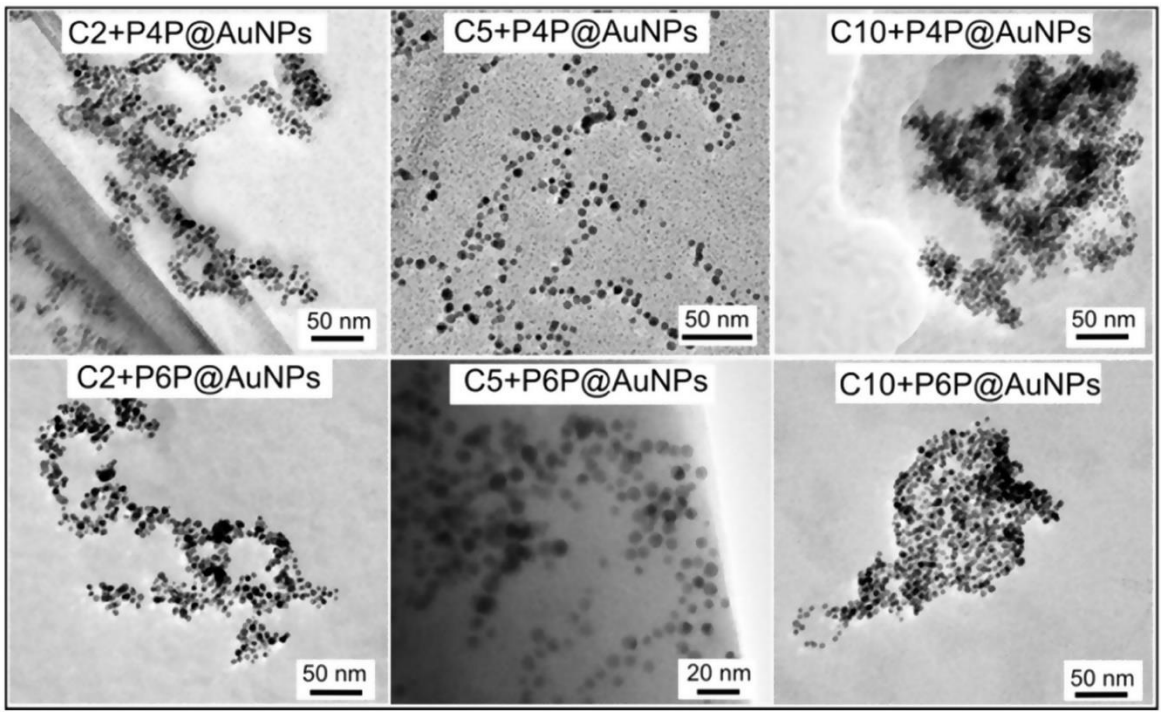

Figure 102. TEM images of the P4P@AuNPs and P6P@AuNPs after mixing with short (C2), medium (C5) and long (C10) diacids.

An interesting observation was also the "zig-zag" structure of the plasmon response (Figure 100A). We attribute this to the odd-even alteration of the aliphatic chain[135], which results in different orientations of the terminal carboxylic groups, and, hence, a non-linear increase in the interparticle distance. Interestingly, the order for the P4P@AuNPs and P6P@AuNPs samples is different, which might be related to the different degree of guests inclusion into the hosts, and subsequent changes in conformation. However, this tendency is noticeable only for weakly aggregated samples (C3-C7). With time, the NP aggregation obscures this effect.

The extent of aggregation of the gold nanoparticles in the presence of aliphatic dicarboxylic acids was measured by DLS (Figure 103A and 103B). In the case of P4P@AuNPs, the largest aggregates were detected in the presence of C2 (766 nm, 5 min) and C10 (336 nm, 5 min). For other diacids (C3-C9), the size of aggregates was much smaller (up to 50 nm). In the presence of P6P@AuNPs, the average size of aggregates was significantly larger for C3-C9 acids, but much smaller for C2 (220 nm) and C10 (287 nm) samples. Similarly to P4P@AuNPs, the gold sols became less stable over time, with increase in the aggregate size (Figure 104). A summary of the extent of the aggregation is shown in **Table 3**.

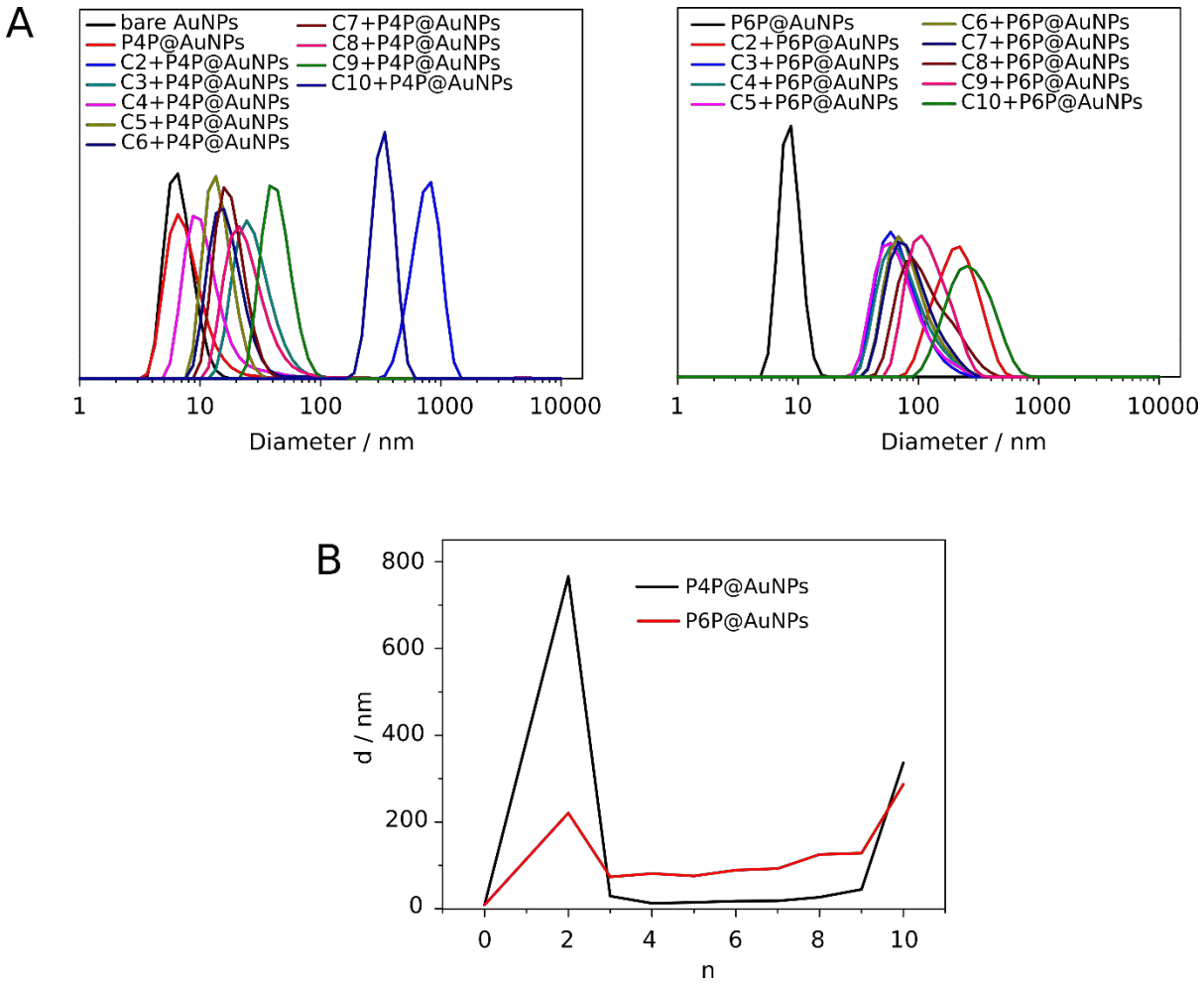

Figure 103. A) Particle size distribution 5 min after mixing the NPs with diacids; B) dependencies of aggregate size on the length of the diacid.

Table 3. Mean particle diameters measured by DLS.

Sample	d, nm	Sample	d, nm
P4P@AuNPs	8,26	**P6P@AuNPs**	8,672
C2+P4P@AuNPs	766,40	**C2+P6P@AuNPs**	220,60
C3+P4P@AuNPs	29,14	**C3+P6P@AuNPs**	73,57
C4+P4P@AuNPs	12,27	**C4+P6P@AuNPs**	81,24
C5+P4P@AuNPs	14,65	**C5+P6P@AuNPs**	75,35
C6+P4P@AuNPs	17,26	**C6+P6P@AuNPs**	89,23
C7+P4P@AuNPs	18,24	**C7+P6P@AuNPs**	92,74
C8+P4P@AuNPs	26,41	**C8+P6P@AuNPs**	125,10
C9+P4P@AuNPs	44,41	**C9+P6P@AuNPs**	127,90
C10+P4P@AuNPs	336,30	**C10+P6P@AuNPs**	287,10

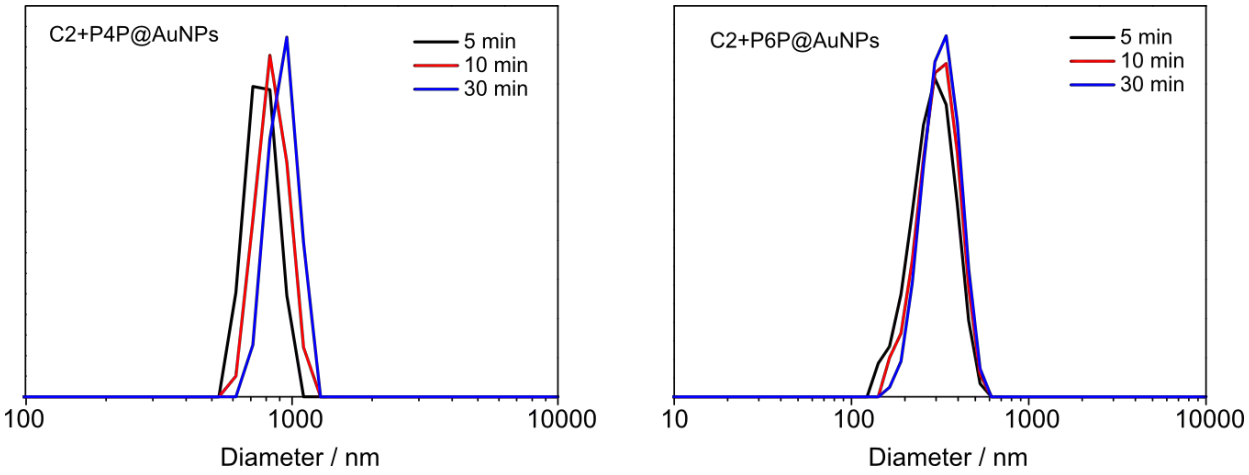

Figure 104. Changes in particle size for the P4P@AuNPs and P6P@AuNPs sensors as time elapsed.

The decrease in stability of the gold nanoparticles after mixing with the aliphatic dicarboxylic acids additionally was confirmed by ξ-potential measurements. It was found that ξ-potential changed from 45 mV (for both macrocycles) to 26-29 mV after the introduction of selected diacids (Figure 105A). Interestingly, in the presence of P6P@AuNPs sensor, ξ-

potentials were slightly lower than those for P4P@AuNPs, indicating the decreased stability (Figure 105B).

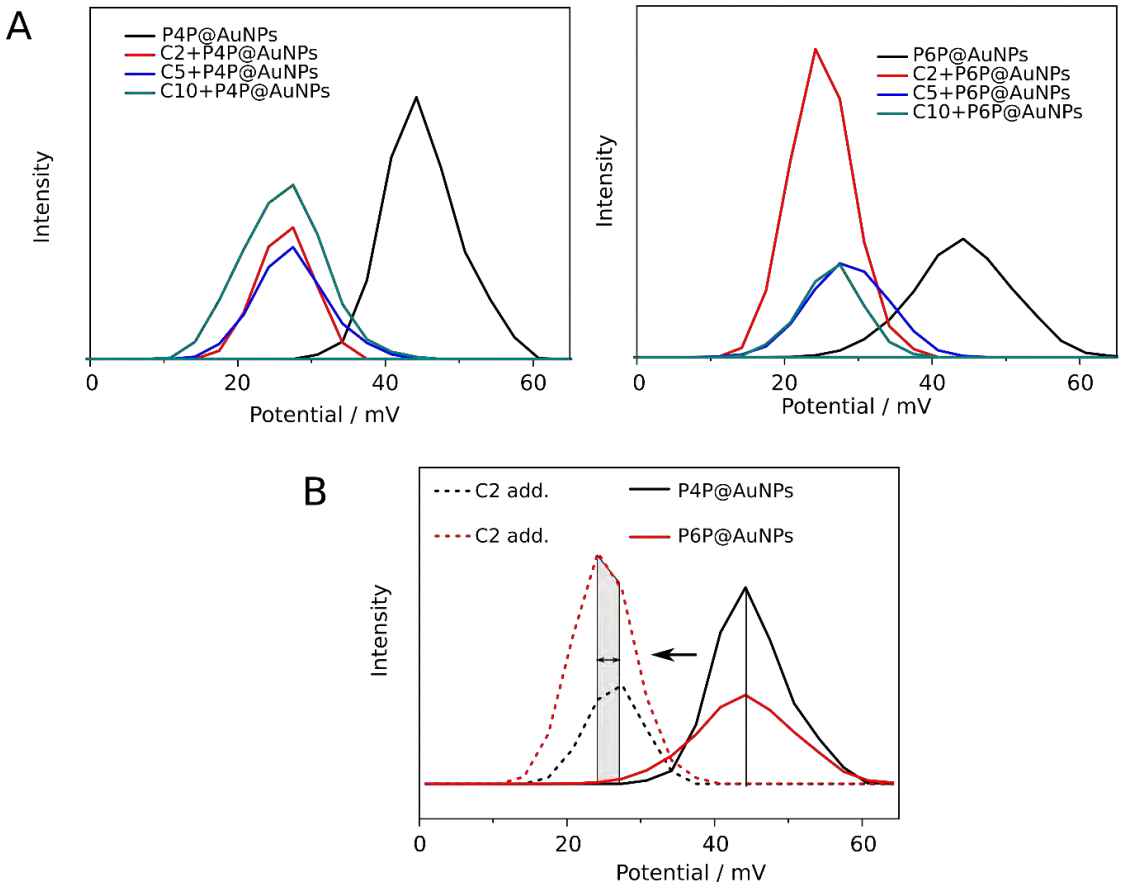

Figure 105. A) Charge distributions of the sample 5 min after mixing the gold nanoparticles with the diacids; B) changes in ξ-potential of the NPs after the addition of C2.

Table 4. Summary of ξ-potentials for different samples.

Sample	ζ-potential, mV	Sample	ζ-potential, mV
P4P@AuNPs	45,0	**P6P@AuNPs**	45,0
C2+P4P@AuNPs	26,9	**C2+P6P@AuNPs**	26,3
C5+P4P@AuNPs	29,0	**C5+P6P@AuNPs**	28,0
C10+P4P@AuNPs	27,2	**C10+P6P@AuNPs**	27,0

Similarly to phthalic acids we attempted to grow single crystals suitable for the X-ray diffraction analysis with C2, C5, C6, and C10 by slow evaporation method. We mixed 19.6 mM aqueous solution of P4P (100 µL) with 100 µL of 19.6 mM solution of C2 (or C5, or C6, or C10) and left the resulting solution for the slow evaporation. Unfortunately, we did not obtain suitable crystals.

2.5 Recognition of geometric isomers

2.5.1 Optical properties of geometric isomers

As model systems we chose three diacids: butendioic acid, azobenzene-4,4'-dicarboxylic acid (ADA) and stilbene-4,4'-dicarboxylic acid (SBDA). Butendioic acid may exist in two forms: *trans* (E) called fumaric acid (Fum) and *cis* (Z) called maleic acid (Mal). Both forms are stable and there is no interconversion between them under normal conditions. On the other hand, ADA and SBDA can be easily interconverted between *trans* and *cis* forms. ADA and SBDA exist predominantly in *trans* form. However, upon 350 nm light exposure, they switch to *cis* configuration. The *trans* isomers may be restored using 430 nm and 254 nm irradiation for ADA and SBDA, respectively (Figure 106).

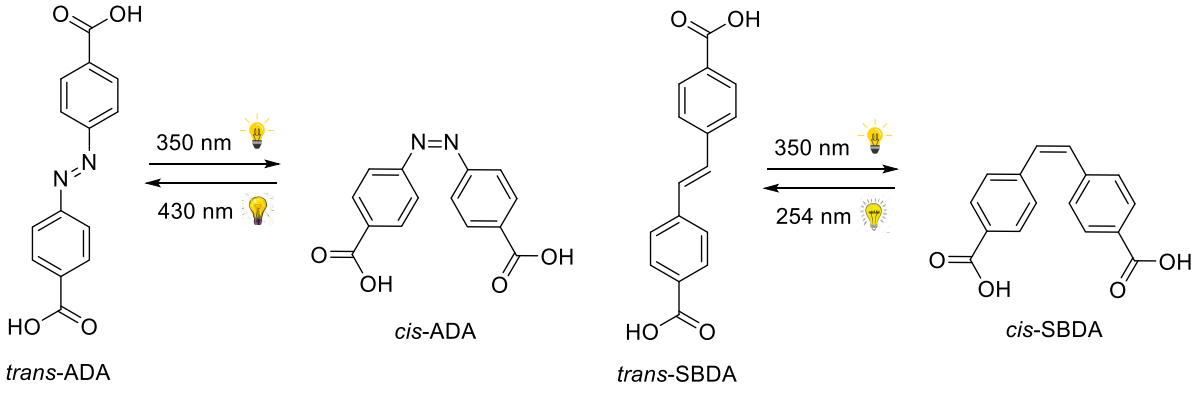

Figure 106. Photoisomerization of ADA and SBDA

Figure 107 shows the UV-Vis spectra of ADA in water. The high-intensity peak at 330 nm belongs to *trans* isomer and is attributed to the π-π^* transition. Irradiation of the solution with UV light (350 nm) results in a decrease of absorbance band with a maximum at 330 nm and the appearance of a new band centered at 430 nm. The latter corresponds to the *cis* isomer, and

is attributed to the n-π^* transition. The main absorption peak of *trans*-SDBA is at 326 nm. Under irradiation with UV light (350 nm), this peak decreases indicating the isomerization to *cis* from. For both acids, the photostationary state, that is, the state in which two forms are in equilibrium, is reached after 10 min of the irradiation.

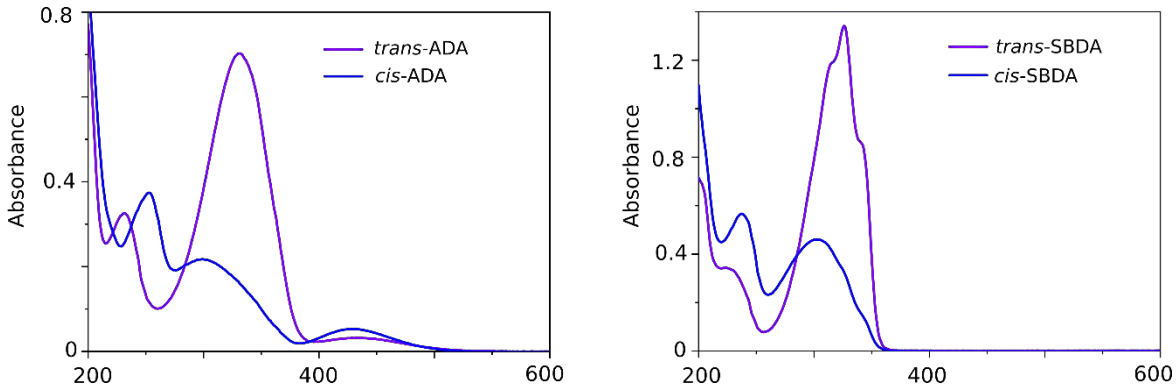

Figure 107. UV-Vis spectra of ADA and SBDA before and after irradiation. The samples were irradiated until the spectra no longer exhibited noticeable changes.

2.5.2 Recognition of E/Z dicarboxylic acids

Since the previous study showed that P6P@AuNPs are less versatile, we continued with the P4P@AuNPs sensor. The diacids were again used in the form of sodium salts. Firstly, we probed the discrimination of the isomers of butendioic acid. For this, we used UV-Vis spectroscopy (Figure 108). A perceivable colorimetric response was obtained with a sevenfold excess of the acid (C =4.5 mM) with respect to the P4P@AuNPs (C=0.6 mM). Only fumaric acid gave a strong shift (+25 nm) and intensity increase (+10%) of the plasmon band, indicating NPs approaching each other and plasmon coupling. The *cis* form (maleic acid) changed the plasmon band only a little (+8 nm) with almost no increase in intensity. Evidently, this is related to the directionality of carboxylic groups (Figure 109). In the case of fumaric acid, carboxylic groups have opposite directions and therefore the space between them is enough to interact with positively charged P4P on the nanoparticle surface. In contrast, maleic acid, whose carboxylic groups lie close to each other and on the same side of the C=C bond, is unable to cross-link gold nanoparticles. DLS analysis revealed the formation of large aggregates (220 nm) for fumaric acid and almost no increase in the particle size for maleic acid (10.11 nm) in

comparison to P4P@AuNPs (9.26 nm). Additionally, we carried out an experiment with monocarboxylic acid (sodium acetate, C=4.5 mM) to confirm the necessity of two opposite carboxylic groups for efficient cross-linking. For acetate (AcONa), only little change in plasmon band was observed (Figure 110).

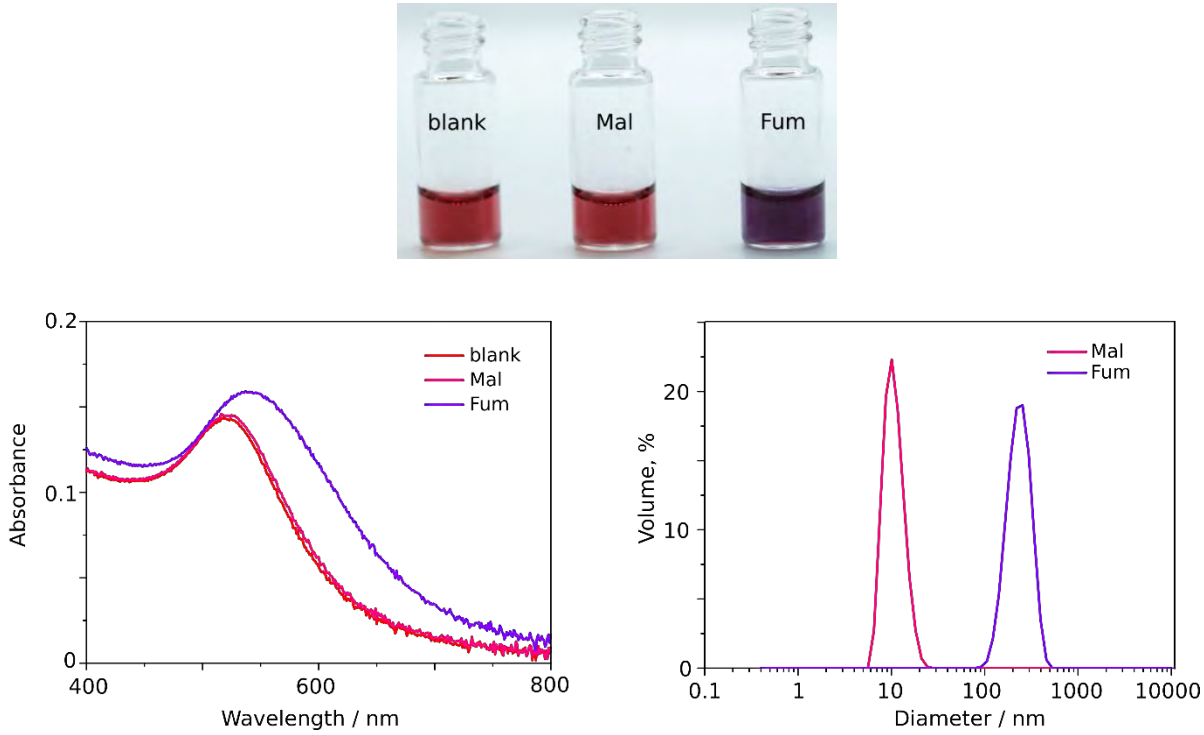

Figure 108. Top: photograph of glass vials filled with P4P@AuNPs taken 10 min after mixing with maleate and fumarate. Bottom: absorption spectra and average particle size of the modified AuNPs after the addition of maleic and fumaric acid.

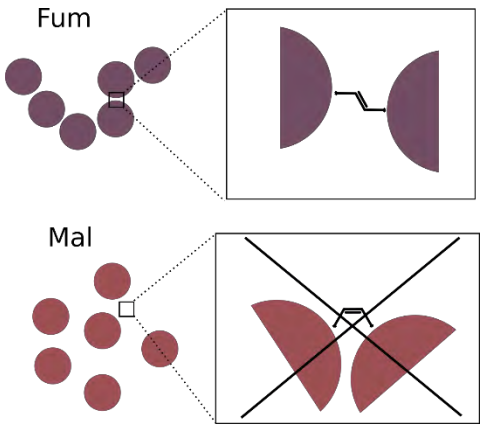

Figure 109. Possible mechanism of interaction of the P4P@AuNPs with fumaric and maleic acids.

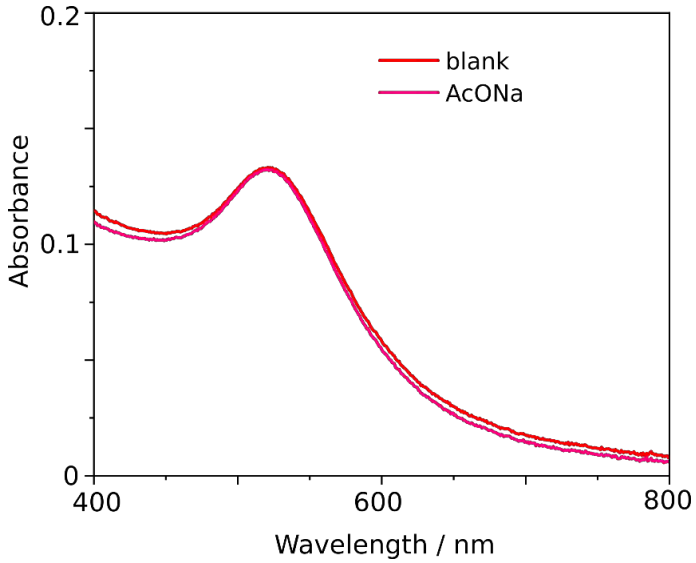

Figure 110. Absorption spectra of the modified AuNPs after the addition of AcONa.

Then, we tested aromatic E/Z dicarboxylic acids (ADA and SBDA, C=0.54 mM). Surprisingly, the sedimentation of the cotton-like red precipitate was observed. This effect occurred regardless of whether the diacids were in *trans* or *cis* forms. Surprisingly, UV-Vis spectra revealed only small changes in plasmon band position, suggesting no or weak interactions between the NPs (Figure 111).

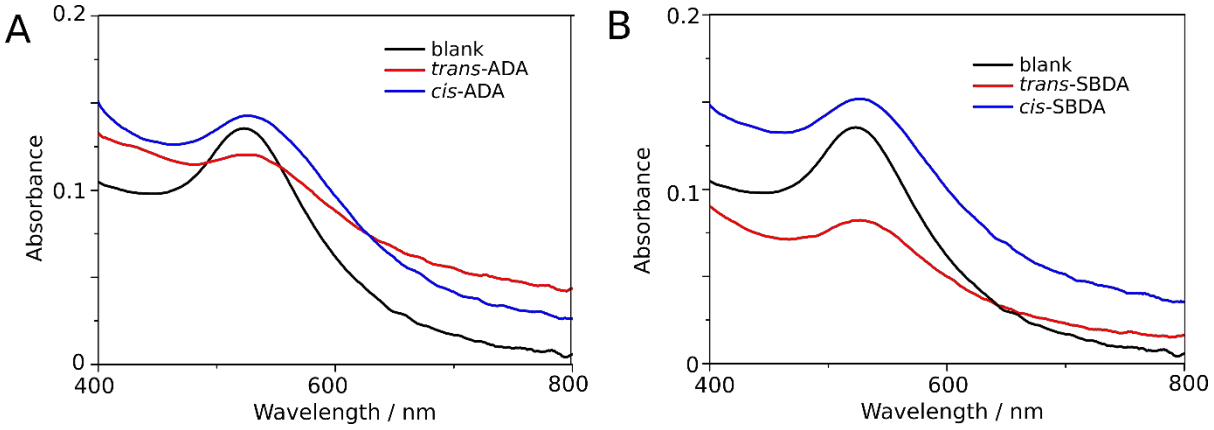

Figure 111. A) Absorption spectra of the P4P@AuNPs after the addition of *trans*-ADA and *cis*-ADA (pH(P4P@AuNPs)=3.2); B) absorption spectra of the P4P@AuNPs after the addition of *trans*-SBDA and *cis*-SBDA (pH(P4P@AuNPs)=3.2).

A TEM examination of the precipitate showed microns long folded ribbons, each consisting of filaments with the average thickness of 1.7 Å and only few NPs around (Figure 112). These

TEM images explained the absence of plasmon coupling between gold nanoparticles and indicated the presence of an organic material. The formation of the ribbons was probably due to the hydrogen bond-mediated self-assembly of protonated ADA and SBDA as well as π-π stacking of the resultant polymeric chains.

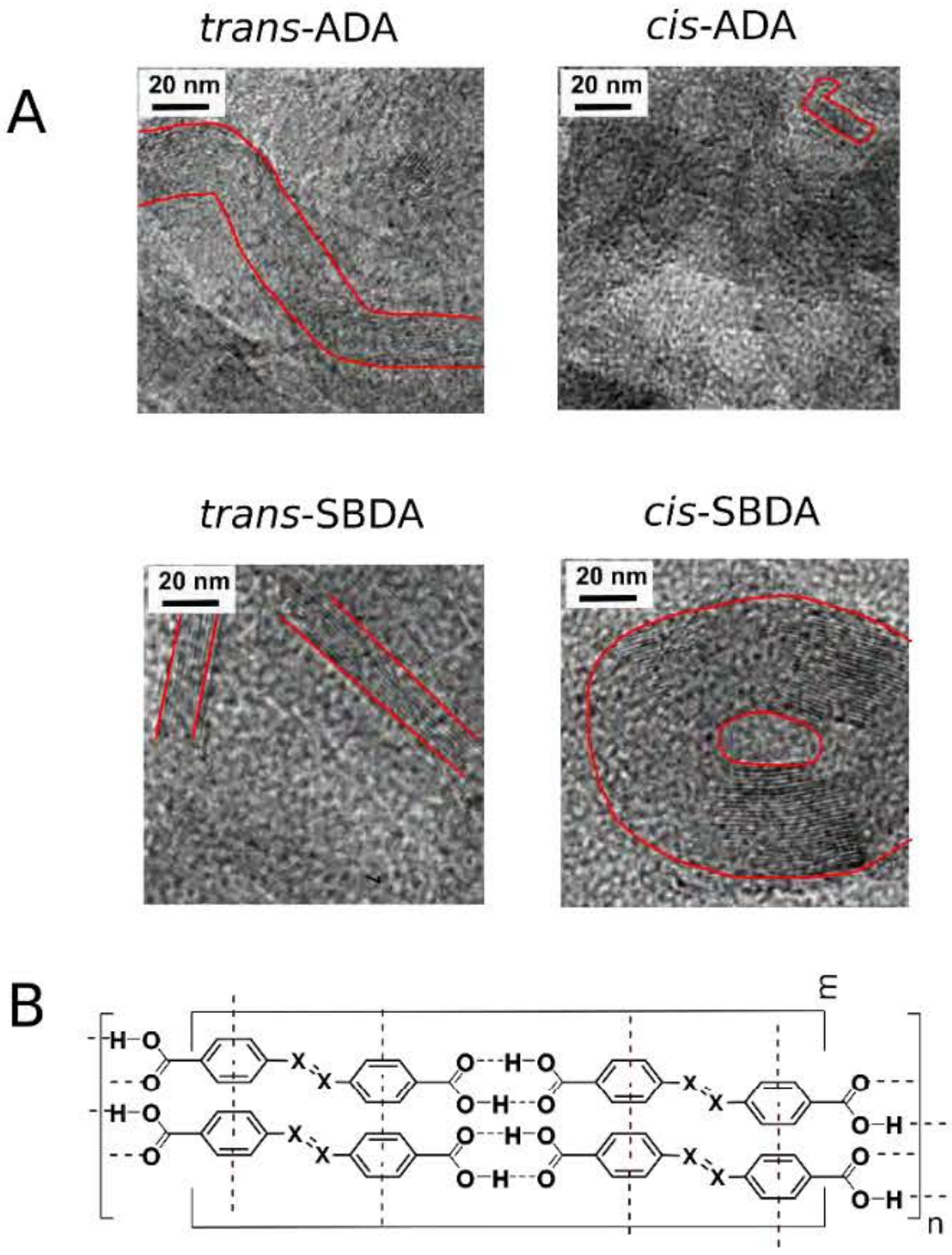

Figure 112. A) TEM images of the cotton-like red precipitates (*trans*- and *cis*-ADA and *trans*- and *cis*-SBDA) (pH(P4P@AuNPs)=3.2). The edges of the ribbons are highlighted by the red lines; B) possible chemical structure of the cotton-like red precipitate.

Since at low pH we observed protonation and precipitation of the diacids, we decided to increase the pH of the initial P4P@AuNP solutions from 3.2 to 4.25. This allowed us to deprotonate the diacids and unable their interactions with the NPs (Figure 113). Due to the shorter distance between the carboxylic groups, *cis* isomers gave stronger shifts of the plasmon band than *trans* isomers (+36 nm (*cis*-ADA) vs. +32 nm (*trans*-ADA) and +36 nm (*cis*-SBDA) vs. +29 nm (*trans*-SBDA)). In addition, we increased the pH of the initial solutions to 4.25 for fumaric and maleic acids. In this case, much larger shifts for both fumaric (+50 nm) and maleic (+20 nm) acids were also observed (Figure 114).

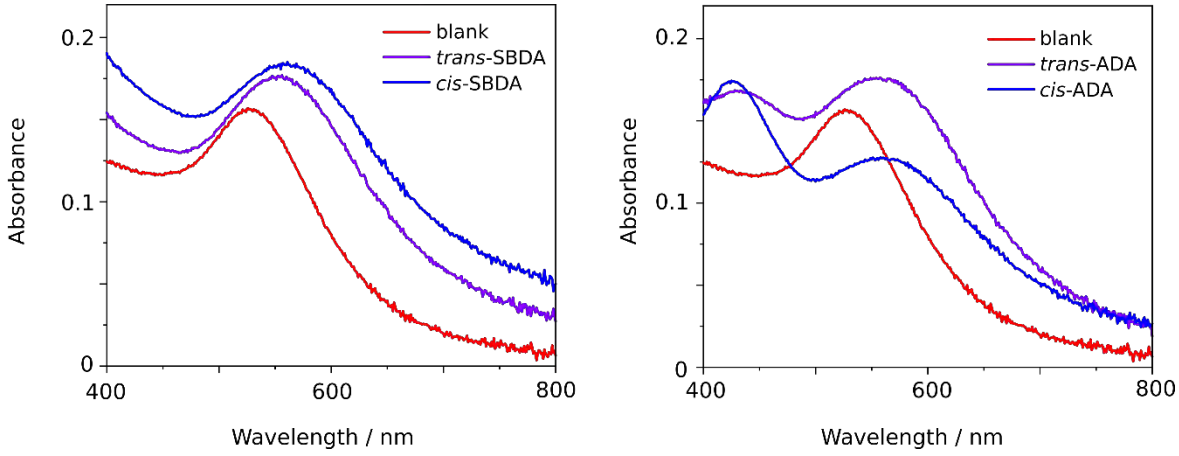

Figure 113. Absorption spectra of the P4P@AuNPs 10 min after the addition of isomeric SBDA and ADA at a higher pH.

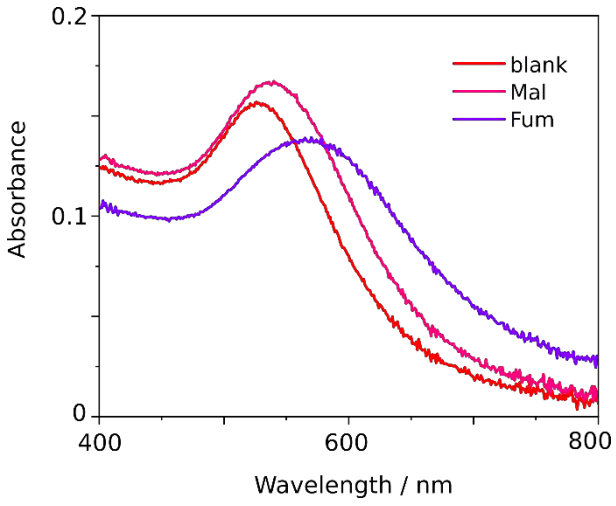

Figure 114. Absorption spectra of the P4P@AuNPs 10 min after the addition of Fum and Mal acids at a higher pH.

These shifts indicated that in addition to the aggregation triggered by the gold nanoparticle cross-linking ("specific" aggregation), there is also an aggregation induced by the pH increase, probably due to the positive surface charge neutralization and NP attraction ("nonspecific" aggregation). To confirm the occurrence of the second type of aggregation we performed experiments at different pH values for the neat colloid without the E/Z diacids (Figure 115). Firstly, we increased the pH of the P4P@AuNPs solution to 4.5, which resulted in a slight bathochromic shift of the plasmon (+4 nm) and an insignificant increase in its intensity (5.5%). DLS analysis revealed almost no difference in the nanoparticle size (9.69 nm vs. 9.26 nm) but considerable decrease in ξ-potential (29.8 mV vs. 43.1 mV). Then, we adjusted the pH of the gold sol to 6.5. Again, UV-Vis spectrum showed only a small change in the plasmon band (+5 nm), but a noticeable increase in intensity (15.8 %). Additionally, DLS measurement indicated the formation of small aggregates (22.0 nm) and further decrease in ξ-potential (27.5 mV). Finally, we increased the pH of the solution to 7.5 and measured the UV-Vis spectrum, which revealed a further shift of the plasmon band (+12 nm) and intensity increase (22.3%). Under these conditions, even larger aggregates (32.9 nm) were detected by DLS analysis (Figure 116). These results confirm that pH affects the stability of the colloid, however, its contribution to overall aggregation is not significant. That is, the crucial role in the aggregation is played by E/Z dicarboxylic acids ("specific" aggregation). This is clearly seen for butendioic acid isomers. Maleic acid sample despite the higher final pH of the solution (pH=6.59), aggregated to much lower extent than fumaric acid (pH=5.35) (Figure 114).

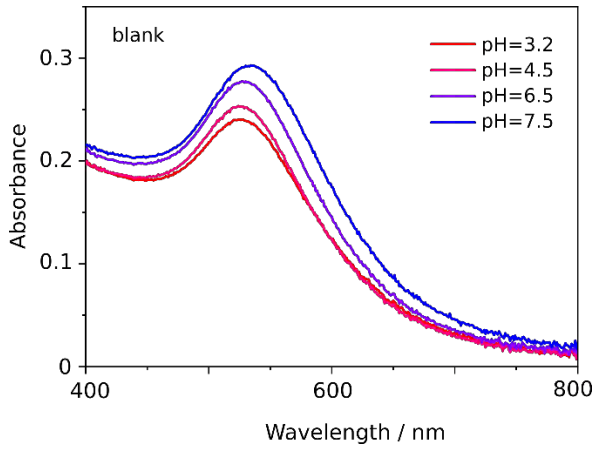

Figure 115. Absorption spectra of the P4P@AuNPs at different pHs.

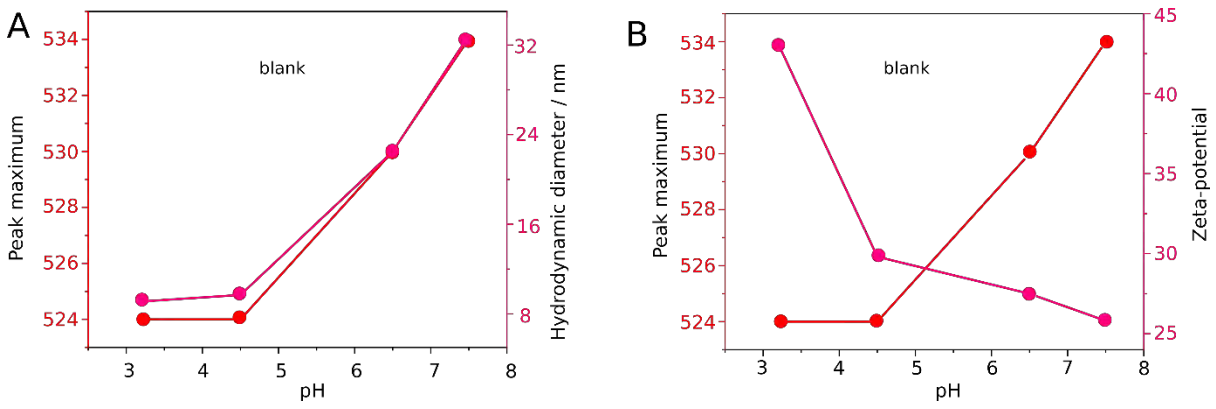

Figure 116. A) Absorption peak maximum and hydrodynamic size at different pH values; B) absorption peak maximums and ξ-potential at different pH values.

The aggregation of samples containing ADA and SBDA was monitored by DLS (Figure 117). Interestingly, the average size of *cis*-aggregates was larger than for *trans*-aggregates, 340 nm vs. 150 nm for ADA and 450 nm vs. 270 nm for SBDA, respectively.

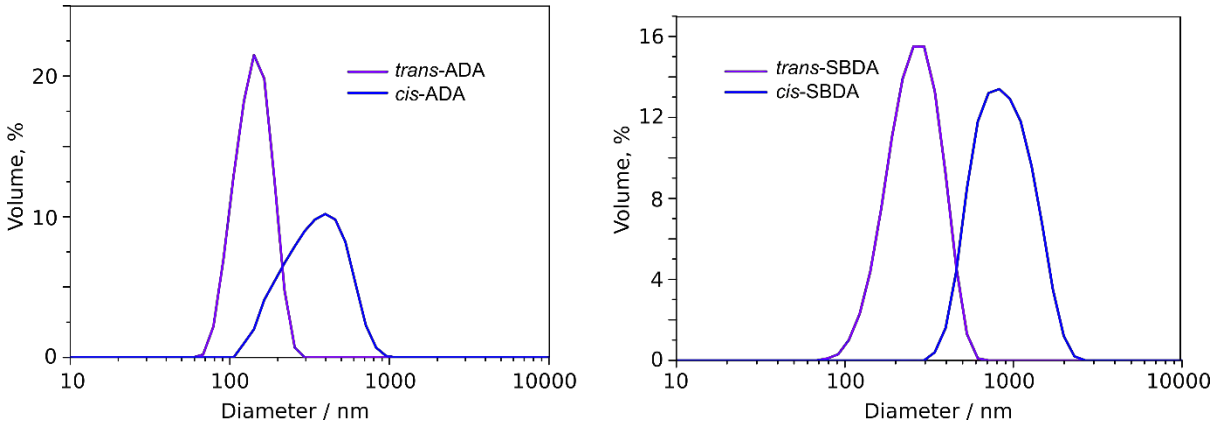

Figure 117. Particle size distribution 5 min after mixing the P4P@AuNPs with ADA and SBDA.

The different size of aggregates may be explained by better surface charge neutralization in *cis* form (Figure 118). This is supported by ξ-potential measurements. The solution containing *trans*-ADA gave 15.7 mV while *cis*-ADA afforded 14.4 mV. Off note, the potentials were not measured for SBDA due to the absence of a cell able to transmit 254 nm light.

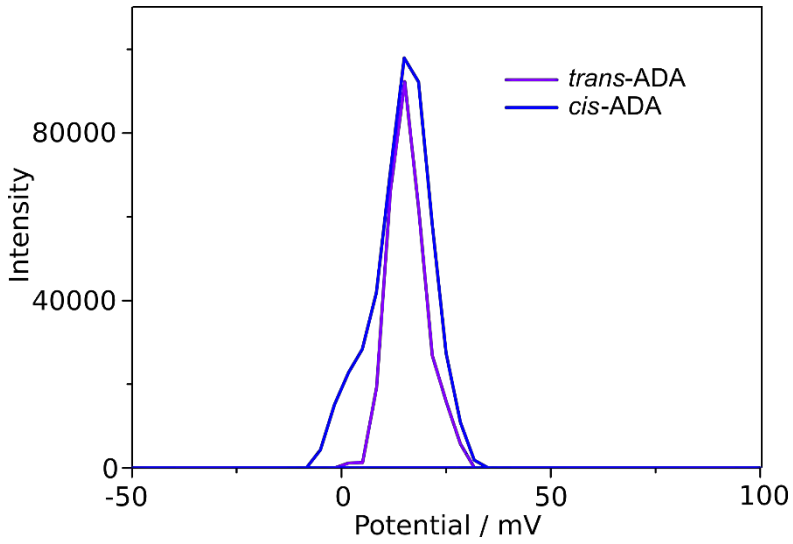

Figure 118. ξ-potential of the P4P@AuNPs solution in the presence of ADA.

2.5.3 Nanoparticle self-assembly

Considering that both ADA and SBDA can be easily interconverted between *cis* and *trans* configurations upon irradiation, we thought to utilize this property in reversible nanoparticle self-assembly. This is usually done by covalently attaching molecular photoswitches to the NP surface.[136] We hypothesized that the P4P@AuNPs sensor could open up the opportunity to perform the process noncovalently using ADA and SBDA as a photoresponsive medium.[137-140]

To make the NPs more stable, we diluted the colloidal solutions threefold. We started with the experiments using ADA. To switch from *trans* to *cis* isomer we irradiated the sample with 350 nm monochromatic light from an arc lamp with a bandwidth of 20 nm, installed in an RF 6000 fluorometer at a distance of 5 cm for 10 min. To restore the *trans* isomer, we used the same set up with 430 nm monochromatic light. In the case of SBDA, 350 nm light was used to switch from *trans* to *cis* forms, and 254 nm light for the reverse process. In that way, we managed to assemble and disassemble the NPs into larger and smaller aggregates at least three times in a row (Figure 119). For both samples, the average aggregate size increased after the first cycle, but then, depending on the diacid, the size of aggregate remained unchanged (SBDA) or increased further (ADA). This may again be explained by different contributions of "nonspecific" aggregation. Indeed, the final pH of the solution containing the ADA sample was more basic (6.88) than that containing the SBDA (6.69). The destabilization and partial

temporal restoration of the gold sol in the presence of ADA, upon light illumination was also corroborated by ξ-potential experiments (Figure 120). Importantly, the gold nanoparticles can be assembled and disassembled starting not only from the *trans* but also from the *cis* form, which renders the system highly versatile.

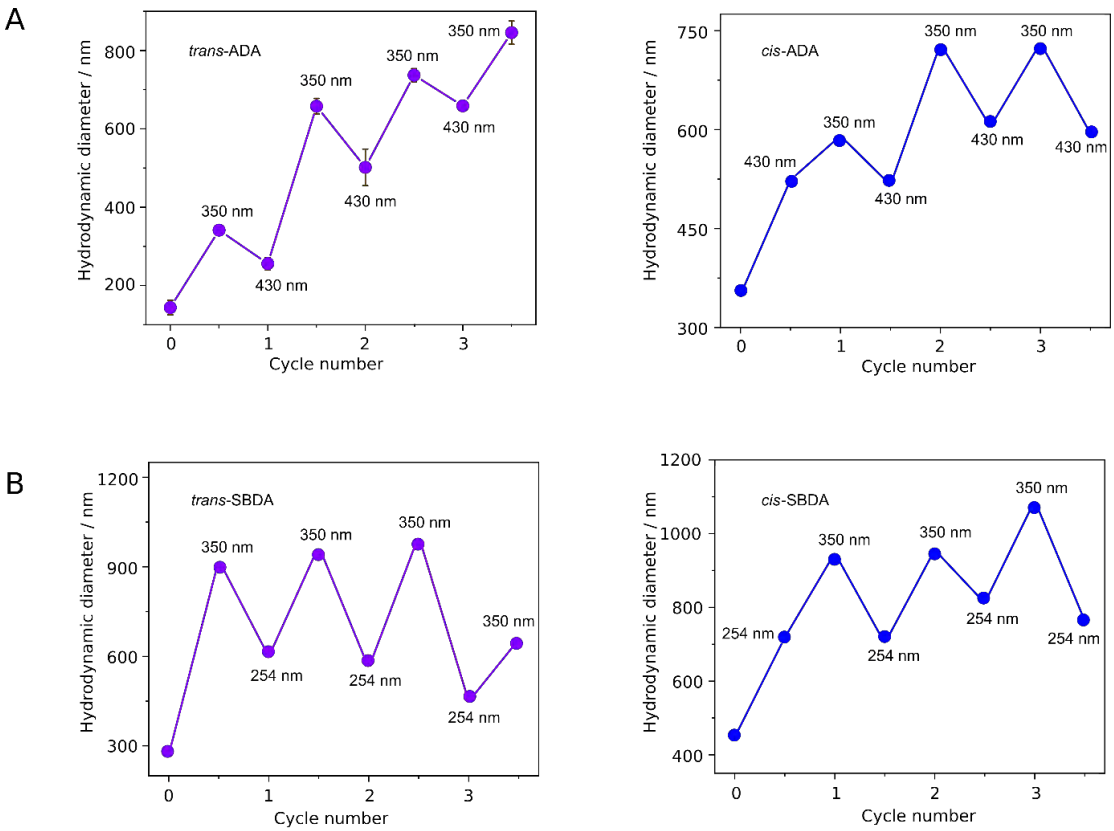

Figure 119. Changes in average particle size upon alternate irradiation of ADA (A) and SBDA (B) containing samples.

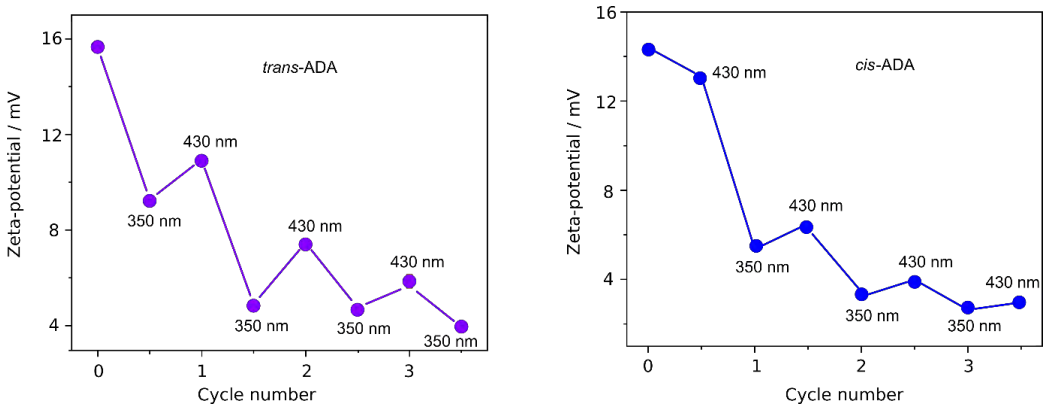

Figure 120. Changes in average ξ-potential upon alternate irradiation of ADA sample.

Finally, the changes induced by ADA and SBDA were clearly seen in TEM images, which revealed the presence of on average larger aggregates in the samples containing the *cis* forms of the diacids (Figure 121).

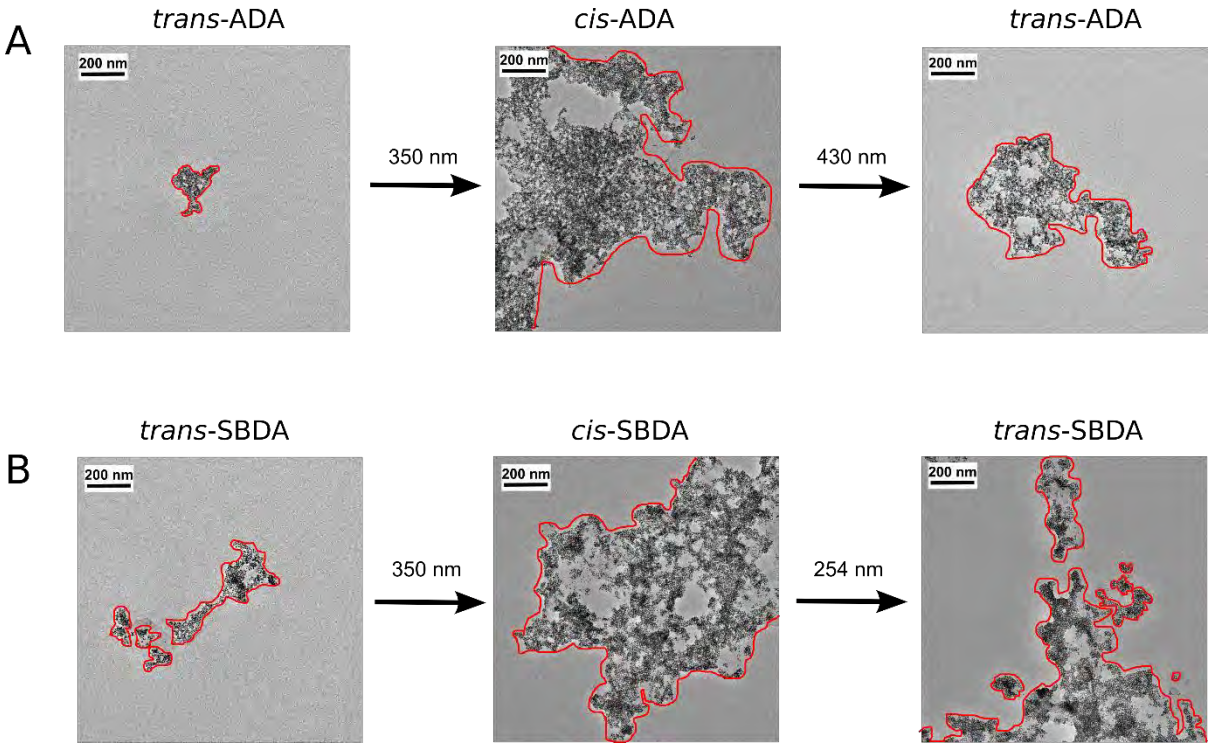

Figure 121. A) TEM images of the *trans*-ADA sample after subsequent ultraviolet and visible light irradiation; B) TEM images of the *trans*-SBDA sample after subsequent ultraviolet and blue light irradiation. The edges of aggregates are highlighted by red lines.

3. EXPERIMENTAL PART

3.1 General information

Quartz cuvettes were purchased from Hellma Analytics, a disposable folded capillary cell (DTS 1070) for ξ-potential measurement and regular polystyrene cuvettes for particle size measurements from Malvern Panalytical, TEM grids from Ted Pella.

UV-Vis spectra were recorded on Evolution 220 spectrophotometer from Thermo Scientific. TEM images were taken with FEI TECNAI and analysed by ImageJ. DLS and ξ-potential were measured on Malvern Zetasizer NANO. FTIR spectra were recorded on a Shimadzu IRTracer-100 spectrometer. Color coordinates for CIE diagrams were determined by taking the photographs of the sample and using Microsoft Paint software. pH was measured using a HI 3220 pH meter equipped with an InLab Micro glass electrode (Mettler Toledo). X-ray data were collected at 100 K on the SuperNova Agilent diffractometer using CuK_α radiation (λ = 1.54184 Å) and processed with CrysAlisPro. Solution and refinement of the structure were done using the programs integrated in WinGX software system. Structure was solved and refined using SHELX-2013. Chemical structures were drawn using ChemDraw 20.1. UV-Vis, FTIR, DLS, TEM data were processed using Origin software.

All chemicals, except *trans*-ADA[141] and pillar[n]pyridiniums[22,120] synthesized by us, were purchased as a reagent grade from commercial suppliers and used without further purification. All experiments were performed at room temperature unless noted otherwise. Deionized water (18.3 MΩ cm) was obtained from Milli-Q station.

3.2 Synthesis and modification of gold nanoparticles

Synthesis of "naked" gold nanoparticles

To a stirred solution of 495 μL (24.3 mM) aqueous $HAuCl_4$ solution in 10 mL of water, 600 μL of 100 mM freshly prepared aqueous $NaBH_4$ solution was added in a single injection. The final solution was stirred for 2 min and left for two days to allow unreacted BH_4^- ions to decompose.

Synthesis of P4P (P6P) coated gold nanoparticles

To a stirred solution of 100 μL (58.82 mM) aqueous pillar[4]pyridinium (P4P) or pillar[6]pyridinium (P6P) chloride salt solution 1200 μL of the "naked" 1.08 mM gold nanoparticles (in terms of gold atoms) were added in 200 μL portions in 10 s intervals with constant stirring for 2 min. The obtained solution was immediately used for sensing applications.

Synthesis of TMA coated gold nanoparticles

To a stirred solution of 100 μL (13.0 mM) aqueous TMA solution 1200 μL of the "naked" 1.08 mM gold nanoparticles (in terms of gold atoms) were added in 200 μL portions in 10 s intervals with constant stirring for 2 min. The obtained solution was immediately used for sensing applications.

3.3 Acids sensing

Phthalic acid isomers sensing by P4P-coated AuNPs

The P4P-coated gold nanoparticles solution was divided into 300 μL portions. To each portion 140 μL (5 mM) of a single acid (1,2-acid, 1,3-acid and 1,4-acid) was added, in the form of sodium salt. Accordingly, blank solution was diluted with the same volume of pure water.

Phthalic acid isomers sensing by TMA-coated AuNPs

The TMA-coated gold nanoparticles solution was divided into 300 μL portions. To each portion 140 μL (5 mM) of a single acid (1,2-acid, 1,3-acid and 1,4-acid) was added, in the form of sodium salt. Accordingly, blank solution was diluted with the same volume of pure water.

α,ω-Alkanedicarboxylic acids sensing by P4P-coated AuNPs and P6P-coated AuNPs

The P4P-coated gold nanoparticles and P6P-coated gold nanoparticles solutions were divided into 300 μL portions. To each portion 240 μL (9 mM) of a single acid (C2-C10) was added, in the form of sodium salt. Accordingly, blank solutions were diluted with the same volume of pure water.

Geometric dicarboxylic acids sensing by P4P-coated AuNPs

The P4P-coated gold nanoparticles solution was divided into 300 μL portions. To each portion a single acid (200 μL; 11 mM in the case of fumaric and maleic acids, and 0.433 mM in the case of ADA and SBDA) was added. Accordingly, blank solutions were diluted with the same volume of pure water.

UV-Vis measurements

The obtained solutions (with and without the diacids) were transferred in 300 μL quartz cuvettes and spectra were recorded.

DLS measurements

The obtained solutions were transferred in 3 mL polystyrene cuvettes and diluted threefold. The average size of particles was recorded for PnPs@AuNPs before and after the addition of the dicarboxylic acids.

ξ-Potential measurements

The obtained solutions were transferred in 1 mL folded capillary cells and diluted twice. The charge of particles was recorded for PnPs@AuNPs before and after the addition of the dicarboxylic acids.

TEM analysis

The resultant solutions were diluted by 25 times. In every case 1 μL of the final solution was deposited and dried on TEM grids for further analysis.

IR analysis

The solutions containing C5 and C10 diacids were concentrated under a vacuum and dried. All samples were analyzed by the ATR method on a ZnSe support.

CONCLUSIONS AND FUTURE PROSPECTS

We developed a versatile nanosensor that can recognize and, in some cases, visualize homologous and isomeric dicarboxylic diacids.

The sensor was prepared by mixing ≈4 nm gold nanoparticles with P4P or P6P macrocycles in aqueous solutions. In the case of phthalic acids, which are positional isomers, the visual discrimination of each acid is possible. This is due to different directionality of carboxylic groups which through electrostatic attractions interact with the adsorbed macrocycles and cross-link the NPs (with the exception of 1,2-acid) giving a distinct plasmonic response for each acid, and hence a change in color.

In the case of homologous aliphatic dicarboxylic diacids, where the carboxylic groups have practically the same directionality, the differences in a plasmonic response were not so pronounced. Therefore, we were only able to visually discriminate the shortest and the longest acids from the medium-length acids. For the recognition of remaining acids, UV-Vis spectroscopy was necessary. Interestingly, the changes in the plasmon band varied non-linearly with the elongation of the aliphatic chain, allowing the sensor to probe its bending and odd-even character. These studies also revealed that the system based on P4P is superior over the one containing P6P, most likely due to larger size and higher charge of the latter, resulting in lower versatility.

The last group of the diacids we studied were geometric isomers. In this type of isomerism, carboxylic groups are differently oriented in *trans* and *cis* configurations. Therefore, we obtained a strong color change for fumaric acid, and no changes for maleic acid. For other diacids (ADA and SBDA), the orientation of the carboxylic groups was less important, as the acid lengths enabled cross-linking the NPs in both cases. Thus, to see the optical changes, UV-Vis spectroscopy had to be used. On the other hand, the changes in the orientation and charge were enough to cause considerable aggregation, opening the opportunity to utilize these acids for reversible control of the dispersion state of the nanoparticles with light.

We foresee that the use of the sensor is not only limited to the recognition of carboxylic moieties, and can be extended for other anionic groups. This opens up the opportunity for differentiating other types of chemically similar compounds.

REFERENCES

1. He, X.; Huang, X. H. H.; Chow, K. S.; Wang, Q.; Zhang, T.; Wu, D.; Yu, J. Z., Abundance and Sources of Phthalic Acids, Benzene-Tricarboxylic Acids, and Phenolic Acids in PM2.5 at Urban and Suburban Sites in Southern China. *ACS Earth and Space Chemistry* **2018,** *2* (2), 147-158.

2. Tan, W.; Zhang, Y.; He, X.; Xi, B.; Gao, R.; Mao, X.; Huang, C. Zhang, H.; Li, D.; Liang, Q.; Cui, D.; Alshawabkeh, A. N., Distribution patterns of phthalic acid esters in soil particle-size fractions determine biouptake in soil-cereal crop systems. *Scientific Reports* **2016,** *6* (1), 31987.

3. Liu, X.; Shi, J.; Bo, T.; Zhang, H.; Wu, W.; Chen, Q.; Zhan, X., Occurrence of phthalic acid esters in source waters: a nationwide survey in China during the period of 2009–2012. *Environmental Pollution* **2014,** *184*, 262-270.

4. Matsumoto, M.; Hirata-Koizumi, M.; Ema, M., Potential adverse effects of phthalic acid esters on human health: A review of recent studies on reproduction. *Regulatory Toxicology and Pharmacology* **2008,** *50* (1), 37-49.

5. Yen, Y.-P.; Ho, K.-W., Development of colorimetric receptors for selective discrimination between isomeric dicarboxylate anions. *Tetrahedron Letters* **2006,** *47* (41), 7357-7361.

6. Tseng, Y.-P.; Tu, G.-M.; Lin, C.-H.; Chang, C.-T.; Lin, C.-Y.; Yen, Y.-P., Synthesis of colorimetric sensors for isomeric dicarboxylate anions: selective discrimination between maleate and fumarate. *Organic & Biomolecular Chemistry* **2007,** *5* (22), 3592-3598.

7. Chatterjee, A.; Oh, D. J.; Kim, K. M.; Youk, K.-S.; Ahn, K. H., Selective Colorimetric Sensing of Geometrical Isomers of Dicarboxylates in Water by Using Functionalized Gold Nanoparticles. *Chemistry – An Asian Journal* **2008,** *3* (11), 1962-1967.

8. Zhang, Z.; Hashim, M. I.; Wu, C.-H.; Wu, J. I.; Miljanić, O. Š., Discrimination of dicarboxylic acids via assembly-induced emission. *Chemical Communications* **2018,** *54* (82), 11578-11581.

9. Chen, W.; Guo, C.; He, Q.; Chi, X.; Lynch, V. M.; Zhang, Z.; Su, J.; Tian, H.; Sessler, J. L., Molecular Cursor Caliper: A Fluorescent Sensor for Dicarboxylate Dianions. *Journal of the American Chemical Society* **2019,** *141* (37), 14798-14806.

10. Qin, D.-B.; Xu, F.-B.; Wan, X.-J.; Zhao, Y.-J.; Zhang, Z.-Z., Effectively selective fluorescent chemosensor for terephthalate. *Tetrahedron Letters* **2006,** *47* (32), 5641-5643.

11. Yoon, J.; Jadhav, J. R.; Kim, J. M.; Cheong, M.; Kim, H.-S.; Kim, J., Electrochemical

discrimination of phthalic acid among three phthalic acid isomers based on an N-butylaminomethyl-ferrocene derivative. *Chemical Communications* **2014,** *50* (57), 7670-7672.

12. Hernandez, S.; Perales-Rondon, J. V.; Heras, A.; Colina, A., Enhancement factors in electrochemical surface oxidation enhanced Raman scattering. *Electrochimica Acta* **2021,** *380*, 138223.

13. Cui, X.; Delgado, R.; Carapuça, H. M.; Drew, M. G. B.; Félix, V., Carboxylate anions binding and sensing by a novel tetraazamacrocycle containing ferrocene as receptor. *Dalton Transactions* **2005,** (20), 3297-3306.

14. Hamase, K.; Nakamura, H.; Nakajima, T., Curdlan Gel, Evaluated as a Polysaccharide Support by Electrophoresis of Substituted Benzenes. *Analytical Sciences* **1993,** *9* (6), 799-802.

15. Bhattacharjee, S.; Bhattacharya, S., Phthalate mediated hydrogelation of a pyrene based system: a novel scaffold for shape-persistent, self-healing luminescent soft material. *Journal of Materials Chemistry A* **2014,** *2* (42), 17889-17898.

16. Comba, P.; Lampeka, Y. D.; Prikhod'ko, A. I.; Pritzkow, H., A New Receptor of Aromatic Carboxylates Based on a Trismacrocyclic Complex of Copper(II) and Operating According to the Molecular Recognition Principle. *Theoretical and Experimental Chemistry* **2001,** *37* (4), 236-240.

17. Kalita, D.; Baruah, J. B., 1-Phenyl-3-(quinolin-5-yl)urea as a host for distinction of phthalic acid and terephthalic acid. *Journal of Chemical Sciences* **2013,** *125* (2), 267-273.

18. Sannasy, D.; Marques, H. M.; Fernandes, M. A.; de Sousa, A. S., Outer-sphere anion recognition by a cyclen-based octadentate europium(iii) complex: pH dependent recognition of ortho-phthalic acid. *Chemical Communications* **2014,** *50* (13), 1582-1584.

19. Užarević, K.; Halasz, I.; Đilović, I.; Bregović, N.; Rubčić, M.; Matković-Čalogović, D.; Tomišić, V., Dynamic Molecular Recognition in Solid State for Separating Mixtures of Isomeric Dicarboxylic Acids. *Angewandte Chemie International Edition* **2013,** *52* (21), 5504-5508.

20. Duran, M.; Arar, Ö.; Arda, M., REMOVAL OF PHTHALIC ACID AND ISOPHTHALIC ACID FROM AQUEOUS SOLUTION BY ANION EXCHANGE RESIN. *Journal of the Chilean Chemical Society* **2019,** *64*, 4399-4403.

21. Ma, H.; Luo, D.; Zhao, Q.; Liu, R.; Zhang, Z.; Hou, X.; Sun, X.; Wang, Y., Crown ether and crown ether/K+ complex assisted DOSY NMR: A versatile tool for positional isomers identification in aqueous solution. *Journal of Molecular Liquids* **2022,** *345*, 117884.

22. Kosiorek, S.; Butkiewicz, H.; Danylyuk, O.; Sashuk, V., Pillar[6]pyridinium: a hexagonally shaped molecular box that selectively recognizes multicharged anionic species.

Chemical Communications **2018,** *54* (49), 6316-6319.

23. Torvinen, M.; Kalenius, E.; Sansone, F.; Casnati, A.; Jänis, J., Noncovalent complexation of glucosylthioureidocalix[4]arenes with carboxylates and their gas-phase characteristics: an ESI-FTICR mass spectrometric study. *Journal of Mass Spectrometry* **2011,** *46* (8), 787-793.

24. Lee, D. H.; Lee, H. Y.; Lee, K. H.; Hong, J.-I., Selective anion sensing based on a dual-chromophore approach. *Chemical Communications* **2001,** (13), 1188-1189.

25. Anzenbacher, P.; Try, A. C.; Miyaji, H.; Jursíková, K.; Lynch, V. M.; Marquez, M.; Sessler, J. L., Fluorinated Calix[4]pyrrole and Dipyrrolylquinoxaline: Neutral Anion Receptors with Augmented Affinities and Enhanced Selectivities. *Journal of the American Chemical Society* **2000,** *122* (42), 10268-10272.

26. Miyaji, H.; Sato, W.; Sessler, J. L., Naked-Eye Detection of Anions in Dichloromethane: Colorimetric Anion Sensors Based on Calix[4]pyrrole. *Angewandte Chemie International Edition* **2000,** *39* (10), 1777-1780.

27. Sancenón, F.; Martínez-Máñez, R.; Soto, J., A Selective Chromogenic Reagent for Nitrate. *Angewandte Chemie International Edition* **2002,** *41* (8), 1416-1419.

28. Jiménez, D.; Martínez-Máñez, R.; Sancenón, F.; Soto, J., Selective fluoride sensing using colorimetric reagents containing anthraquinone and urea or thiourea binding sites. *Tetrahedron Letters* **2002,** *43* (15), 2823-2825.

29. Niikura, K.; Metzger, A.; Anslyn, E. V., Chemosensor Ensemble with Selectivity for Inositol-Trisphosphate. *Journal of the American Chemical Society* **1998,** *120* (33), 8533-8534.

30. Cabell, L. A.; Monahan, M.-K.; Anslyn, E. V., A competition assay for determining glucose-6-phosphate concentration with a tris-boronic acid receptor. *Tetrahedron Letters* **1999,** *40* (44), 7753-7756.

31. Aït-Haddou, H.; Wiskur, S. L.; Lynch, V. M.; Anslyn, E. V., Achieving Large Color Changes in Response to the Presence of Amino Acids: A Molecular Sensing Ensemble with Selectivity for Aspartate. *Journal of the American Chemical Society* **2001,** *123* (45), 11296-11297.

32. Kato, R.; Nishizawa, S.; Hayashita, T.; Teramae, N., A thiourea-based chromoionophore for selective binding and sensing of acetate. *Tetrahedron Letters* **2001,** *42* (30), 5053-5056.

33. Beer, P. D.; Gale, P. A., Anion Recognition and Sensing: The State of the Art and Future Perspectives. *Angewandte Chemie International Edition* **2001,** *40* (3), 486-516.

34. Fitzmaurice, R. J.; Kyne, G. M.; Douheret, D.; Kilburn, J. D., Synthetic receptors for

carboxylic acids and carboxylates. *Journal of the Chemical Society, Perkin Transactions 1* **2002,** (7), 841-864.

35. Wu, J.-l.; He, Y.-b.; Zeng, Z.-y.; Wei, L.-h.; Meng, L.-z.; Yang, T.-x., Synthesis of the anionic fluororeceptors based on thiourea and amide groups and recognition property for α,ω-dicarboxylate. *Tetrahedron* **2004,** *60* (19), 4309-4314.

36. Gunnlaugsson, T.; Davis, A. P.; O'Brien, J. E.; Glynn, M., Fluorescent Sensing of Pyrophosphate and Bis-carboxylates with Charge Neutral PET Chemosensors. *Organic Letters* **2002,** *4* (15), 2449-2452.

37. Knighton, R. C.; Sambrook, M. R.; Vincent, J. C.; Smith, S. A.; Serpell, C. J.; Cookson, J.; Vickers, M. S.; Beer, P. D., Fluorogenic dansyl-ligated gold nanoparticles for the detection of sulfur mustard by displacement assay. *Chemical Communications* **2013,** *49* (23), 2293-2295.

38. Kumar, V.; Anslyn, E. V., A Selective Turn-On Fluorescent Sensor for Sulfur Mustard Simulants. *Journal of the American Chemical Society* **2013,** *135* (16), 6338-6344.

39. Liu, G.; Lu, M.; Huang, X.; Li, T.; Xu, D., Application of Gold-Nanoparticle Colorimetric Sensing to Rapid Food Safety Screening. *Sensors* **2018,** *18* (12), 4166.

40. Bansal, S. A.; Kumar, V.; Karimi, J.; Singh, A. P.; Kumar, S., Role of gold nanoparticles in advanced biomedical applications. *Nanoscale Advances* **2020,** *2* (9), 3764-3787.

41. Martí, A.; Costero, A. M.; Gaviña, P.; Parra, M., Selective colorimetric NO(g) detection based on the use of modified gold nanoparticles using click chemistry. *Chemical Communications* **2015,** *51* (15), 3077-3079.

42. Saha, K.; Agasti, S. S.; Kim, C.; Li, X.; Rotello, V. M., Gold Nanoparticles in Chemical and Biological Sensing. *Chemical Reviews* **2012,** *112* (5), 2739-2779.

43. Wang, Y.; Zhou, X.; Xu, C.; Jin, Y.; Li, B., Gold Nanorods as Visual Sensing Platform for Chiral Recognition with Naked Eyes. *Scientific Reports* **2018,** *8* (1), 5296.

44. Urrutia, A.; Goicoechea, J.; Arregui, F. J., Optical Fiber Sensors Based on Nanoparticle-Embedded Coatings. *Journal of Sensors* **2015,** *2015*, 805053.

45. Wu, D.; Sedgwick, A. C.; Gunnlaugsson, T.; Akkaya, E. U.; Yoon, J.; James, T. D., Fluorescent chemosensors: the past, present and future. *Chemical Society Reviews* **2017,** *46* (23), 7105-7123.

46. Daly, B.; Ling, J.; de Silva, A. P., Current developments in fluorescent PET (photoinduced electron transfer) sensors and switches. *Chemical Society Reviews* **2015,** *44* (13), 4203-4211.

47. Liu, Z.; Nalluri, S. K. M.; Stoddart, J. F., Surveying macrocyclic chemistry: from

flexible crown ethers to rigid cyclophanes. *Chemical Society Reviews* **2017,** *46* (9), 2459-2478.

48. Fyfe, M. C. T.; Lowe, J. N.; Stoddart, J. F.; Williams, D. J., An Extremely Stable Interwoven Supramolecular Bundle. *Organic Letters* **2000,** *2* (9), 1221-1224.

49. Balzani, V.; Clemente-León, M.; Credi, A.; Lowe, J. N.; Badjić, J. D.; Stoddart, J. F.; Williams, D. J., Controlling Multivalent Interactions in Triply-Threaded Two-Component Superbundles. *Chemistry – A European Journal* **2003,** *9* (21), 5348-5360.

50. Jiang, S.; Hu, X.; Qiu, J.; Guo, H.; Yang, F., A fluorescent sensor for folic acid based on crown ether-bridged bis-tetraphenylethylene. *Analyst* **2019,** *144* (8), 2662-2669.

51. Móczár, I.; Huszthy, P., Optically active crown ether-based fluorescent sensor molecules: A mini-review. *Chirality* **2019,** *31* (2), 97-109.

52. Xu, W.; Cheng, M.; Zhang, S.; Wu, Q.; Liu, Z.; Dhinakaran, M. K.; Liang, F.; Kovaleva, E. G.; Li, H., Recent advances in chiral discrimination on host–guest functionalized interfaces. *Chemical Communications* **2021,** *57* (61), 7480-7492.

53. Toro-Vazquez, J. F.; Alvarez-Mitre, F.; Charó-Alonso, M., Physical Properties of Organogels Developed with Selected Low-Molecular-Weight Gelators. In *Crystallization of Lipids*, 2018; pp 353-383.

54. Tian, R.; Chen, J.; Niu, R., The development of low-molecular weight hydrogels for applications in cancer therapy. *Nanoscale* **2014,** *6* (7), 3474-3482.

55. Skilling, K. J.; Citossi, F.; Bradshaw, T. D.; Ashford, M.; Kellam, B.; Marlow, M., Insights into low molecular mass organic gelators: a focus on drug delivery and tissue engineering applications. *Soft Matter* **2014,** *10* (2), 237-256.

56. Ziane, S.; Schlaubitz, S.; Miraux, S.; Patwa, A.; Lalande, C.; Bilem, I.; Lepreux, S.; Rousseau, B.; Le Meins, J. F.; Latxague, L.; Barthélémy, P.; Chassande, O., A thermosensitive low molecular weight hydrogel as scaffold for tissue engineering. *Eur Cell Mater* **2012,** *23*, 147-60; discussion 160.

57. Steed, J. W., Anion-tuned supramolecular gels: a natural evolution from urea supramolecular chemistry. *Chemical Society Reviews* **2010,** *39* (10), 3686-3699.

58. Datta, S.; Bhattacharya, S., Multifarious facets of sugar-derived molecular gels: molecular features, mechanisms of self-assembly and emerging applications. *Chemical Society Reviews* **2015,** *44* (15), 5596-5637.

59. Jadhav, S. R.; Vemula, P. K.; Kumar, R.; Raghavan, S. R.; John, G., Sugar-Derived Phase-Selective Molecular Gelators as Model Solidifiers for Oil Spills. *Angewandte Chemie International Edition* **2010,** *49* (42), 7695-7698.

60. Johnson, E. K.; Adams, D. J.; Cameron, P. J., Peptide based low molecular weight

gelators. *Journal of Materials Chemistry* **2011,** *21* (7), 2024-2027.

61. Stites, W. E., Protein−Protein Interactions: Interface Structure, Binding Thermodynamics, and Mutational Analysis. *Chemical Reviews* **1997,** *97* (5), 1233-1250.

62. Liu, Y.; Sengupta, A.; Raghavachari, K.; Flood, A. H., Anion Binding in Solution: Beyond the Electrostatic Regime. *Chem* **2017,** *3* (3), 411-427.

63. Sommer, F.; Kubik, S., Anion binding of a neutral bis(cyclopeptide) in water–methanol mixtures containing up to 95% water. *Organic & Biomolecular Chemistry* **2014,** *12* (44), 8851-8860.

64. Kubik, S.; Kirchner, R.; Nolting, D.; Seidel, J., A Molecular Oyster: A Neutral Anion Receptor Containing Two Cyclopeptide Subunits with a Remarkable Sulfate Affinity in Aqueous Solution. *Journal of the American Chemical Society* **2002,** *124* (43), 12752-12760.

65. Wu, X.; Wang, P.; Turner, P.; Lewis, W.; Catal, O.; Thomas, D. S.; Gale, P. A., Tetraurea Macrocycles: Aggregation-Driven Binding of Chloride in Aqueous Solutions. *Chem* **2019,** *5* (5), 1210-1222.

66. Užarević, K.; Đilović, I.; Matković-Čalogović, D.; Šišak, D.; Cindrić, M., Anion-Directed Self-Assembly of Flexible Ligands into Anion-Specific and Highly Symmetrical Organic Solids. *Angewandte Chemie International Edition* **2008,** *47* (37), 7022-7025.

67. Užarević, K.; Đilović, I.; Bregović, N.; Tomišić, V.; Matković-Čalogović, D.; Cindrić, M., Anion-Templated Supramolecular C3 Assembly for Efficient Inclusion of Charge-Dispersed Anions into Hydrogen-Bonded Networks. *Chemistry – A European Journal* **2011,** *17* (39), 10889-10897.

68. Friščić, T., Supramolecular concepts and new techniques in mechanochemistry: cocrystals, cages, rotaxanes, open metal–organic frameworks. *Chemical Society Reviews* **2012,** *41* (9), 3493-3510.

69. Imai, Y.; Tajima, N.; Sato, T.; Kuroda, R., Visualization of Molecular Recognition: A Novel System Based on Charge-Transfer Complexes Composed of 1,1‘-Bi-2-naphthol Derivatives and p-Benzoquinone. *Organic Letters* **2006,** *8* (14), 2941-2944.

70. Braga, D.; Grepioni, F.; Lampronti, G. I., Supramolecular metathesis: co-former exchange in co-crystals of pyrazine with (R,R)-, (S,S)-, (R,S)- and (S,S/R,R)-tartaric acid. *CrystEngComm* **2011,** *13* (9), 3122-3124.

71. Rightmire, N. R.; Bruns, D. L.; Hanusa, T. P.; Brennessel, W. W., Mechanochemical Influence on the Stereoselectivity of Halide Metathesis: Synthesis of Group 15 Tris(allyl) Complexes. *Organometallics* **2016,** *35* (11), 1698-1706.

72. Youk, K.-S.; Kim, K. M.; Chatterjee, A.; Ahn, K. H., Selective recognition of fumarate

from maleate with a gold nanoparticle-based colorimetric sensing system. *Tetrahedron Letters* **2008,** *49* (22), 3652-3655.

73. Martí, A.; Costero, A. M.; Gaviña, P.; Parra, M., Selective Recognition and Sensing of Succinate vs. Other Aliphatic Dicarboxylates by Thiourea-Functionalized Gold Nanoparticles. *ChemistrySelect* **2016,** *1* (5), 1057-1060.

74. Liu, Y.; Liu, Y.; Liang, Z.; Li, X.; Liu, S.; Yu, J., Enhanced Sensitivity and Selectivity of Chemosensor for Malonate by Anchoring on Gold Nanoparticles. *Chinese Journal of Chemistry* **2011,** *29* (3), 531-538.

75. Gunnlaugsson, T.; Davis, A. P.; O'Brien, J. E.; Glynn, M., Fluorescent Sensing of Pyrophosphate and Bis-carboxylates with Charge Neutral PET Chemosensors. *Organic Letters* **2002,** *4* (15), 2449-2452.

76. Gunnlaugsson, T.; Davis, A. P.; O'Brien, J. E.; Glynn, M., Synthesis and photophysical evaluation of charge neutral thiourea or urea based fluorescent PET sensors for bis-carboxylates and pyrophosphate. *Organic & Biomolecular Chemistry* **2005,** *3* (1), 48-56.

77. Ghosh, K.; Saha, I.; Masanta, G.; Wang, E. B.; Parish, C. A., Triphenylamine-based receptor for selective recognition of dicarboxylates. *Tetrahedron Letters* **2010,** *51* (2), 343-347.

78. Gotor, R.; Costero, A. M.; Gaviña, P.; Gil, S.; Parra, M., Binding and Fluorescent Sensing of Dicarboxylates by a Bis(calix[4]pyrrole)-Substituted BODIPY Dye. *European Journal of Organic Chemistry* **2013,** *2013* (8), 1515-1520.

79. Más-Montoya, M.; Curiel, D.; Ramírez de Arellano, C.; Tárraga, A.; Molina, P., Preorganized Fluorescent Receptor for the Preferential Binding of the Glutarate Anion. *European Journal of Organic Chemistry* **2016,** *2016* (22), 3878-3883.

80. Pushina, M.; Koutnik, P.; Nishiyabu, R.; Minami, T.; Savechenkov, P.; Anzenbacher Jr., P., Anion Sensing by Fluorescent Expanded Calixpyrroles. *Chemistry – A European Journal* **2018,** *24* (19), 4879-4884.

81. Hu, M.; Feng, G., Highly selective and sensitive fluorescent sensing of oxalate in water. *Chemical Communications* **2012,** *48* (55), 6951-6953.

82. Nakamura, T.; Kaneko, Y.; Nishibori, E.; Nabeshima, T., Molecular recognition by multiple metal coordination inside wavy-stacked macrocycles. *Nature Communications* **2017,** *8* (1), 129.

83. Mateus, P.; Delgado, R.; André, V.; Duarte, M. T., Dicarboxylate Recognition Properties of a Dinuclear Copper(II) Cryptate. *Inorganic Chemistry* **2015,** *54* (1), 229-240.

84. Delori, A.; Suresh, E.; Pedireddi, V. R., pKa-Directed Host–Guest Assemblies: Rational Analysis of Molecular Adducts of 2,4-Diamino-6-methyl-1,3,5-triazine with Various

Aliphatic Dicarboxylic Acids. *Chemistry – A European Journal* **2008,** *14* (23), 6967-6977.

85. Nandy, P.; Nayak, A.; Biswas, S. N.; Pedireddi, V. R., Self-assembly in solvates of 2,4-diamino-6-(4-methyl- phenyl)-1,3,5-triazine and in its molecular adducts with some aliphatic dicarboxylic acids. *Journal of Molecular Structure* **2016,** *1108*, 717-726.

86. Korendovych, I. V.; Cho, M.; Makhlynets, O. V.; Butler, P. L.; Staples, R. J.; Rybak-Akimova, E. V., Anion and Carboxylic Acid Binding to Monotopic and Ditopic Amidopyridine Macrocycles. *The Journal of Organic Chemistry* **2008,** *73* (13), 4771-4782.

87. Bravin, C.; Badetti, E.; Puttreddy, R.; Pan, F.; Rissanen, K.; Licini, G.; Zonta, C., Binding Profiles of Self-Assembled Supramolecular Cages from ESI-MS Based Methodology. *Chemistry – A European Journal* **2018,** *24* (12), 2936-2943.

88. Bravin, C.; Mason, G.; Licini, G.; Zonta, C., A Diastereodynamic Probe Transducing Molecular Length into Chiroptical Readout. *Journal of the American Chemical Society* **2019,** *141* (30), 11963-11969.

89. Liu, S.-Y.; He, Y.-B.; Wu, J.-L.; Wei, L.-H.; Qin, H.-J.; Meng, L.-Z.; Hu, L., Calix[4]arenes containing thiourea and amide moieties: neutral receptors towards α,ω-dicarboxylate anions. *Organic & Biomolecular Chemistry* **2004,** *2* (11), 1582-1586.

90. Andreyko, E. A.; Padnya, P. L.; Daminova, R. R.; Stoikov, I. I., Supramolecular "containers": self-assembly and functionalization of thiacalix[4]arenes for recognition of amino- and dicarboxylic acids. *RSC Advances* **2014,** *4* (7), 3556-3565.

91. Gong, H.-Y.; Rambo, B. M.; Karnas, E.; Lynch, V. M.; Keller, K. M.; Sessler, J. L., Environmentally Responsive Threading, Dethreading, and Fixation of Anion-Induced Pseudorotaxanes. *Journal of the American Chemical Society* **2011,** *133* (5), 1526-1533.

92. Tang, F.; Cao, R.; Gong, H.-Y., Aromatic plane effect study in pseudorotaxane construction between 'Texas-sized' molecular box and carboxylate anions. *Tetrahedron Letters* **2015,** *56* (6), 820-823.

93. Yang, Y.-D.; Fan, C.-C.; Rambo, B. M.; Gong, H.-Y.; Xu, L.-J.; Xiang, J.-F.; Sessler, J. L., Multicomponent Self-Assembled Metal–Organic [3]Rotaxanes. *Journal of the American Chemical Society* **2015,** *137* (40), 12966-12976.

94. Ding, C.-J.; Shen, M.-J.; Xu, L.-J.; Gong, H.-Y., The complexation between 'Texas sized' molecular box and linear n-aliphate dianion: en route to supramolecular organic frameworks (SOFs) for selectively CO2 absorption. *Tetrahedron* **2016,** *72* (3), 431-435.

95. Shang, J.; Rambo, B. M.; Hao, X.; Xiang, J.-F.; Gong, H.-Y.; Sessler, J. L., Post-synthetic modification of a macrocyclic receptor via regioselective imidazolium ring-opening. *Chemical Science* **2016,** *7* (7), 4148-4157.

96. Yang, Y.-D.; Sessler, J. L.; Gong, H.-Y., Flexible imidazolium macrocycles: building blocks for anion-induced self-assembly. *Chemical Communications* **2017,** *53* (70), 9684-9696.
97. Duan, Q.; Zhao, W.; Lu, K., Synthesis of a water-soluble pillar[6]arene dodecaamine and its selective binding of acidic amino acids in water. *Tetrahedron Letters* **2017,** *58* (46), 4403-4406.
98. Berry, S. N.; Qin, L.; Lewis, W.; Jolliffe, K. A., Conformationally adaptable macrocyclic receptors for ditopic anions: analysis of chelate cooperativity in aqueous containing media. *Chemical Science* **2020,** *11* (27), 7015-7022.
99. Cruz, C.; Delgado, R.; Drew, M. G. B.; Félix, V., Supramolecular aggregates between carboxylate anions and an octaaza macrocyclic receptor. *Organic & Biomolecular Chemistry* **2004,** *2* (20), 2911-2918.
100. Khayyami, A.; Karppinen, M., Reversible Photoswitching Function in Atomic/Molecular-Layer-Deposited ZnO:Azobenzene Superlattice Thin Films. *Chemistry of Materials* **2018,** *30* (17), 5904-5911.
101. Pang, Z. h.; Dang, L. l.; Yang, L. x.; Luo, F., Azo-MOFs showing controllable framework flexibility and consequently fine-tuned photomechanical crystal motion. *Journal of Solid State Chemistry* **2019,** *277*, 182-186.
102. Zhang, C.-C.; Zhang, Y.-M.; Liu, Y., Photocontrolled reversible conversion of a lamellar supramolecular assembly based on cucurbiturils and a naphthalenediimide derivative. *Chemical Communications* **2018,** *54* (96), 13591-13594.
103. Wang, J.; Zhang, H.-Y.; Zhang, X.-J.; Song, Z.-H.; Zhao, X.-J.; Liu, Y., Light-controlled reversible formation and dissociation of nanorods via interconversion of pseudorotaxanes. *Chemical Communications* **2015,** *51* (34), 7329-7332.
104. Samanta, M.; Siva Rama Krishna, V.; Bandyopadhyay, S., A photoresponsive glycosidase mimic. *Chemical Communications* **2014,** *50* (73), 10577-10579.
105. Roth Stefaniak, K.; Epley, C. C.; Novak, J. J.; McAndrew, M. L.; Cornell, H. D.; Zhu, J.; McDaniel, D. K.; Davis, J. L.; Allen, I. C.; Morris, A. J.; Grove, T. Z., Photo-triggered release of 5-fluorouracil from a MOF drug delivery vehicle. *Chemical Communications* **2018,** *54* (55), 7617-7620.
106. Lin, Y.-S.; Tu, G.-M.; Lin, C.-Y.; Chang, Y.-T.; Yen, Y.-P., Colorimetric anion chemosensors based on anthraquinone: naked-eye detection of isomeric dicarboxylate and tricarboxylate anions. *New Journal of Chemistry* **2009,** *33* (4), 860-867.
107. Madhuprasad; Trivedi, D. R., A new colorimetric receptor for selective detection of maleate vs. fumarate and ratiometric detection of F− ions. *Analytical Methods* **2014,** *6* (11),

3817-3825.

108. Singh, A.; Mohan, M.; Trivedi, D. R., Design and synthesis of malonohydrazide based colorimetric receptors for discrimination of maleate over fumarate and detection of F−, AcO− and AsO2− ions. *Spectrochimica Acta Part A: Molecular and Biomolecular Spectroscopy* **2020,** *229*, 117883.

109. Kim, E.-J.; Haldar, U.; Lee, H.-i., Tuning the ability to discriminate between geometric isomers maleic acid and fumaric acid of water-soluble polymeric probes with a donor-π-acceptor skeleton. *Polymer* **2020,** *186*, 122040.

110. Samanta, S.; Kar, C.; Das, G., Colorimetric and Fluorometric Discrimination of Geometrical Isomers (Maleic Acid vs Fumaric Acid) with Real-Time Detection of Maleic Acid in Solution and Food Additives. *Analytical Chemistry* **2015,** *87* (17), 9002-9008.

111. Shanmugaraju, S.; Bar, A. K.; Jadhav, H.; Moon, D.; Mukherjee, P. S., Coordination self-assembly of tetranuclear Pt(ii) macrocycles with an organometallic backbone for sensing of acyclic dicarboxylic acids. *Dalton Transactions* **2013,** *42* (8), 2998-3008.

112. Mateus, P.; Delgado, R.; Brandão, P.; Félix, V., Dicarboxylate Recognition by Two Macrobicyclic Receptors: Selectivity for Fumarate over Maleate. *The Journal of Organic Chemistry* **2012,** *77* (10), 4611-4621.

113. Gale, P. A., Anion receptor chemistry: highlights from 2008 and 2009. *Chemical Society Reviews* **2010,** *39* (10), 3746-3771.

114. Steed, J. W., Anion-tuned supramolecular gels: a natural evolution from urea supramolecular chemistry. *Chemical Society Reviews* **2010,** *39* (10), 3686-3699.

115. Hay, B. P., De novo structure-based design of anion receptors. *Chemical Society Reviews* **2010,** *39* (10), 3700-3708.

116. Li, A.-F.; Wang, J.-H.; Wang, F.; Jiang, Y.-B., Anion complexation and sensing using modified urea and thiourea-based receptors. *Chemical Society Reviews* **2010,** *39* (10), 3729-3745.

117. Amendola, V.; Fabbrizzi, L.; Mosca, L., Anion recognition by hydrogen bonding: urea-based receptors. *Chemical Society Reviews* **2010,** *39* (10), 3889-3915.

118. Duke, R. M.; Veale, E. B.; Pfeffer, F. M.; Kruger, P. E.; Gunnlaugsson, T., Colorimetric and fluorescent anion sensors: an overview of recent developments in the use of 1,8-naphthalimide-based chemosensors. *Chemical Society Reviews* **2010,** *39* (10), 3936-3953.

119. Amendola, V.; Esteban-Gómez, D.; Fabbrizzi, L.; Licchelli, M., What Anions Do to N−H-Containing Receptors. *Accounts of Chemical Research* **2006,** *39* (5), 343-353.

120. Kosiorek, S.; Rosa, B.; Boinski, T.; Butkiewicz, H.; Szymański, M. P.; Danylyuk, O.;

Szumna, A.; Sashuk, V., Pillar[4]pyridinium: a square-shaped molecular box. *Chemical Communications* **2017,** *53* (100), 13320-13323.

121. Xie, F.; Bai, Q.; Jiang, X.; Yu, X.; Xia, Z.; Wei, W., Visual and Colorimetric High-Throughput Analysis if Chiral Carboxylic Acids Based on Enantioselective Charge Shielding of Gold Nanoparticles. *Applied Materials and Interfaces* **2018,** *10* (14), 11872-11879.

122. Langille, M. R.; Personick, M. L.; Zhang, J.; Mirkin, C. A., Defining Rules for the Shape Evolution of Gold Nanoparticles. *Journal of the American Chemical Society* **2012,** *134* (35), 14542-14554

123. Afrooz, N.; Sivalapalan, S.; Murphy, C.; Hussain, S.; Schlager, J.; Saleh, N., Spheres vs. rods: The shape of gold nanoparticles influences aggregation and deposition behaviour. *Chemosphere* **2013,** *91* (1), 93-98.

124. Chithrani, B. D.; Ghazani, A. A; Chan, W. C., Determining the Size and Shape Dependence of Gold Nanoparticles Uptake into Mammalian Cells. *Nano Letters* **2006,** *6* (4), 662-668.

125. Li, H.; Chen, D.-X.; Sun, Y.-L.; Zheng, Y. B.; Tan, L.-L.; Weiss, P. S.; Yang, Y.-W., Viologen-Mediated Assembly of and Sensing with Carboxylatopillar[5]arene-Modified Gold Nanoparticles. *Journal of the American Chemical Society* **2013,** *135* (4), 1570-1576.

126. Su, K. H.; Wei, Q. H.; Zhang, X.; Mock, J. J.; Smith, D. R.; Schultz, S., Interparticle Coupling Effects on Plasmon Resonances of Nanogold Particles. *Nano Letters* **2003,** *3* (8), 1087-1090.

127. Jain, P. K.; Huang, W.; El-Sayed, M. A., On the Universal Scaling Behaviour of the Distance Decay of Plasmon Coupling in Metal Nanoparticle Pairs: A Plasmon Ruler Equation. *Nano Letters* **2007,** *7* (7), 2080-2088.

128. Zhang, W.; Li, Q.; Qiu, M., A plasmon ruler based on nanoscale photothermal effect. *Opt. Express* **2013,** *21* (1), 172-181.

129. Wende, T.; Wanko, M.; Jiang, L.; Meijer, G.; Asmis, K. R.; Rubio, A., Spectroscopic Characterization of Solvent-Mediated Folding in Dicarboxylate Dianions. *Angewandte Chemie International Edition* **2011,** *50* (16), 3807-3810.

130. Minofar, B.; Mucha, M.; Jungwirth, P.; Yang, X.; Fu, Y.-J.; Wang, X.-B.; Wang, L.-S., Bulk versus Interfacial Aqueous Solvation of Dicarboxylate Dianions. *Journal of the American Chemical Society* **2004,** *126* (37), 11691-11698.

131. Herbert, J. M.; Ortiz, J. V., Ab Initio Investigation of Electron Detachment in Dicarboxylate Dianions. *The Journal of Physical Chemistry A* **2000,** *104* (50), 11786-11795.

132. Wanko, M.; Wende, T.; Saralegui, M. M.; Jiang, L.; Rubio, A.; Asmis, K. R., Solvent-

mediated folding of dicarboxylate dianions: aliphatic chain length dependence and origin of the IR intensity quenching. *Physical Chemistry Chemical Physics* **2013,** *15* (47), 20463-20472.

133. Viana, R. B.; da Silva, A. B. F.; Pimentel, A. S., Infrared Spectroscopy of Anionic, Cationic, and Zwitterionic Surfactants. *Advances in Physical Chemistry* **2012,** *2012*, 903272.

134. Abbott, H. E.; Hey, J. C.; Britton, M. M.; Johnston, R. L., Effects of Hydration on the Conformational Behavior of Flexible Molecules with Two Charge Centers. *The Journal of Physical Chemistry A* **2020,** *124* (26), 5323-5330.

135. Mishra, M. K.; Varughese, S.; Ramamurty, U.; Desiraju, G. R., Odd–Even Effect in the Elastic Modulii of α,ω-Alkanedicarboxylic Acids. *Journal of the American Chemical Society* **2013,** *135* (22), 8121-8124.

136. Bian, T.; Chu, Z.; Klajn, R., The Many Ways to Assemble Nanoparticles Using Light. *Advanced Materials* **2020,** *32* (20), 1905866.

137. Kundu, P. K.; Samanta, D.; Leizrowice, R.; Margulis, B.; Zhao, H.; Börner, M.; Udayabhaskararao, T.; Manna, D.; Klajn, R., Light-controlled self-assembly of non-photoresponsive nanoparticles. *Nature Chemistry* **2015,** *7* (8), 646-652.

138. Niehues, M.; Engel, S.; Ravoo, B. J., Photo-Responsive Self-Assembly of Plasmonic Magnetic Janus Nanoparticles. *Langmuir* **2021,** *37* (37), 11123-11130.

139. Cheng, Y.; Dong, J.; Li, X., Light-Switchable Self-Assembly of Non-Photoresponsive Gold Nanoparticles. *Langmuir* **2018,** *34* (21), 6117-6124.

140. Ryssy, J.; Natarajan, A. K.; Wang, J.; Lehtonen, A. J.; Nguyen, M.-K.; Klajn, R.; Kuzyk, A., Light-Responsive Dynamic DNA-Origami-Based Plasmonic Assemblies. *Angewandte Chemie International Edition* **2021,** *60* (11), 5859-5863.

141. Peng, X.; Gao, H.; Xiao, Y.; Cheng, H.; Huang, F.; Cheng, X., Synthesis and self-assembly of photoresponsive and luminescent polycatenar liquid crystals incorporating an azobenzene unit interconnecting two 1,3,4-thiadiazoles. *New Journal of Chemistry* **2017,** *41* (5), 2004-2012.